Preparation and properties of the mercury based thin films of very High Tc superconductors and their possible applications in cryoelectronics

Valerianova Michaela

SLOVAK TECHNICAL UNIVERSITY OF BRATISLAVA

UNIVERSITÉ JOSEPH FOURIER - GRENOBLE I

ECOLE DOCTORALE

Physique / Slovak Academy of Science

THESE

Pour obtenir le grade de

DOCTEUR DE L'UNIVERSITE JOSEPH FOURIER

Spécialité : Physique des Matériaux et Nanostructures

Présentée et soutenue publiquement par

Michaela VALERIANOVA

Le 27 septembre 2007

Elaboration et propriétés de films minces à base de mercure supraconducteurs de très haute température critique et leurs applications possibles à la cryoélectronic
_____

Preparation and properties of the mercury based thin films of very High Tc superconductors and their possible applications in cryoelectronics
_____

Thèse dirigée par : Štefan Chromik / Philippe Odier

Composition du Jury :

Juraj BANSKY   - Président
Philippe GALEZ   - Rapporteur
Matej JERGEL   - Rapporteur
Luc ORTEGA   - Examinateur
Stefan CHROMIK   - Examinateur
Philippe ODIER   - Examinateur

Institute of Electrical Engineering

Slovak Academy of Sciences

Bratislava

Néel Institute

Centre National de la Recherche Scientifique

Grenoble

MSc. Michaela Valeriánová

Preparation and properties of the mercury based thin films
of very high Tc superconductors
and their possible application in cryoelectronics

Dissertation thesis

Supervisors:

Dr. Štefan Chromik

Dr. Philippe Odier

Bratislava 2007

Table of contents

I. Introduction

The first observation of the disappearance of the electrical resistance of mercury at helium temperature in 1911 by Kammerling Onnes started the research of the superconductivity phenomenon in various materials. Since the 1960s, researchers have explored the possibility that the superconducting properties of films may be superior to, or at least different from, those of bulk materials. Thin films studies have opened many new and interesting areas of solid-state research, such as superconductive tunneling and enhanced superconductivity.

The recent discovery of high temperature superconductors brings us a giant step closer to the dream of early scientists. Applications currently being explored are mostly extensions of current technology used with the low temperature superconductors. Current applications of high temperature superconductors include: magnetic shielding devices, medical imaging systems, superconducting quantum interference devices (SQUIDs), infrared sensors, analog signal processing devices, and microwave devices. As our understanding of the properties of superconducting material increases, applications such as power transmission, superconducting magnets in generators, energy storage devices, particle accelerators, levitated vehicle transportation, rotating machinery, and magnetic separators will become more practical.

Hg-based superconductors posses the highest critical temperature from all known superconductors and thus they are very promising candidates for the applications thanks to their high operating temperature. The first step to approach the application of these materials in the everyday life is to improve and simplify their fabrication.

The goal of my thesis was to prepare Re-doped thin superconducting films based on mercury (HgBa$_2$Ca$_{n-1}$Cu$_n$O$_{2n+2}$, n = 1, 2) on the CeO$_2$ buffered R-plane sapphire and LaAlO$_3$ substrate. In this work we present the study of the mercuration process with effort to optimize the synthesis conditions to find out reproducible process of the thin film preparation. We tried to find the convenient conditions to obtain HgBa$_2$Ca$_2$Cu$_3$O$_{10}$. We report also the fabrication of the superconducting structures using patterning of the precursor films by lift-off process and their characterization.

This dissertation thesis is devoted to the synthesis and characterization of the thin superconducting films based on mercury. The introduction is the first chapter of the thesis. Then, some basic concepts of the superconductivity, Hg-based superconductors and of the thin films formation are described in the second chapter. The third chapter involves the

present state of status of ongoing research in the field of the synthesis of the mercury cuprates. The aims of the thesis are precised in the fourth chapter. The fifth chapter is concerned with the characterization techniques used in my work. Then, the sixth one involves results and discusion and the last ones contain conclusion of my results and perspectives of the application of Hg-based films and structures in the cryoelectronics as well as the perspectives of the future research.

Introduction

Les premières observations de la disparition de la résistance électrique du mercure dans l'hélium liquide faites par Kammerling Onnes en 1911, ont initiées une recherche du phénomène de la supraconductivité dans les différents matériaux. Depuis les années 1960, les scientifiques ont exploré la possibilité que les propriétés des couches minces supraconductrices puissent être supérieures ou peu différentes des propriétés des matériaux "bulk". La recherche sur les couches minces a ouvert beaucoup des nouveaux domaines intéressants dans la physique du solide comme par exemple l'effet de tunnel supraconducteur.

La découverte récente des supraconducteurs de haute température critique nous a rapproché d'un rêve des premiers chercheurs. Les applications actuellement explorées concernent les supraconducteurs dits bas T_C. Il y a aussi quelque application utilisant les supraconducteurs à HTC comme par exemple les dispositifs de protection magnétiques, les systèmes à stockage d'énergie, les systèmes d'imagerie médicale, les dispositifs supraconducteur à interférence quantiques (SQUID), les capteurs infrarouges, les dispositifs à signal analogique et à micro-ondes. Comme notre compréhension des propriétés des matériaux supraconducteurs s'améliore, les possibilités d'applications dans le domaine du transport de puissance, des aimants supraconducteurs dans les générateurs électriques, des dispositifs de stockage d'énergie, des accélérateurs de particules, du transport de véhicule en lévitation et des séparateurs magnétiques deviendra plus proche.

Les supraconducteurs à la base de mercure ont les températures critiques les plus grandes de tous les matériaux connus. Grace à leur haute température de travail, ils sont les candidats très prometteurs pour les applications. La simplification et l'amélioration de la fabrication des supraconducteurs à la base de mercure seront la première étape de l'approche vers les applications de ces matériaux pour la vie quotidienne.

Le but de ma thèse était la préparation des couches minces supraconductrices à la base de mercure dopées par le rhénium ($HgBa_2Ca_{n-1}Cu_nO_{2n+2}$, $n = 1, 2$) sur les substrats suivants: R-plane saphir avec la couche tampon de CeO_2 et $LaAlO_3$. Dans cette thèse on présent les études de la procède de mercuration et l'objectif de mon travail était une optimisation les conditions de la synthèse pour obtenir le procède reproductible pour la préparation des couches minces a la base de mercure. On a essayé de trouver les conditions appropriées pour obtenir la phase $HgBa_2Ca_2Cu_3O_{10}$. On présent aussi la fabrication des structures

supraconductrices préparées par la gravure des couches précurseurs par lift-off procède et les caractérisations des structures.

II. Basic concepts

Concepts de Base:

Dans ce chapitre on présent le phénomène de supraconductivité en général, mais aussi les matériaux supraconducteurs à hautes températures critique et en particulier les cuprates de mercure. On décrit les applications pratiques où les types différentes de supraconducteurs sont utilisés. On décrit aussi la technologie d'obtention des couches minces (dépôt, choix et le rôle de substrat) et les différentes techniques de gravure.

1. Superconductivity

1.1 Introduction to superconductivity

Superconductors have the ability to conduct electricity without loss of energy [1]. When a current flows in an ordinary conductor, for example a copper wire, some energy is lost. In a light bulb or electric heater, the electrical resistance creates a light and a heat. In metals such as copper and aluminium, the electricity is conducted as outer energy level electrons migrate as individuals from one atom to another. These atoms form a vibrating lattice within the metal conductor; the warmer the metal the more it vibrates. As the electrons begin moving through the maze, they collide with tiny impurities or imperfections in the lattice. When the electrons bump into these obstacles they fly off in all directions and lose their energy in the form of the heat.

Inside a superconductor the behaviour of the electrons is different. The impurities and the lattice are still there, but the movement of the superconducting particles through the obstacle course is quite different. As the superconducting electrons travel through the conductor they pass unobstructed through the complex lattice. Because they bump into nothing and create no friction they can transmit the electricity with no loss in the current of energy.

BCS theory (named for its inventors, Bardeen, Cooper, and Schrieffer) explains the conventional superconductivity, the ability of certain metals at low temperatures to conduct the electricity without an electrical resistance [1]. The BCS theory views the superconductivity as a macroscopic quantum mechanical effect. It proposes that the electrons with an opposite spin can become paired, forming Cooper pairs. In many superconductors, the

attractive interaction between the electrons (necessary for pairing) is brought about indirectly by the interaction between the electrons and the vibrating crystal lattice (the phonons).

An electron moving through a conductor will attract nearby positive charges in the lattice. This deformation of the lattice causes another electron, with an opposite "spin", to move into the region of higher positive charge density. The two electrons are then held together with a certain binding energy. If this binding energy is higher than the energy provided by kicks from oscillating atoms in the conductor (which is true at low temperatures), then the electron pair will stick together and resist all kicks, thus not experiencing resistance.

The BCS theory starts from the assumption that there is some attraction between the electrons, which can overcome the Coulomb repulsion. In most materials (in low temperature superconductors), this attraction is brought about indirectly by the coupling of electrons to the crystal lattice (as explained above). However, the results of the BCS theory do not depend on the origin of the attractive interaction. The original results of the BCS (discussed below) described an "s-wave" superconducting state, which is the rule among the low-temperature superconductors but is not realized in many "unconventional superconductors", such as the "d-wave" high-temperature superconductors. Extensions of the BCS theory has been made to describe these other cases, although they are insufficient to describe the observed features of the high-temperature superconductivity.

The BCS were able to give an approximation for the quantum-mechanical state of the system of (attractively interacting) the electrons inside the metal. This state is now known as the "BCS state". Whereas in the normal metal electrons move independently, in the BCS state they are bound into "Cooper pairs" by the attractive interaction.

In 1986, the "high-temperature superconductivity" was discovered. BCS theory is not appropriate to fully describe this new type of superconductivity. Strong theoretical debates still exist at present to explain the superconductivity above 40 K and peculiarities of "high-T_C" compounds.

1.2 General characteristics of superconductors

The critical temperature T_C is the temperature below which materials have no electrical resistance. This temperature depends on the chemical composition and crystal structure of the superconducting material. The critical temperature is usually represented by Kelvin K.

High temperature superconductors have a broader transition to the superconducting state (from few mK up to few K) than low temperature superconductors and the some important temperature points of the transition are defined according to the Fig. 1.

The critical current I_C is the maximum amount of the current which can pass through the sample without the loss of superconducting properties. Its value is often represented by its density J_C (ratio I_C / S where I_C is the value of the current passing through the surface S). The unit of the critical current density is Am^{-2} (Fig. 2).
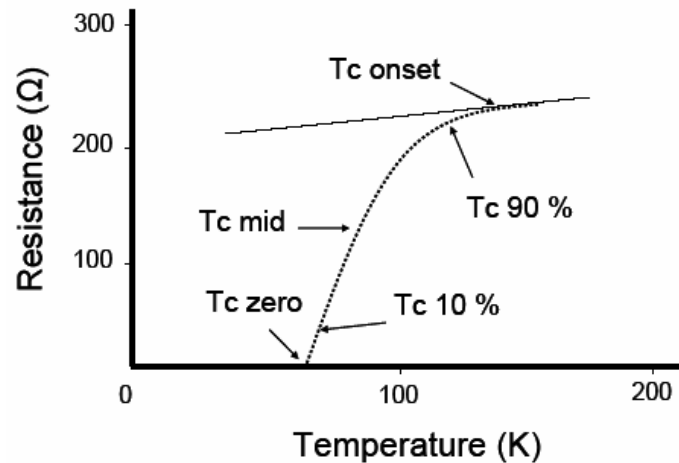
Fig. 1 The characteristic points of the resistance vs. the temperature ($R(T)$) curve for a high temperature superconductor.

The critical magnetic field H_C characterizes the maximum value of the external or self magnetic field which could not be exceeded to not to loose the superconducting properties (Fig. 2). The unit of the critical magnetic induction is Am^{-1}.
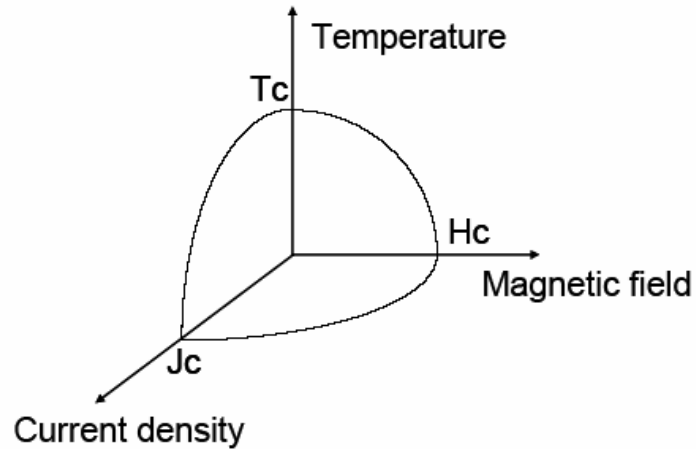
Fig. 2 The critical surface of a superconductor. (T_C - critical temperature, J_C - critical current density, H_C - critical magnetic field).

When a material makes the transition from the normal to the superconducting state, it actively excludes magnetic fields from its interior when $H < H_{C1}$ this is called the ***Meissner effect***.

One of the theoretical explanations of the Meissner effect comes from the London equation. It shows that the magnetic field decays exponentially inside the superconductor over a distance λ (1-40 nm) depending on the material called the London penetration depth.

The magnetic behaviour of a superconductor is illustrated in the Fig. 1.3. It will actively exclude any magnetic field present when it makes the phase change to the superconducting state (Fig. 3) when $H < H_{C1}$.
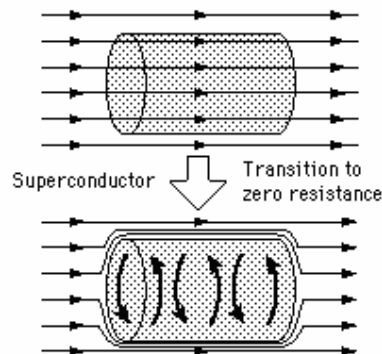
Fig. 3 A superconductor in a magnetic field.

There are thirty pure metals which exhibit zero resistivity at low temperatures and have the property of excluding magnetic fields from the interior of the superconductor

(Meissner effect). They are called Type I superconductors (Fig. 4a). The superconductivity exists only below their critical temperatures and below a critical magnetic field strength. The type I superconductors are well described by the BCS theory.

While instructive for understanding the superconductivity, the Type I superconductors have been of limited practical usefulness because the critical magnetic fields so small and field cannot be trapped.

Starting in 1930 with lead-bismuth alloys, a number of alloys were found which exhibited the superconductivity; they are called Type II superconductors (Fig. 4b). They were found to have much higher critical fields and therefore could carry much higher current densities while remaining in the superconducting state. The type I superconductors are sometimes called "soft" superconductors while the Type II are "hard", maintaining the superconducting state to higher temperatures and magnetic fields.
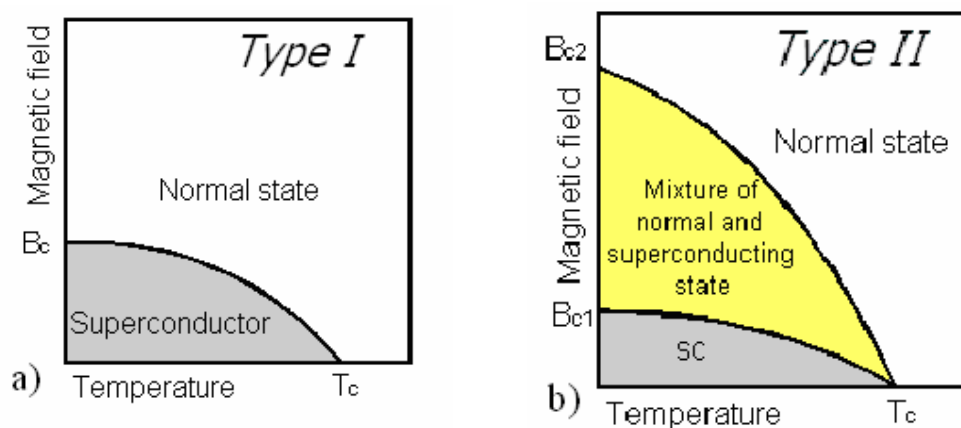
Fig. 4 A type I (a) and type II (b) superconductor.

The yttrium-barium-copper-oxide ceramics which achieved the superconducting state at much higher temperatures are often just referred to as high temperature superconductors and form a class of their own (see chapter 2 in this section).

The irreversibility field (H_{irr}) can be observed in the H_{C1}–H_{C2} interval. The term "irreversibility" is related to the hysteretic behaviour of the magnetization (M) in an applied magnetic field. A typical $M(H)$ dependence for the superconductors is schematically represented in the Fig. 5a. It has been established that the hysteresis loop width (ΔM) is proportional to the critical current density (J_C). For instance, according to a model proposed by Bean:

$$J_C = k \times \Delta M / d$$

where d is an average sample thickness perpendicular to the direction of the applied magnetic field, and k is a constant related to the sample shape. Increasing the magnetic field results in the ΔM decrease (see Fig. 5b), and finally at $H = H_{irr}$ $\Delta M \rightarrow 0$ and therefore $J_C \rightarrow 0$. It is obvious that the H_{irr} value must be considered to be one of the crucial parameters for superconducting materials, since its value is important for different potential applications. H_{irr} is also often used for the characterization and the comparison of different high-T_C superconducting cuprates. The existence of an irreversibility field is explained by several theories, for instance, by "melting" of the so-called vortex lattice present in the mixed state between H_{C1} and H_{irr}.
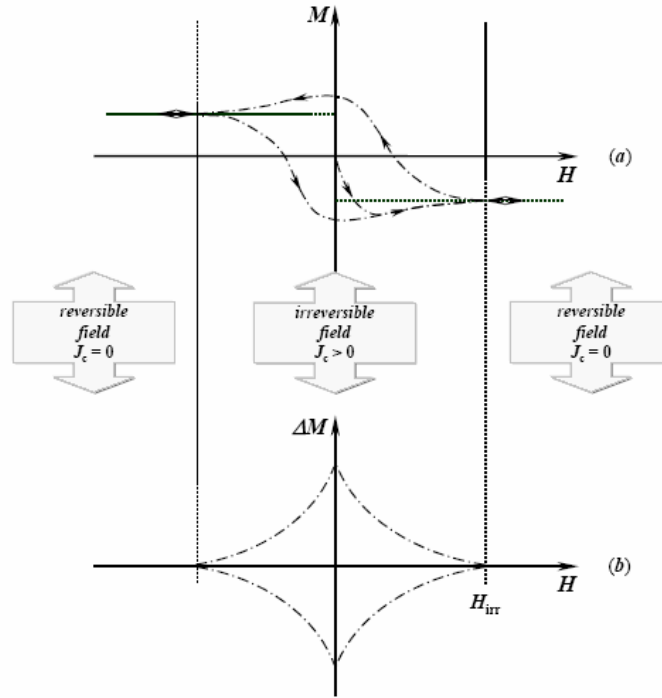
Fig. 5 M(H) (*a*) and ΔM(H) (*b*) dependencies. A schematic division into reversible ($\Delta M = 0$, $J_C = 0$) and irreversible ($\Delta M > 0$, $J_C > 0$) fields is shown.

The temperature dependence of the irreversibility field $H_{irr}(T)$ is called the ***irreversibility line*** (**IL**). This line in fact divides the mixed-state region into an irreversible ($\Delta M > 0$, $J_C > 0$) and a reversible field ($\Delta M = 0$, $J_C = 0$). The irreversibility line belongs to the main limitations to critical currents. It is very rapid thermally activated motion of flux lines which occurs above a combination of the field and temperature. It is not a strict line since the different measurements of the DC magnetization, the loss peak in the AC susceptibility and the zero resistance point give different values. However, all the measurements are consistent

with the idea that it is a resistive transition. That is to say that the magnetic measurement produce a line where the skin depth is comparable to the sample dimensions. It is associated with thermal activation since flux creep increases rapidly as the irreversibility line is approached and the process has been termed 'melting'. Whether this melting is a phase change or not is of interest to physicists but not of much practical importance.

The irreversibility line is much more dependent on basic superconducting properties than the pinning and is less easy to improve. It is strongly related to the degree of coupling between planes. As the number of insulating layers increase and the number of superconducting layers decrease the irreversibility line comes down.

The Josephson effect is the phenomenon of the current flow across two superconductors weakly coupled, separated by a very thin insulating barrier for example (grain boundary, thin oxide layer, etc). This arrangement – two superconductors linked by a non-conducting oxide barrier – is known as a Josephson junction; the current that crosses the barrier is the Josephson current. The terms are named eponymously after a British physicist Brian David Josephson, who predicted the existence of the effect in 1962. It has important applications in quantum – mechanical circuits, such as SQUIDs.

The basic equations governing the dynamics of the Josephson effect are

$$I(t) = I_C \sin \phi(t) \qquad \text{(Josephson or weak-link current-phase relation)}$$

$$U(t) = \frac{h}{2e} \frac{\partial \phi}{\partial t} \qquad \text{(superconducting phase evolution equation)}$$

where $U(t)$ and $I(t)$ are the voltage and current across the Josephson junction, $\varphi(t)$ is the phase difference between the wave functions in the two superconductors comprising the junction, and I_C is a constant, the critical current of the junction. The critical current is an important phenomenological parameter of the device that can be affected by a temperature as well as by an applied magnetic field. The physical constant, $h/2e$, is the magnetic flux quantum, the inverse of which is the Josephson constant.

The two main effects predicted by Josephson follow from these relations:

1. *The DC Josephson effect.* This refers to the phenomenon of a direct current crossing the insulator in the absence of any external electromagnetic field, owing to the tunneling. This DC Josephson current is proportional to the sine of the phase difference across the insulator, and may take values between $(-I_C)$ and I_C.

2. *The AC Josephson effect.* With a fixed voltage U_{DC} across the junctions, the phase will vary linearly with time and the current will be an AC current with amplitude I_C and frequency $2e/h$

U_{DC}. This means that the Josephson junction can act as a perfect voltage-to-frequency converter.

The wave function can be regarded as giving the probability of a given particle existing in a certain place at a certain time. In the superconductors on both sides of a Josephson junction, all the Cooper pairs in each are defined by a single wave function. The wave function does not go immediately to zero at the insulating barrier, however, and if the barrier is thin enough, the two wave functions will overlap, forming a single, continuous wave function. This means that since the wave function in the insulating junction is not zero, the Cooper pairs will leak, or "tunnel", through the barrier.

This tunneling makes the insulating barrier a weak superconductor, with the maximum or "critical" current dependent on the temperature, the material, and the size of the junction. This "direct-current" Josephson effect was quickly verified, and a similar "alternating current" Josephson effect was discovered soon afterwards.
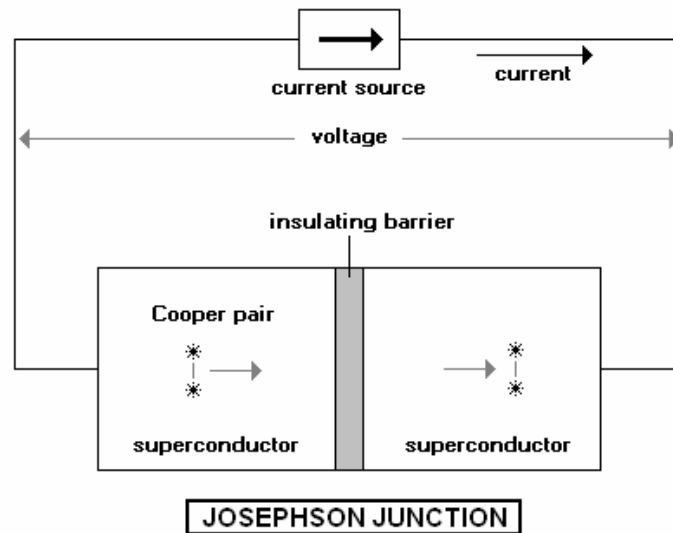
Fig. 6 Schematic representation of the Josephson junction.

2. Hg-based superconductors

High temperature superconductors (HTS) are the materials having the critical temperatures above 40 K. In 1986, the field of superconductivity was revolutionized by the discovery of a new class of superconductors with significantly higher critical temperatures. In that year, $La_{2-x}Ba_xCuO_4$, the first HTS, was discovered [2], and that discovery was soon followed by $YBa_2Cu_3O_{6+\delta}$ in 1987 [3]. $YBa_2Cu_3O_{7-\delta}$ has a T_C greater than 77 K, which made superconductivity obtainable through the use of liquid nitrogen. Unlike the simple conventional superconductors, HTS have complex layered structures (layered perovskite structures).

Superconductivity in the Hg-based cuprate family having the generic formula $HgBa_2Ca_{n-1}Cu_nO_{2n+2}$ ([Hg-12(n-1)n], Hg-Ba-Ca-Cu-O, HgBCCO) was first reported in 1993 [4] for the $n = 1$ compound (Hg-1201). Shortly thereafter, a record high T_C of 133 K was reported for the $n = 3$ compound (Hg-1223) under ambient conditions [5]. Subsequently, it was found that T_C values in excess of 150 K could be induced in the Hg-1223 by the application of a high pressure [6]. Within the next year, compounds covering the full composition range $n = 1$ to 8 were reported [7-10].

2.1 Crystal structure of high temperature superconductors

All the superconducting phases of the $Hg_1Ba_2Ca_{n-1}Cu_nO_{2n+2}$ system crystallize with a tetragonal cell having the symmetry of the space group P4/mmm. The a-parameter is ~ 0.35 nm and the c-parameters of the various phases follow the formula c ~ 0.95 + 0.32 $(n-1)$ nm, n is the number of Cu-O planes in the structure.

Hg-phase	a, b (nm)	c (nm)
Hg-1201	0.3874	0.9505
Hg-1212	0.38425	1.26007
Hg-1223	0.38438	1.57329

Tab. 1 Cell parameters of some phases of the Hg-based superconductors.

The crystal structures are based on the layer sequence:

$$... \{(BaO)\,(HgO)\,(BaO)\,(CuO_2)\,[(n-1)\,(Ca)\,(CuO_2)]\}\,(BaO)...$$
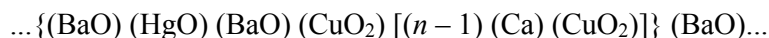
The blocks (BaO) (HgO) (BaO) have the rock-salt structure with a thickness about 0.55 nm (insulating block) and alternate with blocks $(CuO_2)\,[(n-1)\,(Ca)\,(CuO_2)]$ which have a perovskite-like structure with an approximate thickness of $[0.4 + 0.32(n-1)]$ nm (conducting blocks) (Fig. 7).
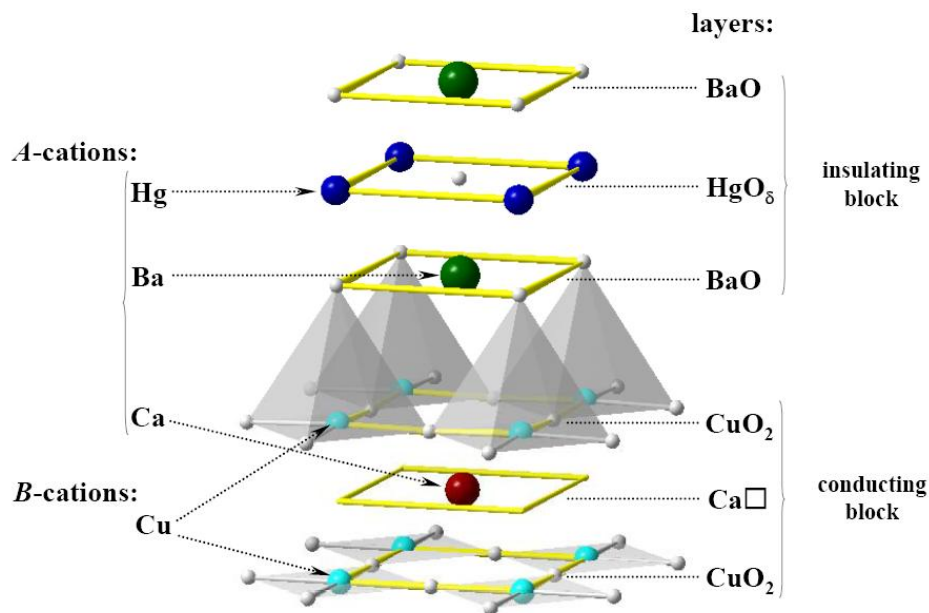
Fig. 7 Stacking sequence of the layers along the c axis for the crystal structure of the $Hg_1Ba_2Ca_{n-1}Cu_nO_{2n+2}$ ($n = 2$).

$Hg_1Ba_2Cu_1O_4$ $Hg_1Ba_2Ca_1Cu_2O_6$ $Hg_1Ba_2Ca_2Cu_3O_8$
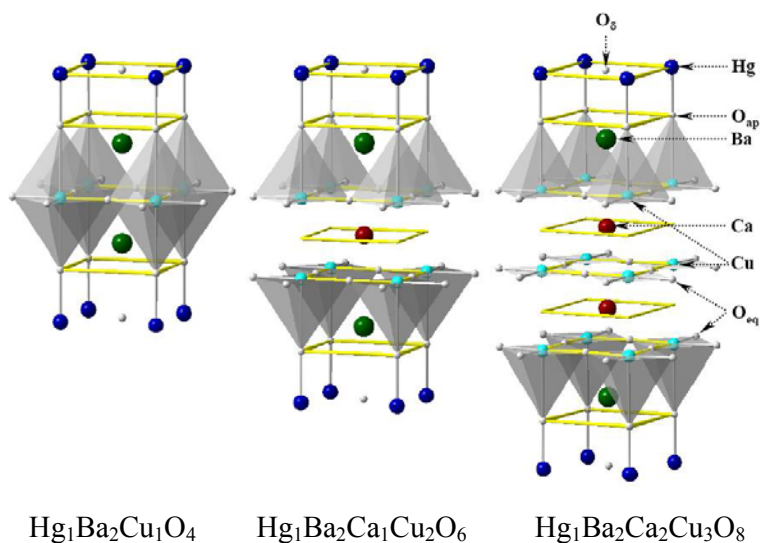
Fig. 8 Crystal structure for the $Hg_1Ba_2Ca_{n-1}Cu_nO_{2n+2}$ ($n = 1, 2, 3$)

The Hg-based superconductors have some structural features which are common for all superconducting cuprates [11]:

a) The copper-oxygen layer (CuO_2) is the main structural unit responsible for the appearance of the superconducting properties.

b) For the appearance of the superconductivity the formal copper valence should be in the range of +1.8-1.9 or +2.05-2.25.

c) For the appearance of the superconductivity the Cu-O distance should be in the 0.188-0.197 nm range.

The crystal structure of the members of homologous series, $Hg_1Ba_2Ca_{n-1}Cu_nO_{2n+2}$ is similar to the other high temperature superconducting cuprate systems [12]. The structure of the Hg-based superconductors is isomorphous to the single layer Tl-based superconductors $Tl_1Ba_2Ca_{n-1}Cu_nO_{2n+2}$ [13-15]. The main difference between the Tl and Hg analogues is that the oxygen occupancy in the Hg layers is only partial, with Hg being only 2-coordinated, whereas in the Tl compounds, Tl is 6-coordinated. The significant oxygen deficiency results in the relative instability of the Hg-based superconducting materials. The partial substitution of Hg by any of several dopants such as Re, Pb, Bi and Cr with a higher valance improves the stability of the Hg layer which facilitates the synthesis. The dopants, being in a higher valance state than Hg, pull additional oxygen atoms into the Hg/M layer, stabilizing the structure [16-20]. For example rhenium atoms in the $(Hg, Re)_1Ba_2Ca_{n-1}Cu_nO_{2n+2}$ (n = 2, 3, 4) substitute at the Hg sites and alter the defect structure of the host layer by pulling in four oxygen atoms to form octahedron around Re [16].

The existence of an extra oxygen anion in the (HgO_δ) layer is one of the specific features of Hg-based cuprates crystal structure. This anion is weakly connected to adjacent Hg^{2+} and Ba^{2+} cations thus opening a possibility to change δ over a wide range. The highest T_C corresponds to the so-called optimal value of δ (δ_{OPT}). Above δ_{OPT}, an increase of oxygen content leads to the T_C reduction. Therefore, each particular sample, depending on its δ value may be either in underdoped, optimally doped or overdoped state. The dependence of the critical temperature on the oxygen content in the Hg-based superconducting phases is shown in the Fig. 9 [21].
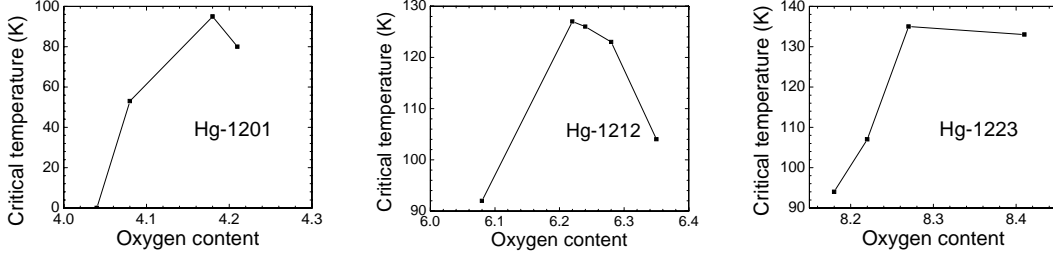
Fig. 9 Dependence of the critical temperature on the oxygen content in the Hg-based superconducting phases.

Intergrowth structures are typical feature of some HTS having the homologous series ($Bi_2Sr_{2-x}La_xCaCu_2O_{8+\delta}$, $Tl_mBa_2Ca_{n-1}Cu_nO_{2n+m+2}$, $Hg_1Ba_2Ca_{n-1}Cu_nO_{2n+2}$). They are built of different structural units (blocks), alternating along the longest period of the unit cell: a perovskite block with superconducting (CuO_2) layers, a rock salt block and/or a fluorite block. The number of the (CuO_2) layers (n) may vary from 1 to 6. If $n \geq 2$, oxygen-depleted cation layers are placed between them. Other insulating layers provide conditions for the stability of the structure compensating the negative charge of the perovskite block, and in particular create the necessary carrier concentration in the conducting band. Their positive charge can be smoothly tuned by a heterovalent substitution or a variation of the oxygen content [11].

The structure of the Tl-based superconductors is very close to the structure of Hg-based HTS and intergrowth structures of TlBCCO compounds was better explored than in the case of HgBCCO. It has been reported that during synthesizing the Tl-based compounds, the $(Tl-O)_2$ bilayer structures are former prior to the monolayer structures regardless the nominal composition [22, 23]. For example, for the Tl-1223 nominal composition, Tl-2223 is first formed and transits to a mixture of Tl-2223 and Tl-1223. This procedure is followed by a formation of the pure Tl-1223 under suitable annealing conditions.

Zhang *et al.* have reported that two intermediate structures between the ideal Tl-Ba-Ca-Cu-O structures [24]. The first structure is based on the Tl-2212 structure but a high density of Tl-deficiency exists in the Tl-O layers (up to 30 %). The second intermediate structure was formed by the ordered *c*-axis intergrowths between the basic phases such as Tl-1223 and the Tl-2223. There are various combinations between the basic phase slabs, resulting in different super periods and symmetries. The average composition of the newly formed phases can be written as $Tl_{1\pm x}Ba_2Ca_2Cu_3O_y$. These new phases have their own structural and superconducting characteristics from which the phase can be defined as

intermediate states between the ideal Tl-based phases. Both types of intermediate structures are closely related to the Tl loss during the processing [24]. Hopfinger *et al*. [25] detected and identified several intergrowth phases between Tl-1223 and Tl-2223 in a non-equilibrium sample with composition $Tl_{1.5}Ba_2Ca_2Cu_3O_y$ prepared by solid-state reaction in a closed system. They suggest that the presence of ordered intergrowth phases in non-equilibrium samples indicates that the transformation from Tl-2223 to Tl-1223 occurs by a progressive de-intercalation of TlO layers from Tl-2223 and also shows that these layers are removed in an ordered way. It appears to be favourable to remove one TlO layer every two, three or four double layers resulting in the formation of the 1:1, 1:2 and 1:3 intergrowth phases.

In many works, it has been reported that before the formation of Hg-1223, the Hg-1212 phase was observed, some authors also observed Hg-1201 phase before the formation of Hg-1212 [7, 26, 27]. In analogy to the Bi-HTS for which the mechanisms of the phase formation have been investigated extensively, two general mechanisms are conceivable also for Hg-HTS [28]: (1) Formation of Hg-1223 (Hg-1212) via intercalation of $CaCuO_2$ double layers into Hg-1212 (Hg-1201); (2) Formation of Hg-1223 via nucleation and growth of this phase. The Hg-1201 and Hg-1212 phases which appear in earlier stages of the synthesis are assumed to dissolve in the later stages and eventually to form liquid phase. Wu *et al*. [29] found that the mechanism for phase formation in the Bi-based HTS depends strongly on the precursor.

Influence of Re doping on the phase formation of Hg-1223 was studied by Reder *et al* [28]. Based on the TEM and XRD analyses, they propose the following model for the formation of the Hg-1223 phase: Already during the heating of the precursor material, nuclei of Hg-1201 develop after the decomposition of HgO. These nuclei compete with the also forming $CaHgO_2$ phase for the free Hg. By Re doping, the formation of $CaHgO_2$ can be reduced strongly enough so that the Hg-1201 development is promoted. Besides planar growth of the Hg-1201 grains, sometimes spiral growth around screw dislocations also takes place. At the latest when all available Hg is incorporated in Hg-1201 grains, the intercalation of Ca, Cu and O into these grains starts which transform them into Hg-1212. By further intercalation, the Hg-1212 grains transform into Hg-1223. Incomplete intercalation due to local lack of Ca and Cu or due to stress fields because of the expansion in the *c*-direction lead to the remaining of many Hg-1212 stacking faults. The intercalation process can take place rapidly where Ca, Cu and O are available. The inhomogeneous distribution of Ca-Cu-rich phases leads to an inhomogeneous distribution of transformed grains at the beginning of the transformation. Especially in later stages of the phase formation, the movement of Hg-1212

stacking faults in the (001) direction towards Ca-Cu-rich neighbouring grains can also contribute to the phase transformation [28].

2.2 Properties of Hg-based superconductors

The superconducting properties of the $HgBa_2Ca_{n-1}Cu_nO_{2n+2}$ system are important for both fundamental and technological reasons. The superconducting properties are important in the efforts to elucidate the mechanism for the superconductivity in the oxides and, because the $n = 3$ compound has the highest T_C of all compounds. From the technological approaches for discovering the compounds with even a higher T_C. Furthermore, from the technological perspective, the T_C gives a preliminary 'necessary but not sufficient' indication of the potential utility of a superconducting material.

The magnetic properties of $HgBa_2Ca_{n-1}Cu_nO_{2n+2}$ have been also studied extensively in the context of the surface versus the bulk pinning. It has been shown that both the Hg-1212 and the Hg-1223, in the as-grown condition, can be dominated by the surface pinning [30-32]. When bulk defects are subsequently introduced by the neutron irradiation, the bulk contribution to the flux pinning improves, while the surface-pinning contribution is destroyed.

The irreversibility line of the undoped and the doped $HgBa_2Ca_{n-1}Cu_nO_{2n+2}$ shows the highest values of the irreversibility field at a high temperature of any known superconductor. Interestingly, it is strongly dependent upon dopants, which is important from both fundamental and technological point-of-view. Consistent with the model that the irreversibility field as a function of the normalized temperature is inversely proportional to the separation between the CuO_2 layers, the H_{irr} versus T/T_C was shown to be above that of the Bi-Sr-Ca-Cu-O double layer compounds, but below that for the Y-Ba-Cu-O [33]. Owing to the record T_C, however, the absolute value of $H_{irr}(T)$ is as high as the Y-Ba-Cu-O around 77 K, and above it for higher temperatures [34]. These early reports estimated H_{irr} (77 K) = 2 T for the Hg-1212 and the Hg-1223 and about 0.5 T for the Hg-1201 [33-35]. Similar conclusions were obtained in the Pb-doped Hg-1223 [36].

Efforts to improve the irreversibility field of $HgBa_2Ca_{n-1}Cu_nO_{2n+2}$ have been both chemical and nuclear. An early report from the University of Tokyo showed that the magnetization hysteresis of the Hg,Re-1223 remained open up to 12 T at 77 K [37]. Although these values have not been confirmed, a significant improvement in the critical current density, depinning activation energy and irreversibility line in the Hg-1212 and the Hg-1223

thin films by Re and Mo doping have been demonstrated [38]. These films showed 77 K irreversibility fields around 6 T as obtained by transport measurements. As the transport is often limited not by the magnetic behaviour but by the phase purity and intergranular connectivity, the actual irreversibility field may be higher. It has been proposed that improvements from the dopants may be inherent and related to the metallization of the blocking layers [32].
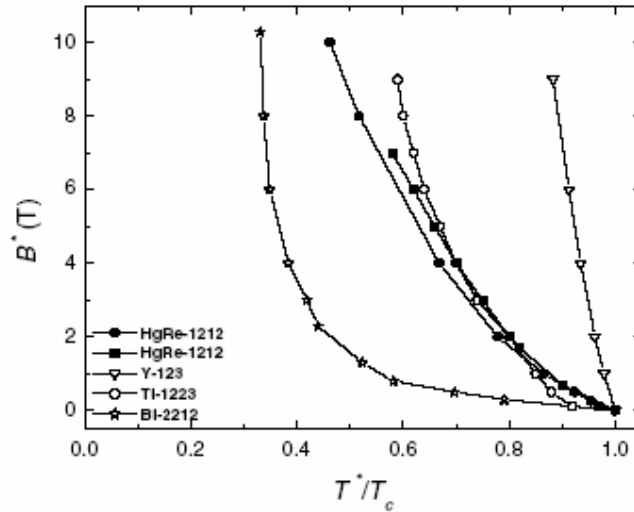
Fig. 10 Irreversibility field B^* as a function of reduced temperature T^* / T_C with the magnetic field oriented parallel to the c-axis for different HTS [39].

The initial discoveries of the superconductivity in the $HgBa_2Ca_{n-1}Cu_nO_{2n+2}$ sparked a flurry of the activity to increase the T_C to new record-high values. A successful approach that significantly increased the T_C of the Hg-1201, Hg-1212 and Hg-1223 was the application of the hydrostatic pressure during the T_C measurement [6, 40-44]. Ultimately, T_Cs of the Hg-1201, Hg-1212 and Hg-1223 reached 118, 154 and 164 K, respectively. Although the pressure is not practical for applications, it demonstrates a great potential of the $HgBa_2Ca_{n-1}Cu_nO_{2n+2}$ and high temperature superconductors in general.

2.3 Applications of high temperature superconductors

Traditionally, low temperature superconductors (LTS) have been used most commonly in applications that require large magnetic fields. The discovery of high temperature superconductors (HTS) in 1986 widened considerably the range of potential applications for

superconducting materials in the electric power and electronic industries. The use of the LTS in electric power applications, in particular, has been driven principally by their successful application in magnetic energy storage units. In these, the LTS is a true enabling technology that allows the protection of sensitive electric machines or even an entire facility from the adverse effects of poor power quality. The most recent discovery of MgB_2 opens up a potential for further application of the superconductivity.

In general the HTS are available in three forms: a bulk, thin films and wires or tapes (LTS are not used practically in the bulk form). Of these, bulk materials have a potential to generate large magnetic fields that are much greater than those achievable with conventional permanent magnets. Thin films have the potential for the use in high-speed electronics, logic and microwave circuits where sharp bandwidth characteristics are required. Wires and tapes have a potential for use in transmission cables, electric rotating machinery and transformers as a more efficient and more compact replacement for copper technology.

Some of applications of superconducting materials are described below.

Electromagnets can be divided into three classes: (1) dissipative windings surrounding a ferromagnetic core; (2) dissipative windings with air cores; and (3) superconducting windings usually with air cores but possibly with ferromagnetic cores. Superconducting electromagnets are partially built from superconducting materials and therefore reach much higher magnetic field intensity.

Current leads are probably the first high-current application of the HTS to be widely used on a commercial basis. In many cases, the HTS current leads enable applications that would be very difficult using conventional technology. Many superconducting devices, for example magnet systems, require the supply of a high current (ranging from tens to tens of thousands of amperes). The current must be transmitted from the room temperature to an operating temperature of the device, typically in the region of 4 K for the LTS and 20 – 80 K for the HTS devices.

AC and DC power transmissions – The early work on superconducting transmission cables using the LTS Nb_3Sn tape although highly successful was not practical due to the use of the liquid helium. As a result, the electric power sector did not seriously consider the installation of these LTS cables. The discovery of the HTS with the promise of the liquid nitrogen operation revitalized the interest for the superconducting transmission within the electric power industry. Superconducting transmission cables can provide two to five times the current transmission capability of a conventional cable with the same cable diameter.

Fault-current limiters – Fault currents are transient currents that flow through an electric power system when a short-circuit occurs. The majority of the ´sustained´ faults typically occur on a three-phase transmission system with one of the phases having a short-circuit to ground. Since most power networks are fed by relatively constant voltage sources through inducting circuits having a low impedance, fault currents exceed normal load currents by more than an order of magnitude, especially on the high-voltage transmission lines. The most common methods for handling fault current use air-core reactors, fuses and circuit breakers. An alternative to these devices is a fault-current limiter. The fault-current limiter (FCL), whether it employs a superconductor or not, is basically a variable impedance that is installed in series with a circuit breaker. During a fault the impedance of the FCL increases rapidly to a value (typically a fraction of an ohm of a distribution system and several ohms on a transmission systems) at which the fault current is reduced to a level that circuit breaker can easily interrupt. In the case of a typical superconducting FCL (SCFCL), a fault causes the device to switch from a superconducting, low-impedance state to a normal, high-impedance state. Use of the FCL is being considered for various applications within the power sector where the potential for large fault currents exists.

Most SCFCL concepts involve the switching of a superconducting element from the superconducting to normal state. A switching speed of several milliseconds would be fast enough to prevent a build up of large fault currents but slow enough to prevent large voltage spikes due to a stray inductance. Several LTS and HTS FCLs have demonstrated acceptable switching characteristics. For example Siemens has developed and tested a resistive FCL using YBCO thin films [45].

Energy storage and transformers – The prospect of using large superconducting magnets for energy storage follows directly from the expression describing energy stored in the magnetic field of an inductor which is simply, $E(J) = \frac{1}{2} L I^2$, where L is in henrys (H) and I the current expressed in amperes. The maximum energy for inductively stored power devices is, thus, dependent on the ability to carry very high currents. A superconducting coil with the ability to carry high currents without power dissipation is therefore, an attractive energy storage candidate.

Transformers consist of inductively coupled coils, of copper or other materials having low electrical resistance, wound around high permeability steel cores. In electric power applications, transformers are used to change voltage/current ratios; i. e. to step voltage up and current down to reduce long distance transmission losses or to step voltage down and current up for distribution and end use.

Microwave resonators and filters – The low surface resistance of the HTS directly translates into extremely high Q-values (Q-value is defined as the ratio of storage energy versus dissipated energy within a RF period) for resonant microwave devices. The orders of the magnitude increase of the Q-value is very attractive to the designers of resonators and filters. This is why resonators and filters have become the most active application for HTS microwave circuits. According to the structures, resonators can be classified into three categories: one-dimensional (transmission line type); two-dimensional (planar type); three-dimensional (cavity or bulk type). Filters can also be classified in the same way as resonators used as their building blocks.

Superconducting transmission lines can be of two types – superconducting coaxial cables and thin film microwave components. Much more widespread in modern electronics are the superconducting microwave microelectronic components. They are applied as interconnections in microwave integrated circuits (MIC), as a fundamental part of resonators and filters based on microstrip lines or coplanar waveguides (CPW), and as feeders in microwave planar antennas.

Josephson devices are active superconducting devices based on the Josephson effects. Josephson junction epitomize one of the most profound macroscopic quantum aspects of the superconductivity, while at the same time enabling a wider range of applications that any aspects of superconducting electronics. Some of Josephson devices employ also another fundamental quantum principle exemplified in superconductors: the magnetic flux quantization. The combination of these two effects has led to two rather different types of device for applications. The first is superconducting logic gates which have been realized in a number of different forms, the front runner for widespread application at the time of writing being rapid single flux quantum (RSFQ) logic.

The second major application device which combines both Josephson effects and flux quantization is the SQUID. In this case the device is an extremely sensitive measuring instrument which essentially determines changes in the magnetic flux applied to a ring of superconductor interrupted by one or more Josephson junctions. Almost any physical parameters may be measured with the extreme sensitivity by coupling a suitable transducer to the input to the SQUID. The Josephson junctions can be used also as mixers and electromagnetic radiation detectors. In general, this function relies on the extreme nonlinearity which is present in the current voltage characteristics of a Josephson or quasi-particle tunnel junction.

Optical sensors – Ultrafast phenomena, optoelectronics and superconductivity are acknowledged fields of technological importance, and a very large amount of research has been performed in these areas in recent years. In modern, highly advanced, digital electronic circuits, the primary function of a high-performance, high-speed signal processing is given to superconducting single-flux-quantum (SFQ) logical devices, based on resistively shunted Josephson tunnel junctions. The development of this branch of the digital electronic requires utrafast and ultrasensitive detectors for fibre optic interconnects between the outside world and the SFQ processor, which must be able to work at cryogenic temperatures and be technologically compatible with SFQ integrated circuits. The superconducting optical-to-electrical transducers can transport the input information coded in the form of a train of ultrafast optical pulses to the electrical domain and, subsequently, feed it into the ultrafast superconducting processor. Superconducting optical sensors also find applications in traditional areas of optoelectronics and infrared (IR) imaging.

Superconducting detectors become the most prominent technology for radiation sensors with an ultimate performance. Typically, they are nanostructures formed from an ultra-thin superconducting film incorporated into an external antenna for an efficient radiation coupling. The operation of so-called hot-electron bolometers and photodetectors (HEBs and HEPs) is based on a nonequilibrium heating of the electron subsystem by the absorbed radiation and results in the film resistance and a corresponding, easily measurable voltage response when the device is current biased. A relatively simple, single-layer manufacturing technology made these devices very popular for needs of the radioastronomy and remote sensing.

The value of the energy gap in a superconductor is two to three orders of magnitude smaller than that in a semiconductor, thus, a photon absorption in a superconductor creates a very significant avalanche of excited electrons. Due to this property, HEBs and HEPs demonstrate very high sensitivity in a broad spectral range from far-infrared to ultraviolet. Moreover, due to their cryogenic operating temperatures, the superconducting detectors are intrinsically low-noise devices.

3. Thin films

3.1 Thin film deposition technology

The deposition techniques for the thin films are more often divided according to the way of the transport and the deposition of the precursors on the top of the substrate.

Chemical vapor deposition (CVD) is the process of chemically reacting a volatile compound of a material to be deposited, with other gases, to produce a nonvolatile solid that deposits atomistically on a suitable placed substrate. This method allows a preparation of the large variety of films and coatings of metals, semiconductors, and compounds in either a crystalline or vitreous form, possessing high purity and desirable properties. It is possible to control the stoichiometry. The CVD could be divided to these reaction types: pyrolysis (thermal decomposition), reduction, oxidation, compound formation, disproportionation and reversible transfer.

Physical deposition is the process where atoms are transferred from a source to a substrate in which the film formation and growth proceed atomistically. All these techniques involve the vacuum which facilitates the transport of the particles from the source on the substrate by decreasing the probability of their collision with the molecules of the atmosphere. The most used techniques for the thin film deposition are thermal evaporation, laser ablation and sputtering.

Epitaxy is the phenomenon of the oriented growth of one substance on the crystal surface of a foreign substance. Because of the anisotropy of the superconducting properties of the Hg-based superconductors the epitaxy of the thin Hg-based films is a very important feature. The oriented growth of the material over itself is termed a homoepitaxy (or auto-epitaxy), and over another material a heteroepitaxy (or simply epitaxy). It is clear that the heteroepitaxy changes over to the homoepitaxy when films are thick enough for the initial substrate to have no orienting influence. Because of the anisotropy of the perovskite structures which are typical for the superconducting cuprates, only a very high degree of the texture in all three dimensions induces the high performance of high-temperature superconductors, therefore, the film deposition is focused on the epitaxy.

3.1.1 RF magnetron sputtering

In sputtering the atoms are sputtered from the surface of a target by bombardment with energetic particles (electrons or ions) and then condensed on the top of the substrate. For convenience we divide sputtering processes into four categories: (1) dc, (2) RF, (3) magnetron, (4) reactive. Several variants exist within each category (e. g. dc bias) and even hybrids between the categories (e. g. reactive RF).

The classical sputter technologies range from the simple DC glow discharge sputtering restricted to conducting target, to the pulsed DC sputtering (typically at 10-200 kHz) preferentially used for the reactive sputtering and to the RF (13.56 MHz) sputtering where even non-conducting target can be sputtered. Various cathode concepts and shapes can be used: planar or hollow cathodes, cylindrical and rectangular cathodes, triodes or even ion beam guns. A further classification of the different technologies into the on-axis and the off-axis sputter deposition is defined by the geometrical arrangement of the cathodes with respect to the substrates. Finally, sputter yields can strongly be enhanced by the use of magnetron assisted targets.

Magnetron sputtering is when the power is supplied to a magnetron and a negative voltage of typically -300 V or more is applied to the target. This negative voltage attracts and accelerates positive ions to the target surface.

RF sputtering was invented as a means of depositing insulating thin films. The ionization can occur in an inert gas or in a mixture of an inert with a reactive gas.

When the AC voltage is applied to the electrodes at a low frequency (< 50 kHz), ions establish a complete discharge at both electrode on each half-cycle. Direct current sputtering conditions essentially prevail at both electrodes, which alternately behave as cathodes and anodes. At high frequency (> 50 kHz), two important effects occur. Electrons oscillating in the glow discharge acquire enough energy to cause ionization, reducing the need for secondary electrons to sustain the discharge. Secondly, RF voltages can be coupled through any kind of impedance so that the electrodes need not to be conductors. This makes it possible to sputter any material irrespective of its resistivity. Typical RF frequencies range from 5 to 30 MHz. 13.56 MHz has been reserved for plasma processing and is widely used.

RF sputtering essentially works because the target self-biases to a negative potential, it then behaves like a DC-target where positive ion bombardment sputters away atoms for subsequent deposition. Negative target bias is a consequence of the fact that the electrons are considerably more mobile that ions and have little difficulty in following the periodic change

in the electric field. The disparity in electron and ion mobilities means that isolated positively charged electrodes draw more electron current than comparably isolated negatively charged electrodes draw positive ion current. For this reasons the discharge current – voltage characteristic are asymmetric (Fig. 11).
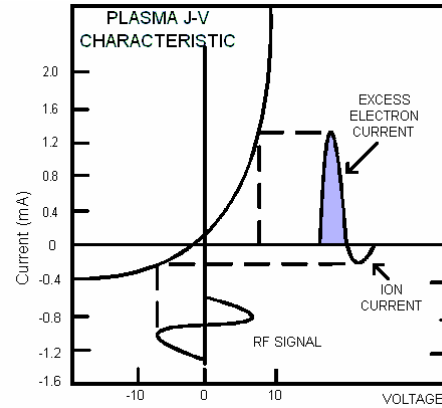
Fig. 11 Formation of pulsating negative sheath on capacitively coupled cathode of RF discharge. Net current/zero self-bias voltage.

Planar magnetron sputtering with an RF potential applied on the cathode (usually 13.56 or 27 MHz) enables the use of nonconducting materials as targets and allows direct or reactive deposition of dielectric films in the same manner as conventional sputtering.

Sputter deposition has been often used for preparing thin films of alloys and complex materials. It was the natural methods to try when the HTS materials were first discovered. However, the problem of resputtering (due to oxygen ions generated in the plasma) was recognized in this class of materials some 18 years before the discovery of the YBCO for $Ba(PbBiO_3)$ deposition [46] and has been thoroughly investigated later [47]. A method to avoid this problem is to thermalize the energetic species either by working at high pressure (which also provides a particularly oxygen-rich environment) or by „off-axis" sputtering at a modestly high sputtering pressure which forces all atoms emanating from the target to undergo a few energy-reducing collisions before approaching the substrate.

Several combinations of different techniques using fully oxygenated stoichiometric targets have been studied, i. e. off-axis techniques using a cylindrical magnetron [48], magnetrons facing the target [49] or a single magnetron [50], and on-axis techniques using non-magnetron sputtering at very pressure [51]. Furthermore, the cathodes can be charged with dc, RF (13.56 MHz) or MF (medium frequency ranging from 20 to 200 kHz) power or combination of these [52].

The sputter deposition process of the HTS material is usually divided into three different parts. In the first part (pre-sputtering), the target is slowly energized, a shutter between the target and the substrate is closed, and the substrate is also slowly heated up to the deposition temperature. When the substrate temperature and the power at the cathode has reached the deposition parameters the second part, i. e. the actual deposition, is started by opening the shutter. The exact choice of the preparation parameters strongly depends upon the sputtering device (size, geometrical arrangement and sputtering mode). The process is terminated by the third part, i. e. the cooling down of the deposited HTS film. During this part of the process the oxygen content of the superconducting film is usually established *in situ*. This can be achieved by applying oxygen at high pressure (standard process, at 10^5 Pa) or alternatively by entering activated oxygen at low pressure [53]. Although the standard process is certainly easier to handle, the alternative process has advantages for sputter deposition (activated oxygen can be generated by the sputter source) and large area deposition (avoidance of the local overheating of the film), it is very reproducible, can be applied to complex high quality multilayers with top- or interlayers, through which oxygen transport is difficult (e. g. dense $NdGaO_3$ top-layers), and it can be integrated more easily into complex or automated preparation process since it is a low pressure procedure.

In conclusion, the different sputter techniques are usually highly reproducible. Advantages of these typically single target deposition techniques are tat they are compatible with high pressures and the use of reactive gas components, and both calibration and rate control are readily obtainable. The presence of plasma can be a great advantage for the process. For instance oxygen can be activated which can make the oxygenation of the HTS thin films very easy. Homogenous composition can be obtained over a rather large area (typically 2.5-5 cm for off-axis sputtering and 10 cm for on-axis sputtering). Recently, a large area deposition was tested with 70 cm long planar cathods [54]. However, it seems to be inherently slow (typically 20-300 nmh^{-1}) due to either off-axis geometries or high levels of thermalization. Higher rates can be achieved by modification of the magnetron (dual magnetrons) or pulsed-DC deposition [52] by which rate could be increased to 1.2 µmh^{-1}. Nevertheless, sputtering has been widely used for the deposition of compounds (e. g. nitrides or oxides) comparable to HTS material as the workhorse technique because it is reliable, cheap and relatively easy to run automatically or semiautomatically and can be scales up to areas larger than 1-3 m. Furthermore, although the presence of a plasma and high deposition pressures hamper the use of most in situ characterizations such as low energy electron diffraction (LEED) or reflection high energy diffraction (RHEED), superlattices and

multilayer HTS thin films have been grown with various sputter techniques [55-58] as well as multilayer heterostructures involving e. g. HTS and magneto-resistive compounds [59]. RHEED can be performed at rather high pressure and is used to follow *in situ* deposition.

3.2 Substrate

The nature and termination of the substrate are extremely important because they greatly influence the properties of the films deposited onto them. Glass, quartz, and ceramic substrates are commonly used for polycrystalline films. Single-crystal substrates (for example sapphire, MgO, $LaAlO_3$ etc.) are used for epitaxial growth. In many cases the substrate does not consist of only one material, but of the main substrate coated with one or several different buffer layers. Different aspects have to be taken into account for the right substrate selection for the superconducting films:

- chemical compatibility
- thermal expansion
- lattice mismatch.

Chemical compatibility – The substrate must be widely inert at the typical deposition conditions of an oxygen-rich ambient atmosphere and high temperatures (650 – 850 ºC). In principle, oxide substrates like $SrTiO_3$, MgO or $LaAlO_3$ are more suitable than metal substrates. It is very important to have no interdiffusion between the substrate and HTS film. An interdiffusion can be avoided if the buffer layers, which do not react with the HTS films, are deposited on the bare substrate. Using oxide buffers like CeO_2, YSZ, MgO, Y_2O_3 or $SrTiO_3$, the HTS films can also be deposited on metals, silicon and sapphire with high J_C values above 1 $MAcm^{-2}$.

Thermal expansion – Because of both the high deposition temperature and the low superconducting transition temperature the difference in the thermal expansion across this temperature range between the substrate, the HTS film and, eventually, additional buffer layers plays a significant role for the choice of the substrate-film combination. If the thermal expansion coefficient of the film exceeds that of the substrate, the film will be in a tension, in the opposite case it will be in a compression. The tensile stress is more critical for ceramic materials.

Lattice mismatch – is the origin of the defects in the buffer layer and in the film (dislocations, islands, etc.) on the growth of the film. For HTS the best properties can only be

reached if the texture of the HTS films is as high as possible. Therefore, an epitaxial growth on single crystalline or very highly textured substrates is desired. The crystallographic structure of the substrate surface or of the surface of a buffer layer on the substrate plays the most important role. The surface atoms should match with the atoms of the first HTS layer. For good superconducting properties HTS films should grow c-oriented (the substrate surface is oriented parallel to the a-b plane of the orthorhombic HTS structure) and also oriented in the a-b plane. The value of the lattice mismatch is defined as $\varepsilon = \{a(\text{film}) - a(\text{substrate})\} / a(\text{substrate})$, where a is the cell parameter.

The surface quality of the substrate is especially important because the film growth is very sensitive to the initial film-substrate interaction. Careful mechanical or chemical polishing (or a combination of both) removes macroscopic defects and creates a smooth substrate surface.

3.2.1 Choice of the substrate and buffer layer

Sapphire (α-Al_2O_3) is an important crystal because of its combination of excellent optical and mechanical properties. It is a material of great technological importance since it is most commonly used as a substrate in a number of solid state devices. The sapphire is a good electrical insulator, and it has a high thermal conductivity, high chemical stability and considerable strength. The sapphire has a hexagonal structure and is highly anisotropic material, with properties that are largely dependent on the crystallographic orientation. The melting point of the sapphire is 2040 °C, and it has an extremely high chemical stability even at high temperatures. The sapphire's energy gap of 9.1 eV is one of the largest for the oxide crystals, which permits an excellent optical transmission with a very little absorption from about 0.250 to 5.0 μm. The sapphire is the material of choice for stringent optical applications involving an exposure to high stresses and harsh environments. The sapphire is one of the strongest and hardest materials available; it has an excellent abrasion resistance and exceptional thermal shock properties. The hardness of the sapphire on the Mohs scale is 9, compared to 10 for the diamond. The strength of the sapphire largely depends on the surface finish quality and the subsurface damage caused by manufacturing processes. The selection of appropriate polishing techniques and heat treatments significantly improves the strength of the sapphire that must be larger than 400 MPa for technical applications.

The typical orientations of the sapphire single crystal are illustrated in the Fig. 12. The summarization of the characteristics of the sapphire is in the Annexe A (A1).
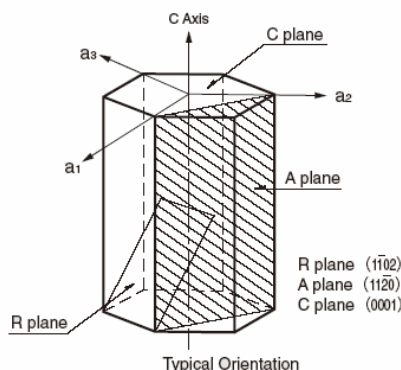
Fig. 12 Unit cell of the sapphire.

The R-plane sapphire is often used as a substrate for the preparation of the thin films of the high temperature superconductors. Since the lattice mismatch between the sapphire and the Hg-based superconductor is about 20 %, an appropriate buffer layer must be used for growth of the epitaxial films.

Lanthanum aluminate $LaAlO_3$ (LAO) has received much attention due to its promising use as a substrate for the high-temperature superconductors and as a filter material in microwave applications. It has a rhomboedral structure, but become pseudo-cubic at high temperatures in a slightly distorted cubic structure. The single crystalline LAO of a permittivity about 24 shows favourable electric, structural and thermal properties combined with high quality factors of the order 10^5 (10 GHz, 77 K).

For the preparation of the HTS thin films the single crystalline (001) LAO is used. Due to the low lattice mismatch between the LAO and HTS ($\varepsilon = 1.4$ %) no buffer layer is needed to.

Buffer layer must be used when the mismatch between the substrate and the thin film is more than 10 %. The list of some appropriate buffer layers with calculated lattice mismatches to the sapphire and to the mercury superconducting phase Hg-1212 is in the Annexe A (A2). The figures of the basic structural types of the materials appropriate for the buffer layers are in the Annexe A (A3).

CeO_2 is an attractive choice for several reasons: it is stable at high temperatures, it has a small lattice mismatch with both, the R-plane sapphire and the HgBCCO and a high dielectric constant, $\varepsilon_0 = 20$. It is also chemically inert to the sapphire and HgBCCO

superconductors. The unit cell compatibilities between the CeO_2 and the R-plane sapphire are illustrated in the Fig. 13.
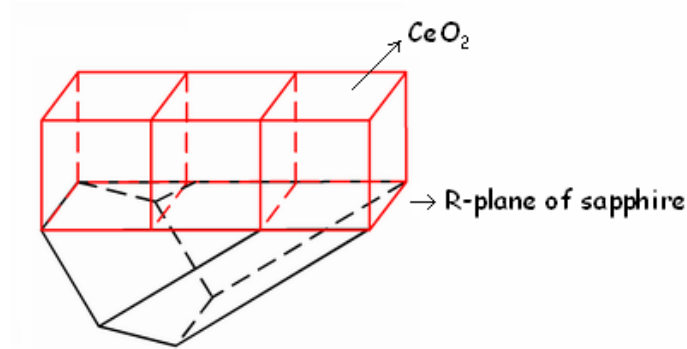
Fig. 13 Schematic of the unit cell compatibilities between the CeO_2 and the R-plane sapphire.

3.3 Patterning of thin superconducting films

To use the thin superconducting films as devices they should be patterned into structures. We distinguish two types of HTS circuits. The simplest are passive microwave devices, which are made by patterning a single superconducting layer and adding normal metal contacts. This technology is in the development process in several industries. Active circuits incorporating Josephson junctions (e. g. SQUIDs and single flux quantum (SQL) logic circuits) require much more complex processing. Successive superconducting layer need to be grown and patterned but interleaved with insulating layers, while maintaining the epitaxy and oxygenation in all the layers. This multilayer circuit technology, particularly Josephson junctions, is much less advanced, and deeper understanding of the processing mechanism is needed if progresses are to be made.

Lithography enables to transfer a specific pattern to the surface of a wafer. The basic aspects of photolithography processes are outlined schematically in the Fig. 14.

A radiation sensitive material, called resist, is coated onto the wafer to record the pattern. Regions of the resist are exposed to the radiation according to the desired pattern (in the photolithography, the radiation is UV light, and the pattern is transferred from the mask). The radiation interacts with the resist to change its chemical or physical properties. Following exposure, the resist is developed to remove the desired regions of the resist. The positive resist remains on the wafer after the development if it has not been exposed; the negative resist remains on the wafer if it has been exposed.
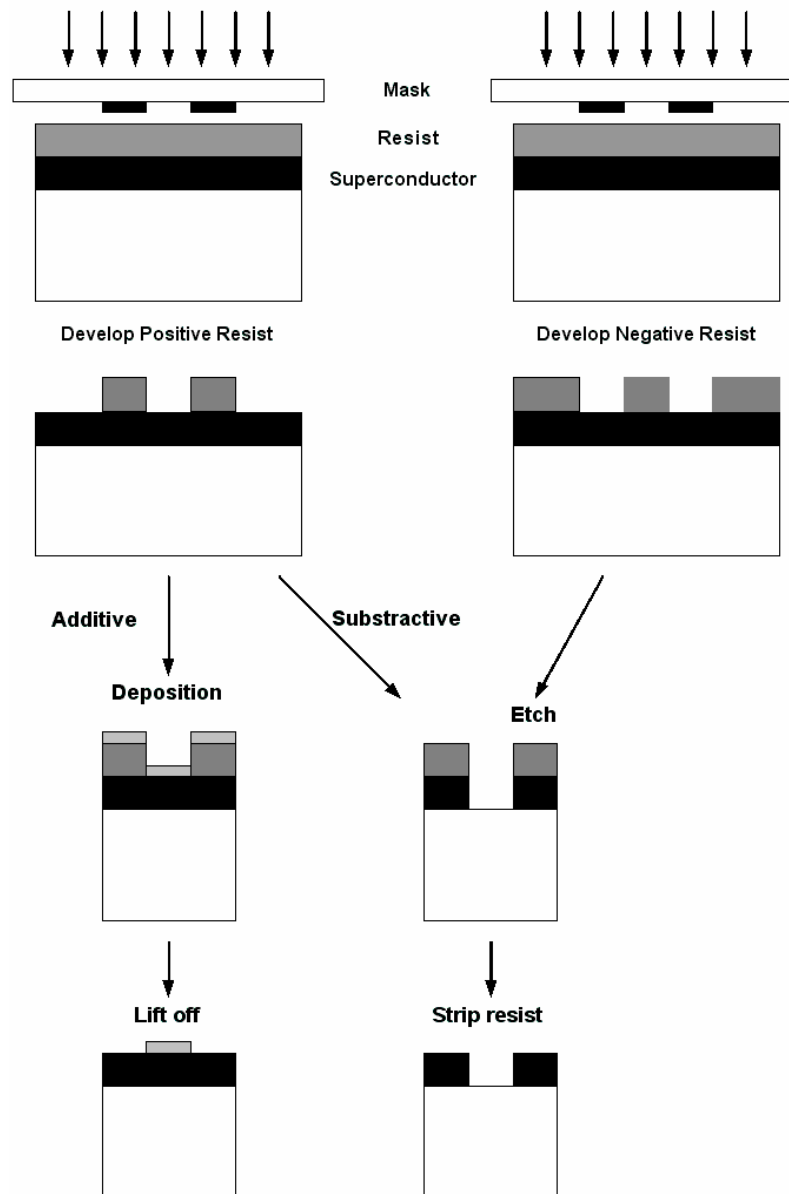
Fig. 14 Photolithography processes.

Once the resist pattern is formed it can be used in two ways. (a) The resist acts as a mask where the exposed superconductor is removed – it is called substractive litography or (b) a subsequent layer (e. g. a metal layer for contacting) is deposited through the resist mask. The resist is then dissolved away by a solvent, detaching the metal layer on the top of it. This leaves an inverse of the pattern of the wafer. This is called an additive lithography or a „lift off". The lift off can only be used with positive resists, as the negative varieties are very difficult to strip with liquid based processes.

The most widely used exposure system is light, usually in the UV region of the spectrum. This has the advantage that the process is a parallel one (i. e. a whole wafer, or at least a large fraction of it, is exposed simultaneously) resulting in a high throughput. However, there are higher resolution lithographic techniques which use beams of electrons or ions. These write the pattern serially (i. e. a point by point) and are comparatively slow.

Etching or subtractive patterning is the most common form of the lithography used for the semiconductor and the superconductor patterning. This is the most crucial stage in the patterning because an error at this stage cannot be undone, unlike the resist pattern.

The ideal process will etch the film uniformly at a controllable rate. The etchant should exhibit a high degree of selectivity i. e. it should etch the film but not the resist, any underlying film or substrate. It must be compatible with the edge slope defined by the designer. For example, the highest resolution demands vertical edges, but this is not possible for epitaxial films because of their anisotropic. The edge slope is controlled by the anisotropy of the etching process (Fig. 15). If the etching is isotropic i. e. the etching rate is the same in all directions, an undercut of the resist mask will result, leading to a loss in pattern resolution. With an etch process that etches in depth faster than laterally the replication of the pattern is better and the edge slope increase.

Fig. 15 Edge profiles obtained with isotropic to anisotropic etches.

Basically, etching mechanisms are either chemical, physical or a combination of both. The main techniques are:

- Wet etching
- Reactive ion etching
- Ion milling

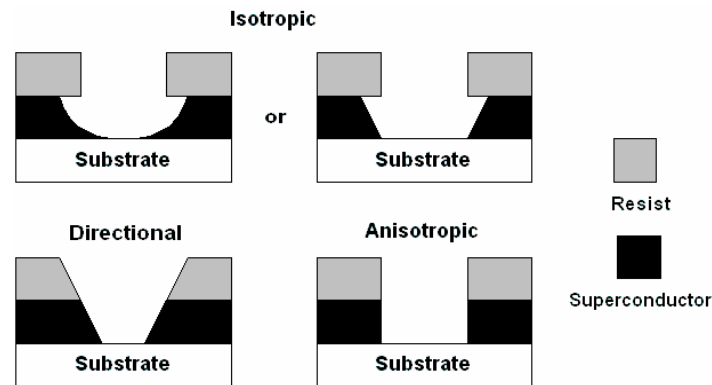*Wet etching* is a very simple and an inexpensive method. The superconductor is merely immersed in an etching solution for a predetermined length of time. In general, the cuprate superconductors are basic oxides and are etched by acid – base reactions. Then a good selectivity to resist is easy to achieve, as polymeric materials tend to be impervious to aqueous acids. However, superconducting cuprates are very sensitive to water and the process must avoid even minor chemical decomposition.

In the *reactive ion etching* (RIE), chemically reactive species are created in plasma and react with the layer being etched to form volatile compounds which are pumped away. In the *ion milling*, inert ions are accelerated by an electric field, and their kinetic energy is used to sputter atoms or molecules from the layer being etched. Using plasma combines often a mixture of both. RIE processes are highly developed for semiconductor circuits, and are used for low temperature superconductors, too. They are very attractive, as they cause a minimal damage to the active material, can be designed to be an anisotropic, and leave the surface clean, as all the reaction products are volatile.

The stability of the HTS films is a particularly important factor to take into consideration for the fabrication of microelectronic circuits. It generally necessitates a micro-patterning process for the fabrication of the desired superconducting structure. The most frequently used process for the patterning of the HTS materials involves photolithographic patterning which exposes the HTS material to photoresist, heat, developer and chemical etchants, all which may have determinal effects to the HTS material. Such a degradation would most likely reduce the performance and yield of the patterned device as well. This degradation is actually a common observation after the photolitografic patterning process of the HTS materials. Aytug *et al.* studied the response of Hg-based thin films to photolithographic process [60]. They found out, that after the treatment process of the photoresist material, the superconducting properties of the Hg-1212 samples are degraded as evidenced by a visible change in the surface terrace edges. However, there was no obvious surface contamination of the films observed after the etching in an acid solution of HCl / H_2O. Although the Hg-based superconductors are very promising materials for applications due to their high values of T_C, there is very few reports concerning the fabrication of the Hg-based devices. Tsukamoto *et al.* prepared high-performance (Hg,Re)-1212 grain-boundary Josephson junctions and DC SQUIDs on the $SrTiO_3$ bicrystals using a patterning by the electron-beam lithography and ion-beam etching [61, 62]. The junctions show RSJ-like properties close to the theoretical even at 113 K and $I_C R_N$ products of 400-460 μV at 77 K, which have a great potential for the use in the development of Josephson devices such as

SQUIDs with high operating temperatures above 100 K. Inoue *et al.* fabricated (Hg,Re)-1212 bicrystal junctions on the STO (001)-tilt symmetric bicrystal substrates with misorientation angles of 5-45° [63]. They observed a monotonical decrease of the J_C values with an increase in θ from 0 to 24°. For the higher values of θ (24-45°) the J_C values were almost identical. Another way of the fabrication of the Hg-based superconducting structures was presented by Aga *et al.* [64]. They prepared Tl-based films which were patterned using the standard photolithographic process and wet etching. The as prepared structures were mercurated using the Tl-Hg cation exchange process. This method avoided direct moisture exposure of the Hg-1212 films and therefore minimized the postsample degradation after the device is fabricated.

III. Present state of status of ongoing research

Etat de l'art des recherches

Ce chapitre est axé sur les difficultés générales de synthèse des cuprates de mercure. On décrit les procédés de préparation de ce composé sous forme volumique, de couches minces et aussi des couches épaisses et de rubans.

Synthesis methods of Hg-based superconductors

The superconductor family $HgBa_2Ca_{n-1}Cu_nO_y$ (n = 1, 2, 3...) has been intensively studied since its discovery in 1993 [4]. The n = 3 member of this Hg-superconductor series has the record T_C of 135 K at ambient pressure [5] and under high pressures a T_C of 160 K may be reached (around 30 GPa) [6]. Such material may display current densities as high as 10^6 Acm^{-2} at 77 K and 10^5 Acm^{-2} at 110 K and 1 T [65]. Irreversibility fields above 5 T at 100 K can be also achieved [66]. These characteristics demonstrate the high potential that these superconductors have. The synthesis process of mercury superconductors is very complex because of the high Hg vapour pressure which requires a preparation of the materials in confined vessels avoiding the loss of Hg vapours. The ceramic materials are usually prepared either at high pressures (0.1-7.5 GPa) or by means of the sealed quartz tube technique (< 5 MPa).

The preparation of the films (thin and thick) usually consists of two steps: (a) a deposition of the precursor phase and (b) a mercuration process using a source of Hg vapour within the same closed tube.

Superconducting materials exist in three different forms for the applications: ceramic materials (bulks), thin films and tapes. The synthesis of every form of the superconductor is different and will be explained below.

1. Bulk synthesis

The main difficulty in the synthesis of Hg-based superconducting ceramic is the loss of mercury at low temperature by evaporation. The mercury oxide, which is used in all

synthesis of Hg-based compounds, decomposes into metallic Hg vapour and oxygen above 460 ºC. Thus, to avoid the loss of stoichiometry, the synthesis of these compounds has to be carried out in closed vessels or in high pressure chambers. Basically, two different processing routes may be followed to prepare the raw materials for the superconducting synthesis: (a) a direct method [8] and (b) a two step method [67]. The direct method consists of the preparation of a green pellet containing a mixture of the stoichiometric simple oxides required to form by reaction the superconducting phase. In the two step method, a multiphase compound corresponding to the stoichiometry $Ba_2Ca_{(n-1)}Cu_nO_x$ is prepared at first starting from nitrates, carbonates or oxides. This first step is very important to control because it has a strong influence on the formation of the superconducting phase [68, 69]. Then, the precursor multiphase powder is mixed in a stoichiometric form with the required HgO and pelletized. Moreover, the binary precursors used for the synthesis are very sensitive to the atmospheric CO_2 and moisture. Therefore it is necessary to handle the materials in a controlled atmosphere to avoid the exposure to air. In addition, it is necessary to pay attention and maintain safety procedures due to the toxicity of the mercury and mercury compounds.

High pressure synthesis of Hg superconductors allows a production of materials with an optimal quality for all members of the series $HgBa_2Ca_{n-1}Cu_nO_y$. This type of synthesis involves the use of external high pressures (0.1-7.5 GPa) to suppress the decomposition of HgO and prevent mercury losses. It is necessary the use of the stable precursors. The external pressure can be mainly generated by two techniques: (a) belt type or Conac system [4, 5, 7, 70, 71] and (b) hot isostatic gas pressing (HIP) [72, 73]. The belt-type apparatus applies a mechanical pressure on the sample and allows a generation of the pressure of around 7.5 GPa. However, their applicability is limited because the sample size is very small (< 1 cm^{-3}). Conac systems offer the possibility to work on high volume (~ 1 cm^3) [71]. The HIP technique allows increasing the quantity of the material but achieves lower pressures (0.2 GPa) than the belt-type system. This technique may be useful to process materials for applications, since the sintered powders may reach a high density and the ceramics can be shaped into specific forms by using stiff metal covers.

The first three members of the series $HgBa_2Ca_{n-1}Cu_nO_y$ can also be synthesized by means of the sealed quartz tube [8, 69], while higher members require high pressure synthesis. With this technique it turns out to be very beneficial to carry out the partial substitution of mercury by higher valence cations, such as Re, because the precursor becomes chemically stable against CO_2 and moisture and the volatility of Hg is decreased.

The synthesis of the Hg-based superconductors has been modelled as a solid-gas reaction [74]. Therefore, one of the most important synthesis parameters to stabilize the superconductor phase is the total pressure produced by Hg (g) and O_2 (g) inside the quartz tube. The pressure influences the competition between the formation of Hg-12(n-1)n cuprates and the binary compound $HgCaO_2$ [75, 76]. This last binary oxide turns out to be the hardest impurity to eliminate, remaining frequently in the final product.

Considering the quartz tube technique, the development of an *in situ* pressure monitoring system within the quartz tube (thermobaric analyzer [75]) has allowed a detailed analysis of the reaction mechanism of the Hg-based superconductors and a determination of the optimized synthesis parameters, such as the filling factor, the heating and cooling ramps, etc. [69, 75]. Additionally, this system allows one to investigate the conditions of the thermodynamic stability of the different phases, and one essential step is to control the crystalline grain growth and the sintering process.

2. Thick films and tapes synthesis

There have been efforts to fabricate thick films of Hg-based superconductors on metallic and ceramic substrates. The choice of metals is limited due to amalgamation and subsequent melting of most metals under the processing conditions required for synthesis. The solubility of mercury in a given metal varies with temperature, making it difficult to optimize the processing conditions. Among the metals investigated, platinum and palladium were found to react severely with HgBCCO [77]. Nickel was found to be stable in the presence of mercury, but Meng *et al*. [78] observed that the adherence of Ba-Ca-Cu-O precursor materials on nickel was poor. Silver and gold were found to be compatible with HgBCCO materials even though both metals absorb significant quantities of mercury [72, 77, 79].

Lechter *et al*. [72] showed that gold was compatible with Hg-based superconductors with little reaction with the components of the superconducting system. They synthesized Hg-1223 phase encapsulated in the gold foil by hot isostatic pressing at 900 ºC. Amm *et al*. [77] showed that the gold foil interface enhances the grain growth and alignment of Hg,Bi-1223 by altering the mercury partial pressure at the gold-oxide interface. Large colonies of aligned

Hg,Bi-1223 grains were synthesized by reacting a coating of the mixture of Bi_2CuO_4 and Ba-Ca-Cu-O on gold at 845 ºC using $CaHgO_2$ as the mercury source [77].

Meng *et al*. [78] fabricated Hg,Re-1223 films on Ni substrates with a Cr buffer layer of 30-50 nm. They also used a 5 nm layer of silver to take advantage of the lower melting temperature of the superconductor on the silver. The coatings were made by spraying a 10-40 μm thick layer of the mixture of ReO_2 and Ba-Ca-Cu-O in alcohol. The reaction was carried out at 850-870 ºC. The reacted tapes had ~ 40 μm thick *c*-axis oriented Hg-1223 film with a self field J_C of ~ 2.5×10^4 Acm^{-2} at 77 K [78].

Sastry and Schwartz [80] fabricated Hg,Pb-1223 on silver at 780 ºC using $CaHgO_2$ as the external mercury source. The precursor coatings were made by dip-coating the mixture $Ba_2Ca_2Cu_3O_7 + 0.2PbO$ on silver foils. The precursor coatings were heated at 700 ºC in flowing oxygen for 10 h. Precursor films were vacuum-sealed in quartz tubes along with $Ba_2Ca_2Cu_3O_7$ and $CaHgO_2$ and were reacted at 780 ºC for 10 h. The films had large regions of aligned grains of Hg,Pb-1223 and showed a resistive transition at 133 K.

There were also some attempts to fabricate Hg-1201 wires/tapes using the powder-in-tube technique [79, 81]. Both studies used silver for the sheath material and reported high volume fraction of Hg-1201 in the composite. Schwartz *et al*. [79] used a two-zone technique to control the mercury pressure inside the sealed quartz reaction tube. The Ag-Hg-1201 composite wires were reacted at 800-850 ºC at a mercury pressure of 15.10^5 Pa achieved by controlling the temperature of the mercury reservoir at 450 ºC. Peacok *et al*. [81] achieved high volume fraction of Hg-1201 from a reaction mixture that contained 50 % excess of HgO. They utilized a progressive thermal cycling process that involves heat treatment for 1 h for each of four different temperatures between 600 and 800 ºC. The final tapes had > 90 % Hg-1201 phase as analysed by X-ray diffraction analysis and magnetization measurements. The tapes, however, were porous with poor intergrain coupling and did not support any transport current [81]. These studies clearly demonstrate that silver is compatible with the Hg-Ba-Ca-Cu-O system. More studies are essential to improve the processing to achieve density and intergrain connectivity.

Thick films of Hg-1223 were fabricated on YSZ, MgO and ZrO_2 ceramic substrates [82-84]. Tsaba and Reich [82, 83] used sol-gel techniques to deposit thick Hg-1223 films on single crystal YSZ substrates. They used minute quantities of In_2O_3 additions to promote the formation and growth of superconducting phase. They obtained films with a T_C of 132 K and magnetic J_C of 10^7 Acm^{-2} at 10 K and 10^5 Acm^{-2} at 100 K. Yoo *et al*. [84] also made thick films of Hg-1223 on polycrystalline MgO using a sol-gel technique. The as-synthesized films

showed a T_C of 118 K, which was enhanced to 130 K after post-annealing in oxygen at 350-400 ºC. Singh *et al*. [85] used spray pyrolysis to make Ag doped Hg,Tl-1223 films on single crystal MgO and ZrO_2. The films showed spiral like growth of the superconducting phase grains. The transport critical current density of the films was $\sim 7 \times 10^4$ Acm^{-2} at 20 K.

3. Thin film synthesis

The deposition of epitaxial thin films of Hg-based superconductors on single crystalline substrates has its own interest due to the possible electronic applications of these materials. Additionally, it must be considered as a necessary step towards the development of coated conductors over metallic substrates, as required for practical use in electrotechnical applications.

The activity developed in this field may be considered as moderate due to the difficulties in mastering the solid-gas reaction. The most common method used to perform the synthesis is based on two steps. The first one consists of a deposition of the precursor multiphase $Ba_2Ca_{(n-1)}Cu_nO_x$ mixture in the substrate. This deposition can be carried out by different techniques such as laser ablation, RF sputtering, spray pyrolysis, sol-gel, etc. [65, 86-94]. The second step involves a mercuration process similar to that described for ceramic materials. The deposition process defines the final thickness of the film, which is limited to about 0.1-0.2 μm in the case of the laser ablation or the sputtering [65, 86-89].

Other techniques may be used to prepare thicker films. Spray pyrolysis uses a precursor nitrate solution to generate an aerosol through a pneumatic nebuliser or by means of a piezoelectric ultrasonic excitation [90-93]. The aerosol is carried by an inert gas (Ar) to a preheated substrate where the deposition occurs and the solvent is vaporized. This technique allows a production of films with a thickness in the range 1-10 μm. After the deposition a high temperature annealing is necessary to remove all traces of nitrates and to adjust the oxygen content of the precursor film.

Attempts to synthesize thin films of $HgBa_2Ca_{n-1}Cu_nO_{2n+2+\delta}$ began shortly after their discovery. Early results on Hg-1212 films were very encouraging for the prospects of $HgBa_2Ca_{n-1}Cu_nO_{2n+2+\delta}$ application in general [65]. Thin films of Hg-1212 and Hg-1223 have been formed with varying degrees of the film quality. Most films have been grown on $SrTiO_3$

(STO) and LaAlO$_3$ (LAO) substrates, but MgO, NdGaO$_3$ and Y$_{0.15}$Zr$_{0.85}$O$_2$ (YSZ) have also been used successfully.

The most common procedure to carry out the vapour reaction of the deposited films with Hg is by means of the quartz tube technique, similar to the reaction leading to ceramic materials. The thermodynamic conditions where the superconducting phase may be formed are very similar to those found in ceramic materials, thus the temperature and pressures which must be used to prepare single phase materials do not differ too much either.

The synthesis of the Hg-based compounds can be described by a general reaction, where the solid component Ba$_2$Ca$_{n-1}$Cu$_n$O$_{2n+1+x}$ might be a mixture of several phases:

$$HgBa_2Ca_{n-1}Cu_nO_{2n+2+\delta} \text{ (s)} \leftrightarrow Ba_2Ca_{n-1}Cu_nO_{2n+1+x} \text{ (s)} + Hg \text{ (g)} + (1-x+\delta)/2 \text{ O}_2 \text{ (g) [4].}$$
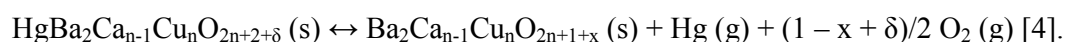
From the thermodynamic point of view the system Hg-Ba-Ca-Cu-O shares two components – mercury and oxygen – with the surrounding atmosphere. In the synthesis of bulk materials, phase equilibria as well as the content in the condensed phase of these compounds is controlled by adjusting their activity. The oxygen partial pressure may be controlled by an oxide redox couple (Co$_2$O$_3$/CoO, CuO/Cu$_2$O [95, 96] or Mn$_2$O$_3$/Mn$_3$O$_4$ [96-98]) and for the activity of mercury HgBa$_2$CuO$_4$/Ba$_2$CuO$_3$ couple has been used [4]. Formation of the particular phases depends on the relation between pHg, pO$_2$ and synthesis temperature. The pHg/pO$_2$ vs. T dependences have been published by several groups [95, 96, 99-103]. There are big differences between p(T) dependences in different publications so these results could not be used as a general technique for the preparation of the single-phase samples. But we can predict that to obtain higher phase from the homologous series we have to increase the mercury pressure. Between the formations of two phases there is some competitive reaction resulting HgCaO$_2$ (or HgBaO$_2$, respectively). Hg-1212 can be stabilised relative to CaHgO$_2$ by using a higher temperature at constant pO$_2$ or at lower oxygen pressure at constant T. This research was performed on the bulk samples. In the case of the thin films, other parameters, e. g. the substrate or the buffer layer, could also influence the formation of superconducting phases but the systematic research in this area was not accomplished.

The growth mechanism of the Hg-phases in the thin films is not well known. Hg-1212 phase is easy to obtain, to grow Hg-1223 phase is more difficult. De Barros *et al.* [93] found out, that the substrate can influence the growth of the Hg-based superconducting phases. On the LAO, which has very small lattice mismatch with the Hg-based compounds, Hg-1212 is preferentially formed while Hg-1223 grows on the MgO (bigger lattice mismatch with Hg-

based superconductors). They suggest that this is linked with nucleation-growth conditions and to the formation path of Hg-1223 involving Hg-1212 as an intermediate step. Hg-1212 grows epitaxially on the LAO, the access of (Ca, Cu, O) being limited to the cross section of the films creates very bad conditions kinetically. On MgO, both large misfit and interfacial conditions favour 3D growth, a better conditions for the conversion Hg-1212 into Hg-1223.

This is in agreement with the study of Reder *et al.* [28]. They propose the following model for the formation of the Hg-1223 phase: Already during the heating of the precursor material, nuclei of Hg-1201 develop after the decomposition of HgO. These nuclei compete with the also forming $CaHgO_2$ phase for the free Hg. By Re doping, the formation of $CaHgO_2$ can be reduced strongly enough so that the Hg-1201 development is promoted. Besides planar growth of the Hg-1201 grains, sometimes spiral growth around screw dislocations also takes place. At the latest when all available Hg is incorporated in Hg-1201 grains, the intercalation of Ca, Cu and O into these grains starts which transforms them into Hg-1212. By further intercalation, the Hg-1212 grains transform into Hg-1223. Incomplete intercalation due to local lack of Ca and Cu or due to stress fields because of the expansion in *c*-direction lead to the remaining of many Hg-1212 stacking faults inside the Hg-1223 grains. Re doping promotes the formation of Hg-1234 stacking faults. The intercalation process can take place rather rapidly where Ca, Cu and O are available (Fig. 16). The inhomogeneous distribution of Ca–Cu-rich phases leads to an inhomogeneous distribution of transformed grains at the beginning of the transformation. Especially in later stages of the phase formation, the movement of Hg-1212 stacking faults in the [0 0 1]-direction towards Ca–Cu-rich neighbouring grains can also contribute to the phase transformation [28].

This model of the Hg-1223 formation is supported also by the work of Yun *et al.* [86]. His group first reported the fabrication of *c*-axis oriented Hg-1223 films in 1995. The film precursor was deposited by an RF sputtering onto the STO with no dopant. A HgO cap layer was deposited atop the film that was subsequently annealed to grow the Hg-1223 phase. Due to this cap layer (Ca, Cu, O) necessary for the formation of the Hg-1223 are kept in the film and thus Hg-1223 is formed easily. The resulting onset T_C was between 130-132 K. Less than one year later, the same group reported significantly improved films that were grown without the cap layer but with unreacted Hg-1223 pellets as the Hg source for the growth reaction [88]. As before, these films were deposited by an RF sputtering on the STO with no dopant. In this case, oxygen annealing was introduced after the growth reaction. A high magnetization J_C was reported (2.3×10^7 Acm^{-2} at 5 K, zero-field; 5×10^5 Acm^{-2} at 100 K). As with their Hg-1212 films, this group also used a fast temperature ramping technique to grow the Hg-

1223 films on the LAO with success [87]. They have shown also that doping with Li significantly reduces the required sintering temperature for the growth of the Hg-1223 phase, while maintaining good phase purity (73 %) [104].
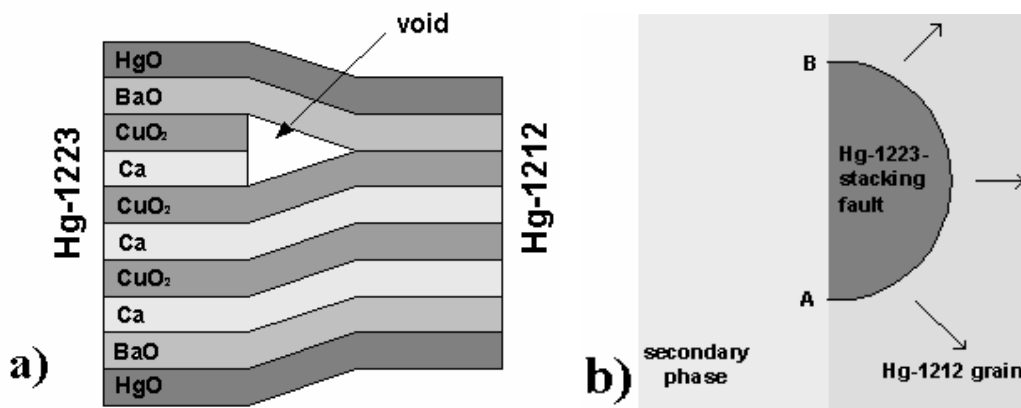
Fig. 16 (a) Schematic drawing of the stacking sequence at the transition of a (0 0 1) plane from $n = 2$ to $n = 3$. The partial dislocation surrounding an Hg-1223 stacking fault inside Hg-1212 grain is linked with a tubelike void (marked by circle). (b) Sectional drawing along a (0 0 1) plane through a Hg-1212 grain with an incomplete Hg-1223 stacking fault. The void channel parallel to the partial dislocation limiting the stacking fault intersects the grain boundary at the points A and B [28].

The HgO cap layer was used also by Moriwaki *et al*. [38, 94]. They prepared undoped and Re-doped *c*-axis Hg-1223 superconducting thin films on $SrTiO_3$ (100) substrates by using the two-step process which comprises pulsed laser deposition of precursor films and subsequent annealing in mercury-vapor atmosphere. The use of $HgO/Re_xBa_2Ca_2Cu_3O_y$ (*x*=0, 0.1) multilayer precursor films capped with an HgO protective layer was found to be effective to obtain more than 75% phase-pure Hg-1223 films, while the absence of the protective layer leads to appearance of a substantial amount of impurities phases. Re-doped Hg-1223 films exhibit a T_C (zero) as high as 127.5 K and a slightly lower T_C (zero) of 123 K is observed for undoped Hg-1223 films. Re-doped films also show a high J_C (transport) at 77 K of 1.5×10^6 Acm^{-2} in a self-field and 1.2×10^5 Acm^{-2} under a magnetic field of 1 T parallel to the *c*-axis. It is demonstrated that the Re-doping improves the superconducting properties, as well as the film morphology. Moreover, the irreversibility field above 77 K evaluated from the resistive

transitions of the Re-doped Hg-1223 films is found to be substantially higher than those for undoped Hg-1212 and Tl-1223 thin films.

The mercuration using HgO cap layer has been found very effective for the fabrication of the thin films containing Hg-1223, however the deposition of the HgO is dangerous and contaminates all the deposition apparatus.

Another method for the preparation of the thin films with the Hg-1223 phase was reported by Kang *et al*. [105, 106]. They fabricated high quality *c*-axis oriented $HgBa_2Ca_2Cu_3O_8$ thin films with the stable Re-doped $Ba_2Ca_2Cu_3O_x$ precursor powder by pulsed laser deposition followed by postannealing without any special handling. As-grown films on (100) $SrTiO_3$ exhibit a zero-resistance transition (T_{C0}) at ~ 131 K with a narrow transition width $\Delta T \sim 1.5$ K after oxygen annealing at 340 °C for 12 h. The critical current densities are observed 1.1×10^7 Acm^{-2} at 10 K and 1.2×10^5 Acm^{-2} at 120 K in zero field. The x-ray diffraction pattern indicates highly *c*-axis oriented thin films normal to the substrate plane containing also a minor $HgBa_2CaCu_2O_6$ phase. Oxygen annealing increased the T_C to 133 K and the J_C to 1.9×10^7 Acm^{-2} at 10 K and 2.6×10^7 Acm^{-2} at 120 K [106].

A new approach to the formation of the Hg-based films was demonstrated by Wu *et al* [107]. In this approach, the Tl-1212 films are grown on the single crystal LAO and subsequently annealed in the presence of an Hg vapour. The annealing removes the Tl from the film and replaces it with the Hg. Using this cation exchange process, the authors obtained films with J_Cs close to 1 $MAcm^{-2}$ at 110 K. At 5 K, the J_C of the Hg-1212 film is about twice that of the original the Tl-1212 film. At 77 K, the Hg-1212 film has a J_C about two orders of magnitude greater than Tl-1212 counterpart (note that the T_C of the Tl-1212 is about 90-95 K, while that of the Hg-1212 is about 115 K).

Stelzner and Schneidewind [108, 109] double sided high critical current density $HgBa_2CaCu_2O_{6+\delta}$ films on lanthanum aluminate as well as on CeO_2 buffered R-plane sapphire substrates using an improved Tl–Hg cation-exchange process. The films on the LAO exhibited critical current densities (J_C) of up to 7 $MAcm^{-2}$, and films on sapphire substrates showed J_C values of up to 5 $MAcm^{-2}$ in a self-field. The superconducting transition temperatures (T_C) were in the range of 121–124 K for films on LAO substrates and 118–122 K for films on sapphire substrates.

Xie *et al*. published the only work on the fabrication of the Hg-1223 phase using Tl–Hg cation-exchange process [110]. They used cation-exchange process developed by Wu *et al*. [107] was applied to convert $Tl_2Ba_2Ca_2Cu_3O_{10}$ (Tl-2223) superconductors to $HgBa_2Ca_2Cu_3O_{8+\delta}$ (Hg-1223) superconductors via Tl–Hg cation-exchange in Hg-vapor at

processing temperatures ranging from 700 to 800 °C for 6–24 h. Oxygen annealing process at 350 °C for 10 h was followed to optimize the content of oxygen in the Hg-1223 samples. The Tl-2223 phase has been successfully converted to the Hg-1223 phase with a negligible amount of non-superconducting impurity phase. T_C values up to 135 K have been obtained in the Hg-1223, which are ~ 15 K higher than that of the original Tl-2223 compounds.

IV. Aims of dissertation thesis

Buts de cette thèse

Ce chapitre a pour buts de préciser les objectifs généraux de ma thèse.

Both, Institute of Electrical Engineering in Bratislava and Centre National de la Recherche Scientifique in Grenoble have cooperated since several years with the aim to highlight the potentialities of very high T_C's materials like HgBCCO or TlBCCO in modern electronics. A large effort needs to be done on the material side because all knowledge of the processing has to be built on before electronic applications could be started.

According to the present state of status on ongoing research, technological and experimental equipment of my workplaces the aims of my dissertation thesis are targeted to the following area:

- To master the sol-gel method and its application in the preparation of the sputtering targets and mercuration pellets.

- Fabrication of thin superconducting Hg-based films on the CeO_2 buffered R-plane sapphire and other substrates using an RF magnetron sputtering and an *ex situ* mercuration. Characterization of the prepared films.

- Optimization the mercuration process. Two directions were followed:
  - Study of the influence of the configuration of mercuration on the structural and electrical properties of the prepared films.
  - Optimization of the phase composition of the films to obtain Hg-1223 phase with the best electrical properties.

- Fabrication of the Hg-based superconducting structures with different techniques with the aim to find the best patterning method. Study of the properties of the prepared structures to find some practical applications.

V. Experimental

Partie expérimentale

Tous les procédés nécessaires à la fabrication des couches minces de cuprates de mercure sont décrits dans ce chapitre. On présente aussi les méthodes de caractérisation des couches.

1. Experimental techniques

1.1 Structural characterization of the thin films

For the structural characterization of the prepared samples X-ray diffraction (XRD) (CuK$_\alpha$) analyses in the classical Bragg-Brentano configuration and also using a texture apparatus in the Schultz configuration (4 axis from Seifert) allowing to modify the tilt inclination χ and the rotation angle ϕ were used (Fig. 17).

In the Bragg-Brentano configuration the X-ray diffracts on the planes parallel to the substrates. A maximum positive interference occurs when the path differences between the reflections from successive lattice planes in a family is equal to an integer number of the wavelength, i. e.

$$n\,\lambda = 2d\,\sin\theta,$$

where n is the order of the reflection, λ is the wavelength, d is the lattice plane spacing and θ is the angle of incidence / reflection.
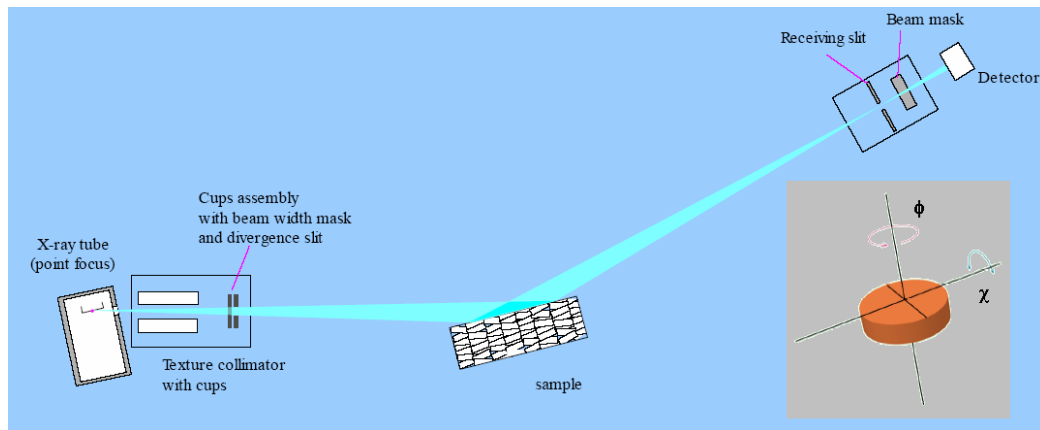

Fig. 17 Experimental set-up for texture measurements in Schulz geometry.

In this configuration of the XRD device we can measure these parameters of the thin film or single crystal:

- Precise lattice constants measurements derived from θ-2θ scans, which provide information about lattice mismatch between the film and the substrate and therefore is indicative of the strain and stress. If the film is textured or epitaxial, only (00l) diffractions are visible in the XRD patterns because only (00l) planes are parallel to the substrate. When the impurities present in the sample are also textured it is very difficult to detect them by θ-2θ scan and another analysis has to be done.

- Rocking curve measurements (ω-scan) made by doing a θ scan at fixed 2θ angle, the width of which is inversely proportionally to the dislocation density in the film and therefore used as a gauge of the quality of the film. This study is useful for the epitaxial films. The Bragg peak is broadened by three factors: thickness, thickness deviation and strain in the normal direction to the film. The rocking curve is broadened by three factors: lateral size of coherent grains, its dispersion, the angle between the normal to atomic planes at the surface (mosaic spread). The full width at a half maximum (FWHM, $\Delta\omega$) of the rocking curve gives us also information about the mosaicity of the film.

- In plane orientation can be established by the sample rotation around the axis perpendicular to the sample surface (ϕ-scan). In this case, however, crystalline planes that are parallel to the surface will not provide the necessary information. The combination of the diffraction from planes inclined with respect to the surface and rotation around the axis parallel to the surface will provide us the information about the in-plane orientation.

- The poles figure gives a representation of the complete texture of a sample. It is then complementary to ϕ-scans (and ω-scans) that give diffraction information of only one sort of atomic planes. In the pole figure measurement, one fixes the Bragg angle to a given value and explores all the orientations that provide diffraction of this plane by changing systematically ϕ and χ. Thus all the orientations of the various atomic planes are detected. The diffracted poles are dispersed on a sphere and a stereographic projection on the plane of the surface of the sample is used to present the data. This mathematical transformation is schematically drawn in the Fig. 18. In this polar representation χ angles are along

the radius (but with a scale ArcTang(χ) while the angles are ϕ. A spot at the centre means that the sample has its atomic planes (hkl) parallel to its surface. In a cube texture $(100)\|(100)_{substrate}$, the pole (100) is observed at the centre and the pole (111) provides four poles at $\chi = 54.7°$. The great advantage of the poles figure over simple ϕ-scans and ω-scans characterisations is that all orientations are studied, not only the one giving ϕ-scans response.
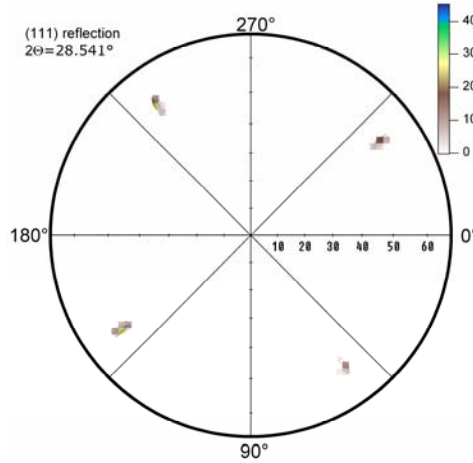
Fig. 18 Pole figure of (111) plane of the CeO_2 thin film.

The diffraction data from the ICDD database of the substrates (sapphire, $LaAlO_3$), the buffer layer (CeO_2) and of the Hg-based superconducting phases (Hg-1212, Hg-1223) use as a standard in our study are shown in the Annexe A (A3-A8).

All the structural characterizations were performed by X-ray diffraction (CuK_α) in the classical Bragg-Brentano configuration and also using a texture apparatus in the Schultz configuration (4 axis from Seifert) allowing to modify the tilt inclination χ and the rotation angle ϕ.

1.2 Scanning electron microscopy

The scanning electron microscope (SEM) is a standard analytical tool used for the study of a wide range of materials. The most basic, and widely used, function of the SEM is an imaging of surface features and topography at magnifications up to 100 000. This type has been used for study of superconducting materials to assess important microstructural features

like the homogeneity, the porosity, the roughness and the connectivity. One of the most attractive aspects of the SEM is the ability to add to this imaging function a range of chemical and crystallographic tools. A standard SEM may be fitted with energy dispersive (EDX) and wavelength dispersive (WDX) X-ray detectors which allow spatially resolved elemental analysis to be performed.

Quantitative analyses were performed using ZAF corrections. ZAF correction is used to offset the effects of atomic number differences (Z), absorption (A), and fluorescence (F) on the EDX spectral data obtained from samples. The calculations of the concentration of the elements present in the samples were made using the standards using following formula:

$$C[\%w] = \left(\frac{Z.A.F._{\cdot \acute{e}ch}}{Z.A.F._{\cdot std}} \right) \cdot x \cdot K \cdot x \cdot Ct_{\%w} \cdot x \cdot 100$$

The morphology of the films was studied by a SEM using HITACHI field emission S-800 and Jeol 840A apparatus. EDX analyses were performed by Jeol 840A apparatus.

1.3 Transport electrical measurements

The critical temperature of the superconducting samples was measured by DC four probe techniques. A four probe resistance measurement is a technique for measuring the resistance of low resistance material, especially superconductors.

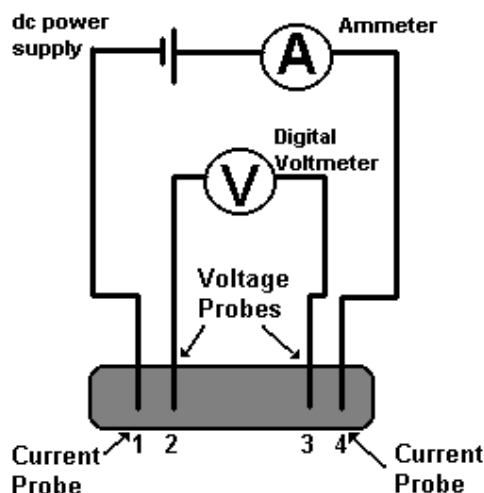A schematic of a four point probe is shown in the Fig. 19 below.

Fig. 19 Schematic of four-point probe.

In this diagram, four wires (or probes) have been attached to the sample. A constant DC current is made to flow the length of the sample through probes labelled 1 and 4 in the figure. This can be done using a current source or a power supply as shown. Many power supplies have a current output readout built into them. If not, an ammeter in series with this circuit can be used to obtain the value of the current. This four probe method eliminates the problem of the resistance of the probe contact (called contact resistance).

A typical measurement current values of 0.1-100 µA for superconducting cryoelectronic structures (Josephson junctions, nano-microbridges), of 0.1-5 mA for thin films (thickness d < 1 µm), of 1-10 mA for thick films (d ~ 1-10 µm), of 20-100 mA for tapes and wires, and of 0.1-1 A for superconducting bulk samples are used.

If the sample has any resistance to the flow of electrical current, then there will be a drop of potential (or voltage) as the current flows along the sample, for example between the two wires (or probes) labeled 2 and 3 in the figure. The voltage drop between probes 2 and 3 can be measured by a digital voltmeter. The resistance of the sample between probes 2 and 3 is the ratio of the voltage registering on the digital voltmeter to the value of the output current of the power supply. The high impedance of the digital voltmeter minimizes the current flow through the portion of the circuit comprising the voltmeter. Thus, since there is no potential drop across the contact resistance associated with probes 2 and 3, only the resistance associated with the superconductor between the probes 2 and 3 is measured.

The contacts for this measurement could be made from different materials (Ag paste or low meltable metals or alloys). The choice of the contact material depends on the type of the measured material, its surface properties, etc. In our case, we found out that In is the most suitable for the thin films of Hg-based superconductors. Indium contacts have a good adhesion to the Hg-based film, did not involve high heating of the sample and did not degrade the electrical properties of the samples.

The measurement of the current-voltage *I-V* characteristics of the thin films and structures was performed in the same configuration as the measurement of the $R(T)$ dependences (Fig. 27). Increasing current in the sample was controlled by a computer. The process of the current increase was stopped when the voltage reached a certain value (for example 1mV).

The temperature dependence of the critical current $I_C(T)$ was obtained by the measurements of the *I-V* characteristics at a given temperature. The criterion for the critical current was the value of the voltage of 5 µV.

1.4 Magnetic measurements

The most important electrical parameters of a superconducting sample are current–voltage J–E characteristics and the value of the critical current density. The direct measurement of the I–V curves with the transport current requires the preparation of very low resistance current contacts and potential contacts. To reduce the sample heating in the current contacts the patterning of the sample to narrow bridges is used [94]. However, the contacted and patterned samples cannot be used for further processing or analysis. AC-susceptibility is widely used and offers advantages with respect to direct electrical measurements [111].

A non-destructive Hall probe method allows determining the J–E curves, the critical current, its dependence on the external magnetic field and its uniformity in the sample. The method also allows determining the type of the currents flowing in the sample (intragranular or intergranular currents); that is important information for the technology. In comparison with the transport experiments, the electric fields induced in the samples can be lower, so that the measuring method is able to detect very low resistances and their effect on the shape of the J–E curve.

From the maxima of the field $B_{SZ} = f(x)$ we can determine the critical current density J_C of the persistent magnetization currents.

Measuring method

The sample is placed in the centre of a copper magnet producing magnetic fields B_e, (perpendicular to the sample surface), which can be changed by various values of the rate of the change, dB_e/dt. Two types of measurements were done:

1. Measurement in the static regime, at which the external magnetic field is changed from 0 to $B_e \sim 0.2$ T and back to zero. By this way we induce persistent magnetization currents in the sample. The magnetic field due to these currents is measured by a micro Hall Probe with the active area of $\sim 100 \times 100$ μm^2. The Hall probe is moved over the sample surface and scans the sample magnetic field, see the Fig. 20. The shape of the profiles of the sample magnetic field due to intragranular currents is very different from those due to intergranular currents. The details of the measurements are given in [112]. It is important to note that the electric field E in this regime is very low ($E \ll 1$ $\mu V/cm$), as it is controlled by the decay of the magnetic flux created by the magnetization currents. Thus, the critical currents obtained by this method are obviously smaller than those determined by the transport measurements.
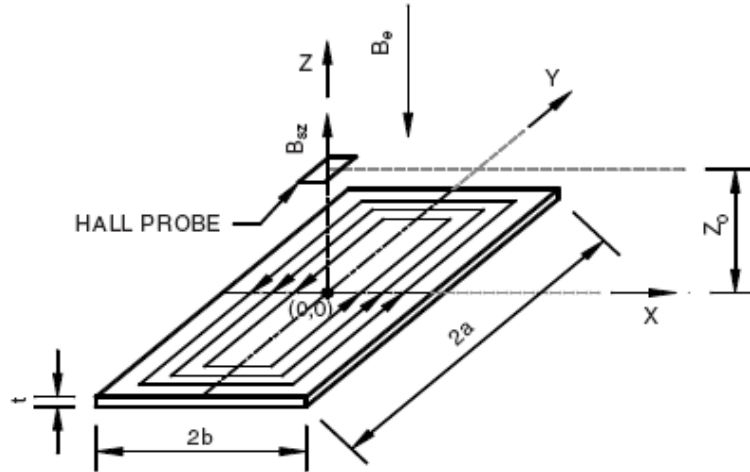
Fig. 20 Measurement arrangement in the coordinate system, z_0—sample to probe distance, 2a—length of the sample, 2b—width of the sample, t— thickness of the film, B_e—external magnetic field, B_{sz}—perpendicular component of measured magnetic field.

2. Measurements in the dynamic regime, which allow to determine J–E characteristics and the critical current density, J_C. The copper magnet produces triangular magnetic field waves $0 \rightarrow B_{em} \rightarrow 0 \rightarrow - B_{em} \rightarrow 0$ with the constant value of dB_e/dt (B_{em} is the amplitude of B_e). The Hall probe signal proportional to the magnetic field above the sample center, B_{sz}, is recorded as a function of B_e. The hysteresis loops are measured at various values of dB_e/dt, which induce different electric field in the sample. From the family of loops $B_{sz} = f(B_e)$ we can determine the electric field–current density curves, as described in [113]. The measurements can be done at various positions along the sample, which allow getting information on the sample uniformity.

All measurements were done in the liquid nitrogen bath at the atmospheric pressure.

1.5 Thickness measurement

The thickness of our films was measured using a stylus profilometry.

The profilometry is a measurement of the surface height variations of an object. It can be divided into two areas; the measurement of the surface shape, or the departure of the shape from an ideal shape, and the measurement of the roughness. Generally, the height variations when measuring roughness have a much smaller period than the variations when measuring

the shape or the form. Therefore the measurement of the roughness requires instruments with both high lateral and vertical resolution. If we have some step on the film (for example patterned structure), the stylus profilometry can be used also for the thickness measurement.

The classical tool and the industrial standard for measuring surface profiles is the mechanical stylus. The stylus probe is passed across the surface and its movement, as it follows the surface profile, is measured. This is still the standard surface profiling technique and can offer high precision allowing the measurement of the surface roughness. However, the stylus technique has its disadvantages. There are limits in lateral resolution, set by the size of the probe tip; peaks that are narrower than the probe tip will be recorded as being broader than they really are, while the probe will be physically incapable of reaching the bottom of narrow troughs. This reduced the lateral resolution results in a loss of surface height information and the results depend on the shape of the stylus.

The thickness measurement was performed using step height measurement, a Hobson Talystep profilometer.

1.6 Microwave absorption measurements

Magnetically Modulated Microwave Absorption (MMMA) is a sensitive differential method to study the magnetoresistence related to the voltage fluctuation in nonhomogeneous superconducting systems with Josephson junctions (JS) and in magnetic systems exhibiting giant magnetoresistence (GMR). The MMMA method has been successfully established after the discovery of polycrystalline high temperature superconductors with high concentration of Josephson junctions. MMMA proved to be the third method besides resistivity and magnetic susceptibility measurements to determine the critical temperature T_C. In magnetic nanostructures the MMMA enables to determine the GMR(H) and magnetization reversal.

The microwave absorption measurements of superconducting films were performed in a cavity resonator filled with a sapphire rod using TE_{011} mode. Resonant frequency was f_0=10 GHz. The dissipated microwave power affects the quality factor Q of the microwave cavity $Q^{-1} \sim f_0 \; \delta P/W$, where $\delta P/W$ is the ratio of the dissipated power and energy stored in the resonator. As results from microwave analysis we determine the temperature dependence of the parameter Q/Q_R where Q_R is the quality of the empty resonator ($\approx$2000).

2. Preparation of the Hg,Re-Ba-Ca-Cu-O films

2.1 Preparation of the precursor powder

The powders for the preparation of the mercury source were prepared by a sol-gel method [114-117]. The synthesis of the Re-Ba-Ca-Cu-O powders is carried out by dissolving separately the $BaCO_3$, $CaCO_3$, CuO and Re in aqueous solution of nitric acid or acetic acid for the former carbonates. The solutions are mixed afterward in stoichiometric ratio. The cations Cu^{2+} and Re^{6+} in the solution are separately complexed with the addition of acid-EDTA : $(H_4Y) = [CH_2N(CH_2\text{-}COOH)_2]_2$ in the ratio 1:1 and pH is adjusted to ≈ 3 with ammoniac addition to obtain H_2Y^{2-}, a species that best complex with these cations. Finally, all solutions are mixed to reach a total volume of approximately 200 ml for obtaining 10 g of the precursor phase. Added to this solution was 6wt. % of acrylamid monomers ($H_2C = CHCONH_2$), 0.6 wt.% of N,N'-methylenebisacrylamid (($H_2C = CHCONH)_2CH_2$) and a few milligrams of a reticulating agent α,α'-azoisobutyronitrile ($C_8H_{12}N_4$) to perform the polymerisation which is easily achieved by heating to 80 °C. This forms rather hard gels that are stable with time.

The gel is then dried a few minutes in a microwave oven. During this process, the dehydration occurs first and is followed by the ignition of the carbon components. It results from this treatment an extremely porous foam material. The xerogels obtained are then homogenized in a ceramic mortar and calcined at 860 °C during 36 h in a muffled furnace with a circulation of the gas (O_2). The oxygenation is important for further mercuration. The powder obtained is then homogenized and calcined again at 860 °C during 12 h. For the total removal of the carbonates a vacuum annealing at 840 °C / 5 h was used. The powders are very fine, the native particles being in the range of 0.1–0.3 μm. They are, however, agglomerated in soft aggregates, reaching a few μm. The prepared powders did not contain barium carbonates (Fig. 21).
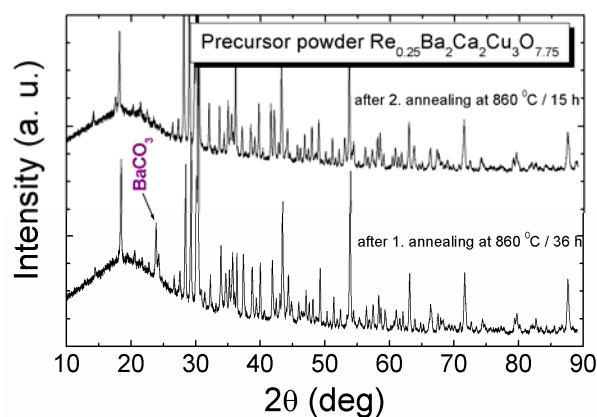
Fig. 21 X-ray diffraction pattern of the precursor powder after annealing at 860 ℃ / 36 h and after the second annealing at 860 ℃ / 15 h. The diffractions of $BaCuO_2$, Ca_2CuO_3, $Re_2Ba_4CaO_2$, CaO and CuO were present in the XRD pattern.

2.2 Preparation of the targets for sputtering

The sputtering targets with a nominal composition of $Re_{0.25}Ba_2Ca_2Cu_2O_x$ and $Re_{0.15}Ba_2Ca_2Cu_2O_x$ were prepared from the precursor powders with the same stoichiometry. Precursor powders were synthesized using sol-gel method (see chapter 1.1). The powders were pressed into pellets with 5 cm diameter using a pressure of about 15 MPa. The pellets were then sintered at 920 – 940 ℃ during 24 h in air.

2.3 Preparation of the CeO₂ buffer layer

The CeO_2 buffer layer as well as the Re-Ba-Ca-Cu-O precursor films were prepared in the Leybold-Heraus Vacumatic 2PS apparatus.

To improve the surface properties, the substrate (R-plane sapphire) was preannealed 3 h at 1000 ℃ in air. The CeO_2 layers were grown by on-axis radiofrequency (RF) magnetron sputtering method [118-120]. For the deposition of a 60 nm thick CeO_2 layer, a mixture of Ar and O_2 at a ratio of 4:1 and a total pressure of 50 Pa was used. The RF power on the target and the substrate temperature were 80 W and 750 ℃, respectively. A post-deposition annealing of the CeO_2 layers (3 h at 1000 ℃ in the air) was applied to improve the FWHM value of the ω-scan from the (002) CeO_2 line. The prepared films of the CeO_2 buffer layer

were then characterized by XRD analysis (θ-2θ scan, ω-scan, Φ-scan, poles figures). The thickness of the films was controlled using step height measurement using a Hobson Talystep profilometer (see part 1.5 in this chapter).

2.4 Preparation of the Re-Ba-Ca-Cu-O precursor films

Precursor films, 300 nm thick, were prepared by the RF magnetron sputtering from two stoichiometric targets with the nominal composition of $Re_{0.25}Ba_2Ca_2Cu_3O_x$ and $Re_{0.15}Ba_2Ca_2Cu_2O_x$. During the sputtering, we used inert atmosphere (Ar) with a total pressure of about 20 Pa. Using the RF power of 80 W, the sputter rate was about 0.3 nm / s. The films were sputtered at the room temperature so after the deposition they were amorphous. The thickness of the films was controlled using step height measurement using a Hobson Talystep profilometer (see part 1.5 in this chapter). The composition of the films was controlled by EDX analysis. The qualitative analysis confirmed the presence of all sputtered elements (Re, Ba, Ca, Cu and O) and we saw also the signal from the substrate (Al_2O_3) and from the buffer layer (CeO_2). The typical EDX spectra are in the Fig. 22a (the precursor film sputtered from the target with the $Re_{0.25}Ba_2Ca_2Cu_2O_x$ composition) and Fig. 22b (the precursor film sputtered from the target with the $Re_{0.15}Ba_2Ca_2Cu_2O_x$ composition).
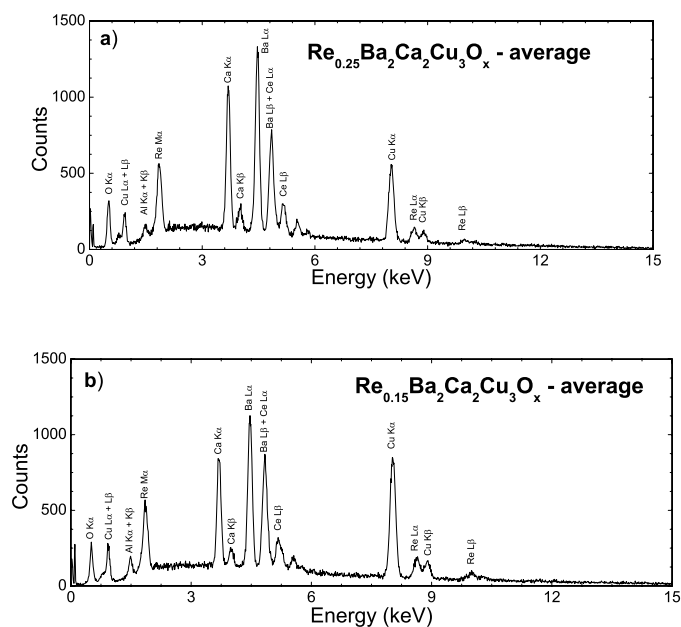

Fig. 22 Typical EDX spectra of the precursor film sputtered from the target with the $Re_{0.25}Ba_2Ca_2Cu_2O_x$ (a) and $Re_{0.15}Ba_2Ca_2Cu_2O_x$ (b) composition.

Quantitative analyses were performed using ZAF corrections in the bigger average area (1 μm^2) as well as in the different points of the sample. These calculations confirmed the stoichiometry of the prepared precursor films close that of the target. An example of the calculation is reported in the Tab. 2.

As prepared precursor films were then used for the preparation of the thin superconducting films based on mercury.

Analysis:	Correction	Method::	ZAF							
	Analysis	Type::	Std							
Quantitative	Results									
	Elt	XRay	Int	Error	K	Kr	W%	A%	ZAF	Theoretical A %
	O	Ka	18	0.3463	1.3376	0.084	22.59	58.72	2.7029	60.4
	Ca	Ka	62.5	0.6451	1.166	0.1043	10.2	10.58	1.0152	11.1
	Cu	Ka	90.8	0.7774	0.9907	0.2705	28.46	18.63	1.0555	16.6
	Ba	La	91.3	0.7797	0.585	0.2976	35.73	10.82	1.2108	11.1
	Re	Ma	29.7	0.4449	0.6034	0.0332	5.6	1.25	1.69	0.8

Tab. 2 The calculations of the concentration in the average area in the precursor film sputtered from the target with the nominal composition $Re_{0.15}Ba_2Ca_2Cu_3O_x$.

2.5 Mercuration

The mercuration was performed in a sealed quartz tube using an external source of the mercury. This source was an unreacted pellet having the composition (Hg,Re)-1223. It was prepared by mixing the mercury oxide HgO with (Re-Ba-Ca-Cu-O) precursor powder in an agate mortar. The source of mercury and the precursor film were wrapped in a gold foil and sealed in the quartz tube under vacuum (1 Pa). The gold foil was used to avoid the reaction between barium oxide and quartz; it is also used to support the additive of liquid mercury. This additive was used to initiate the increase of mercury pressure upon heating and to supply the mercury homogeneously. The mass of the mercury in the source was approximately 3 g and we added a small amount of liquid mercury (0.1 g). The quartz tube had an internal diameter of 8 mm and a length of about 12 cm. A piece of quartz was inserted in the tube to reduce the free volume. Then the total amount of mercury was about 0.001 mol/cm^{-3} taking into account the mercury in the source pellet and liquid Hg. The synthesis temperature was in the range 800-830 °C and the annealing time was and 2-24 h.

VI. Results and discussion

Résultats et discussions

Les principaux résultats sont présentés dans ce chapitre. Ils sont divisés en cinq parties – mercuration sans contact, mesures magnétiques, influence de la pression de mercure, influence de la qualité de la couche tampon en CeO₂ et essais de structuration de films supraconducteurs. Dans chaque partie on a rappelé les motivations et décrit les résultats originaux.

1. Role of the configuration of the mercuration on the properties of the thin superconducting films based on mercury

The synthesis of thin films of the mercury based superconductors is generally made in two steps: the first one is to deposit the precursor film; the second step is its mercuration. In the second operation, the film is put close to a source of mercury, composed of an unreacted pellet of the same composition as the film to mercurate. There is no reference in the literature to the exact position of the precursor film with respect to the mercury source. Sometimes it is reported that the film is placed face to face to the mercury source [121] but it is not clear if they should be at contact or not. In other words, is the mercuration induced by mass transfer from the vapour phase or by solid /or liquid/ state reaction? The first experiments with no contact between the mercury source and the precursor film were performed by De-Barros [92]. He assumed that vapour phase may play an important role in the mercuration. Beside this, the contact can cause sticking of the film on the mercury source – this can be a drawback when the film is then separated from the mercury source. That was the reason why we decided to study the possibility of a mercuration without any physical contact between the precursor film and the source of mercury.

Two methods of the mercuration were compared. In the case of the method I, the precursor film and the source of mercury were placed face to face (Fig. 23a). In the case of the method II, any contact between the precursor film and the source of the mercury was avoided (Fig. 23b), due to the special shape of the sample holder made of porous alumina. The synthesis temperature and the annealing time were 800 °C and 5 h, respectively.
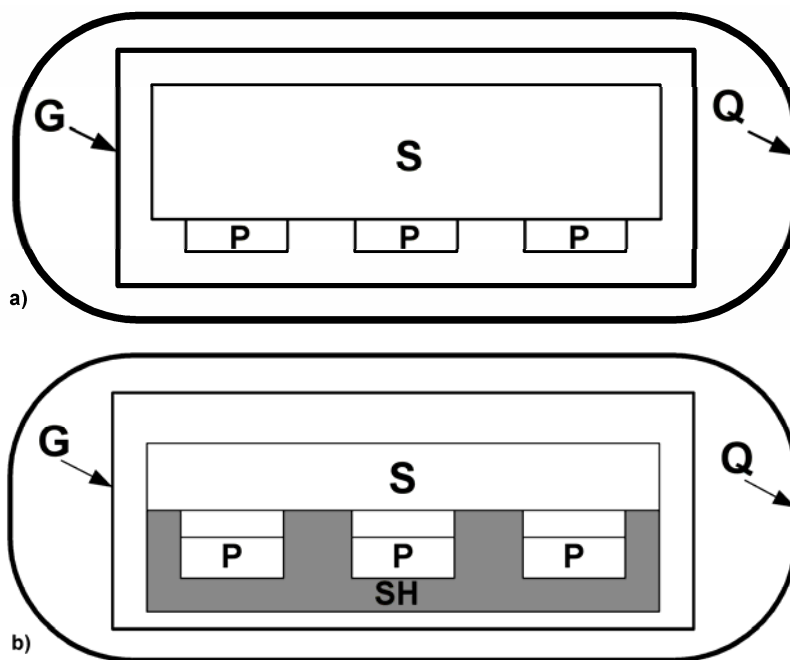
Fig. 23 Scheme of the method I (a) and the method II (b) for the mercuration of the precursor films in the sealed quartz ampoule method. P – precursor film, S – source of mercury, G – gold foil, Q – quartz tube and SH – sample holder.

We have studied the influence of the methods (method I or method II) on the structural and the electrical properties of the films.

The films prepared by the method I were compared with the films prepared by the method II. In both cases the films were superconducting. Three types of films were observed: i) films prepared by both methods were generally black but those grown by the method I were often irregular with some apparently uncovered parts, ii) the films prepared by method II were homogeneous without visible defects on the surface; iii) in some cases, parts of the films (method I) were translucent indicating very small thickness, surprisingly they were also superconducting. We suppose that this was caused by sticking of the films to the surface of the mercury source during the mercuration process.

Using XRD analysis we identified the main phase as Hg -1212. Fig. 24 represents θ-2θ XRD patterns taken from the typical films prepared by the method I (Fig. 24a) and the method II (Fig. 24b). Only (00l) Bragg-peaks were visible, suggesting a strong texturation in the c direction. The in-plane orientation of the Hg-1212 phase was studied by ϕ-scans of the

(102) planes and compared with ϕ-scans from the CeO$_2$ buffer layer and from the sapphire (Fig. 25).
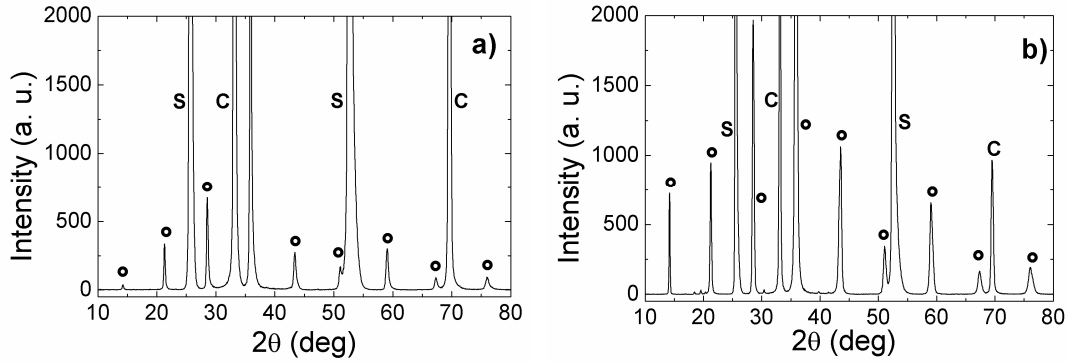
Fig. 24 XRD patterns of films prepared by the method I (a) and the method II (b). Hg-1212 phase (○), sapphire (S), CeO$_2$ buffer layer (C).
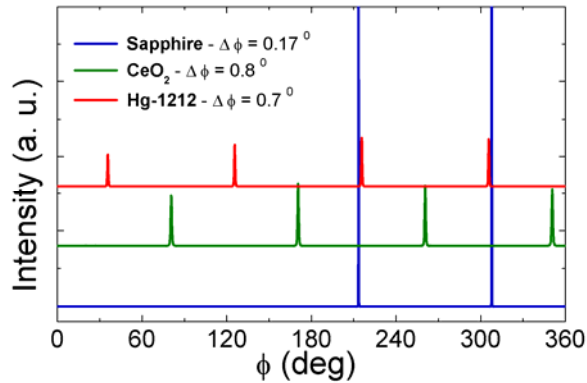
Fig. 25 ϕ-scans of the (102) plane of Hg-1212 phase, (220) plane of the CeO$_2$ and of (110) ((11$\bar{2}$0) using Miller-Bravais indexation for the hexagonal structures) plane of the sapphire.

In the ϕ-scans of the sapphire we observed two reflections corresponding to (110) and (-120) planes in a rhombohedra representation. The angle between these planes was 94° exactly as we expected from the structure. In the case of the CeO$_2$ films we detected (220), (-220), (2-20) and (-2-20) planes at 90° of each other. They are rotated by 45° with respect to the sapphire axes. The reflections of the mercury phase ((102), (-102), (012) and (0-12)) were separated 90° as it is expected and they were rotated by 45° with respect to the CeO$_2$. Using ϕ-scans we did not find big differences between the films prepared by the methods I and II.

To study the texture of these films more precisely we performed measurements of pole figures (see Fig. 26). We measured (103) plane of Hg-1212 superconducting phase. Before the measurements we determined the exact 2θ position of the (103) Bragg reflection that was $2\theta = 31.7°$. The pole figures were composed of four planes (103), (-103), (013) and (0-13) at the position $\chi = 47.5°$ (the angle ϕ depends on the position of the film on the sample holder). This agrees well with the predictions from the structure and shows a bi-axial texturation or an epitaxial growth. From these data we can extract the intensity versus ϕ for different χ values.
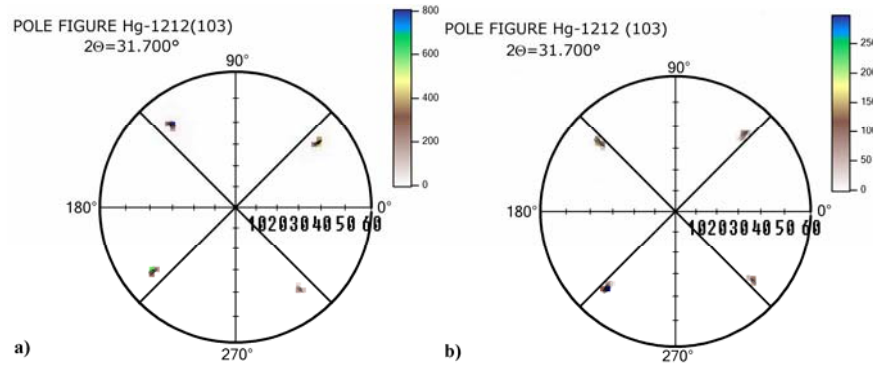
Fig. 26 Pole figures of the (103) plane for the films prepared by the method I (a) and the method II (b).

Seeing that there is no big difference in the pole figures of the films prepared by the method I and the method II, we used a more wide view which was obtained by calculating the mean value of the intensity in the interval $38°<\chi<55°$ and plot it versus ϕ. This is shown in the Fig. 27 for both sets of samples prepared by the method I (Fig. 27a) and method II (Fig. 27b).
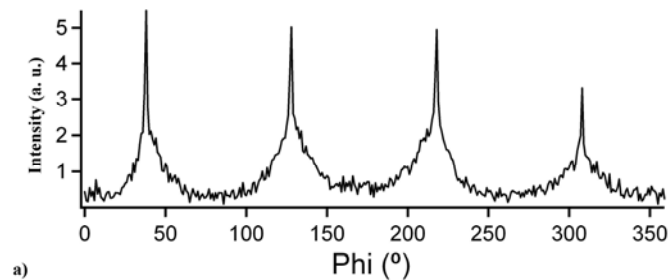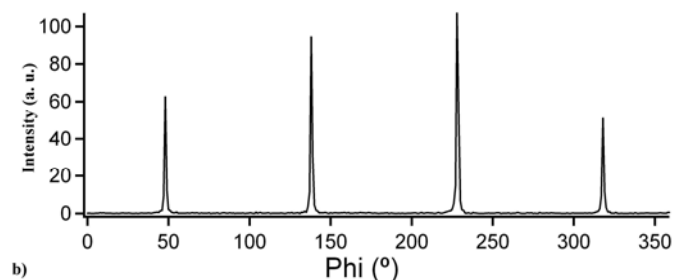
Fig. 27 Average ϕ-scan of the selected area of the mercury based superconducting films prepared by the method I (a) and the method II (b).

From these figures we evidence a significant difference between the films prepared by the methods I and II. The films obtained by mercuration without contact (method II) had thin peaks indicating a small in-plane mosaicity. The films prepared by mercuration with physical contact between the source of mercury and the precursor film (method I) had a broad foot suggesting the presence of another population of grains with weak orientation constrain (Fig. 27a). We suggest that this secondary population of grains could come from the contact with the source of mercury creating a secondary nucleation source competing with the primary one issued from the substrate interface.
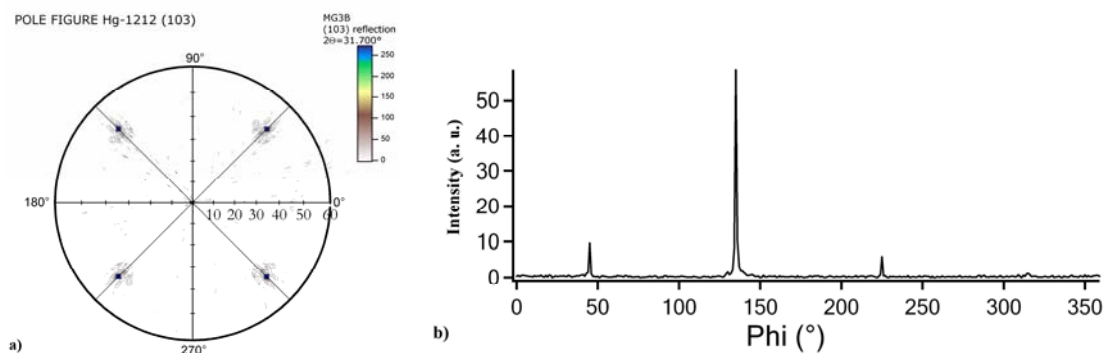
Fig. 28 Pole figures of the (103) peak of Hg-1212 phase (a) and average ϕ-scan of the selected area (b) of the very thin transparent film prepared by the method I.

The very thin translucent films were formed when the film was separated from the source of mercury to which it was bonded after the reaction. This was not systematic but occurs frequently. These films were also bi-axially textured as shown in the Fig. 28. However, the average ϕ-scans show a less pronounced foot compared with the black films prepared by

the method I (Fig. 27a). This support the idea that the upper part of the films prepared according to the method I was contaminated by a secondary population of grains originating from the mercury source.

Measurements of $R(T)$ confirmed the presence of superconducting phases. The films prepared by the method I had critical temperatures comparable with those prepared by the method II (T_{C0} = 100-115 K) (Fig. 29a). The critical temperature of the translucent films was lower (T_{C0} < 77 K) and their resistance was much higher which we attribute to their small thicknesses (Fig. 29b). The black films prepared by the method I and II had low resistance and the zero resistance can be clearly observed. Although the values of the critical temperatures are very similar, the synthesis by the method II is more reproducible than by the method I.
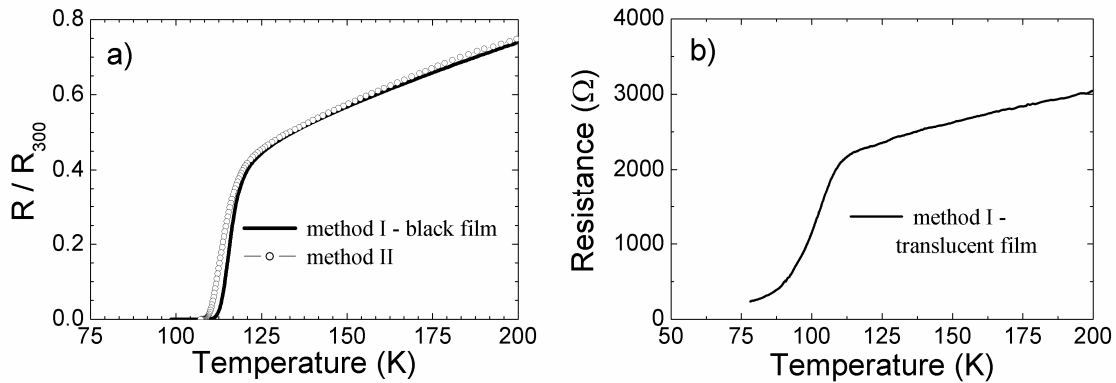
Fig. 29 $R(T)$ dependences of Hg-based films prepared by method I and method II.

EDX analysis confirmed the presence of the Hg-1212 phase in any cases. We observed also some impurities in the form of $CaHgO_2$, $Re_{2-x}Ba_4Ca_{1+y}O_{12}$ and oxides of calcium and copper. These impurities were not easy to distinguish by using XRD analysis (θ-2θ scan) because they were also textured with orientations that do not allows their measurements in θ-2θ scan (at χ = 0°) and their pattern could be hidden below the peaks of the superconducting phase or of the buffer layer and substrate.

From the SEM analysis it is possible to compare the microstructure of the film prepared by the method I and II (Fig. 30). The films, prepared by the method II are smoother than those by the method I. Moreover, the translucent films, Fig. 31, contain many impurities sticked on their surfaces.
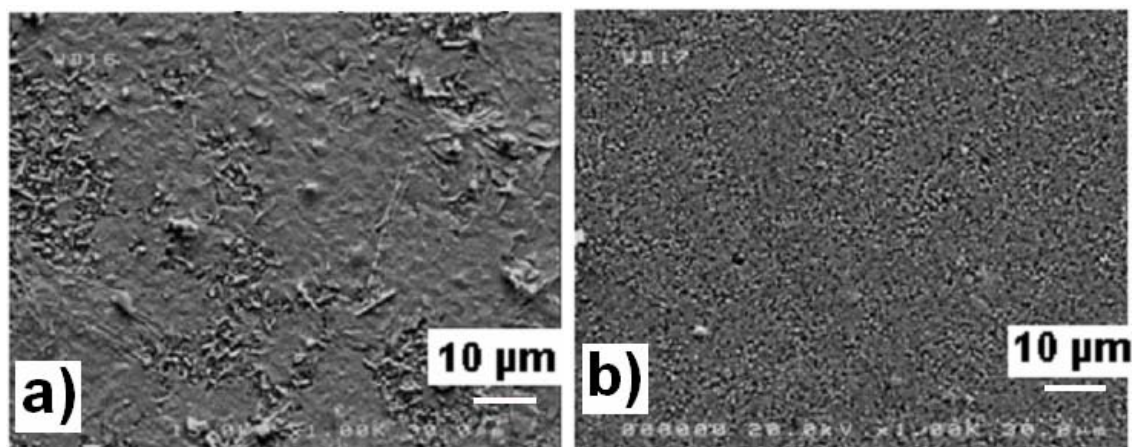
Fig. 30 SEM images of the superconducting film prepared by the method I (a) and the method II (b).
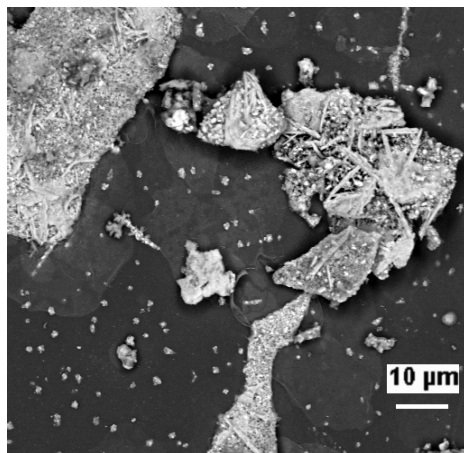
Fig. 31 SEM image of a thin translucent film prepared by the method I.

In summary

Superconducting HgBCCO films (<300 nm) were prepared by RF magnetron sputtering and ex-situ mercuration. We studied the influence of the mercuration process on the textural and electrical properties of the films. The films prepared without contact between the precursor film and the source of the mercury (method II) were bi-axially textured Hg-1212 phase which is evidence that the mercury is incorporated in the precursor film through the mercury vapour. When the films were prepared with contact between the precursor films and the source of mercury (method I), a dominating bi-axially Hg-1212 phase is also formed but another populations of grains is detected, suggesting that the contact caused the secondary nucleation centres. The critical temperatures in both methods were comparable in the range of

100-115 K. However, the method II is more reproducible thus more suitable for the preparation of thin superconducting films based on mercury for cryoelectronic applications. The formation of mercury based films by vapour phase is a quasi unique situation in high tempreture superconducting field and could be a great opportunity to prepare thin films of high quality and useful areas.

These results were published in *Physica C* **435** (2006) 31-36.

2. Magnetic characterization of HgBCCO films according to their method of preparation

The magnetic properties of the films prepared by two types of the mercuration (with (method I) and without (method II) contact between the precursor film and the source of Hg) were studied using Hall probe method with the aim to identify some differences between these two methods. These measurements allow determining the *J-E* curves, the critical current density and its dependence with the external magnetic field and its uniformity in the sample. All measurements were performed at liquid nitrogen temperature ($T = 77$ K).

The list of the measured samples is in the Tab. 3.

Sample	Sample dimensions (mm)	Film thickness (nm)	Mercuration	T_{C0} (K)
1	4×6.7	100	Contact (Method I)	118
2	5×7.0	300	Non-contact (Method II)	108
3	3×3.8	200	Contact (Method I)	98

Tab. 3 Parameters of the measured samples

The static magnetic field map B_{SZ} measured in the distance of 0.65 mm above the sample 1 in various longitudinal positions *y* is presented in the Fig. 32a. It is seen that the sample is inhomogeneous in the longitudinal direction (*y*) and the maximal magnetic field above the sample centre is relatively weak (0.13 mT). The triangular shape of the profiles indicates that the flowing currents have an intergranular character. Similar measurements for the sample 2, Fig. 32b showed larger value of magnetic fields above the sample centre (0.16 mT). The scans of the magnetic field have also the triangular shape; consequently, the intergranular currents are dominant in this sample. From the maxima of the field $B_{SZ} = f(x)$ we can determine the critical current density J_C of the persistent magnetization currents. For rectangular samples with $a > b$ we can calculate J_C as [113]

$$J_C = \frac{2\pi B_{SZ}}{\mu_0 t \ln(1 + b^2 / z_0^2)} \tag{1}$$

where t – thickness of the film, z_0 – sample to probe distance, $2b$ – width of the sample.

For disk or square shaped samples J_C is given by

$$J_C = \frac{2\pi B_{SZ}}{\mu_0 t} \left\{ \frac{-r + \ln\left[r + \left(r^2 + z_0^2\right)^{1/2}\right] \cdot \left(r^2 + z_0^2\right)^{1/2}}{\left(r^2 + z_0^2\right)^{1/2}} - \ln z_0 \right\}^{-1}$$

(2)

where r is the disk radius and z_0 is sample to probe distance.
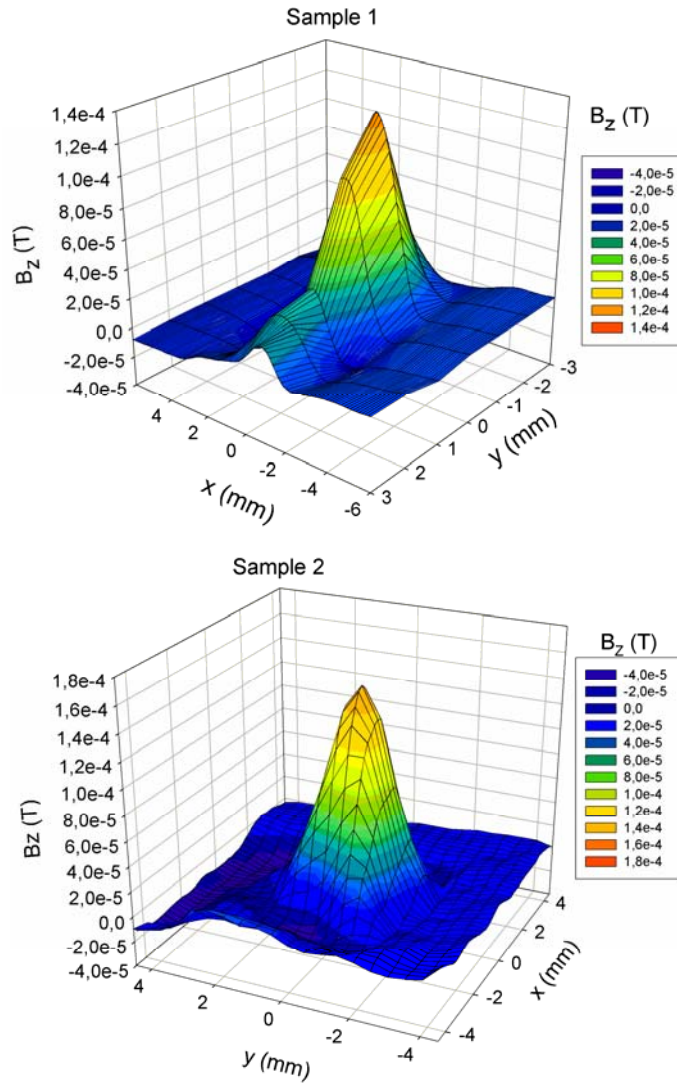
Fig. 32 Magnetic field map above sample (a) sample 1, $z_0 = 0.65$ mm, (b) sample 2, $z_0 = 0.35$ mm.

The profiles measured in the distance $z_0 = 0.25$ mm above the sample 3 are shown in the Fig. 33. As we can see, the slope of the curve $B_{sz} = f(x)$ has a local minimum above the central part of the sample. This profile is characteristics for the samples with intragranular currents. Another sign of intragranular currents is a very small field $B_{sz} \sim 0.1$ G. In comparison to the sample 2 which has typical triangular profile.

The values of the critical density in the self field were $J_C = 2.1 \times 10^5$ Acm^{-2} and $J_C = 6.75 \times 10^4$ Acm^{-2} for the samples 1 and 2, respectively. The sample 3 exhibited only intragranular currents. The J_C value was higher in the case of the film prepared by the method I (sample 1); however the film prepared by the method II (sample 2) was more homogenous than those prepared with the contact.

There is no report in the literature about the critical current densities of the Hg-based thin films prepared on the CeO_2 buffered R-plane sapphire. Only Stelzner and Schneidewind [108, 109] published the fabrication of the Hg-1212 phase on the R-plane sapphire with the CeO_2 using Tl-Hg cation exchange process. They used Tl-2212 films as the precursor films and the final films showed the critical current densities up to 6 MAcm^2 at 77 K in the self field. Our results are slightly lower but comparable to those obtained using Tl-Hg cation exchange process.

The big difference of the magnetic field profiles between the samples 2 and 3 prepared by the method I confirms our proposition that the contact mercuration is not very reproducible.
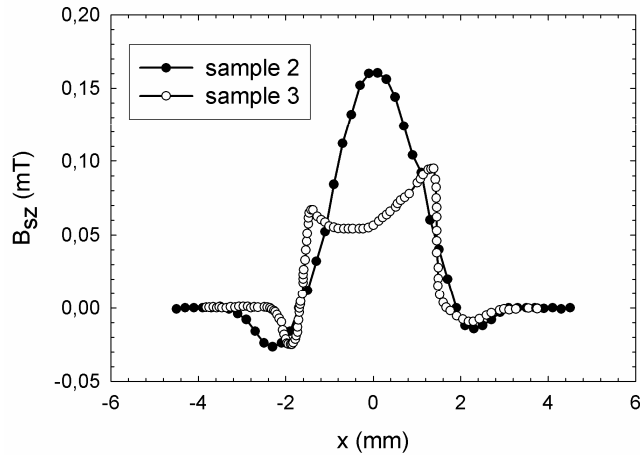
Fig. 33 The magnetic field profiles measured for the sample 2 in the distance $z_0 = 0.35$ mm and for the sample 3 in the distance $z_0 = 0.25$ mm. (The values of the magnetic field B_{sz} for sample 3 are multiplied by the factor 10).

The dynamic measurements are shown with the sample 1. The hysteresis curves $B_{sz} = f(B_e)$ measured at frequencies of the external field from 5 mHz up to 100 mHz with the amplitude of 70 mT, are shown in the Fig. 34. The width of the hysteresis curves increases with the increasing frequency. The Hall probe-superconducting layer distance was $z_0 = 0.8$ mm. The deformation of the magnetization loop is caused by the Hall probe nonlinearity. The width of the curves is not affected by this effect. We see the weak frequency dependence of B_{sz} in the interval of 20 – 100 mHz.

The induced current density can be calculated using Eq. (1) replacing B_{sz} by $\Delta B/2$. The corresponding electric field E in the sample is determined by the frequency f of the external field [113]

$$E = 4fbB_{max}. \tag{3}$$

Choosing several values of B_e (e.g. 0, 30, 60 mT) in the Fig. 42 and determining the width of the magnetization curve ΔB at these fields we can determine the current density J.
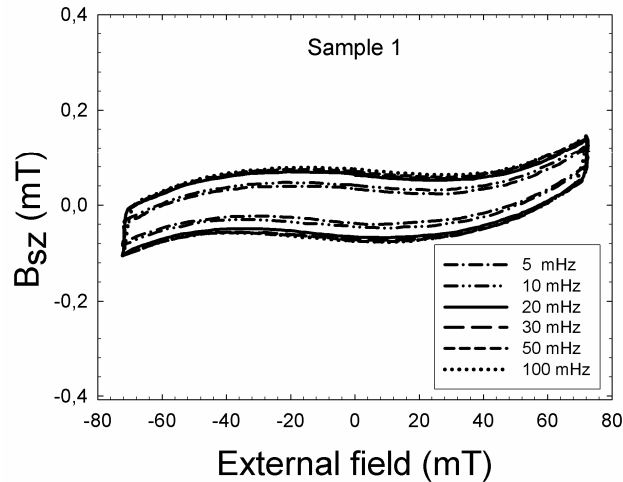
Fig. 34 Hysteresis loops $B_{sz} = f(B_e)$ of the sample 1 for various frequencies of the triangular external magnetic field. The distance $z_0 = 0.8$ mm. ΔB - width of the magnetization loop.

From the set of the calculated values (J,E) we obtained $E = f(J)$ characteristics with B_e as a parameter, see the Fig. 43. In the case of the sample 1 we have observed resistive parts on the curves at all magnetic external fields (0, 30, 60 mT). To determine J_C we extrapolated the values of E for the criterion 1 µV/cm in the Fig. 35. The normalized values of $J_C(B)/J_C(0) = f(B)$ with $J_C(0) = 2.1 \times 10^5$ Acm^{-2} are shown in the Fig. 36. The critical current density of the sample 1 in $B_e = 70$ mT is 60 % of $J_C(0)$.
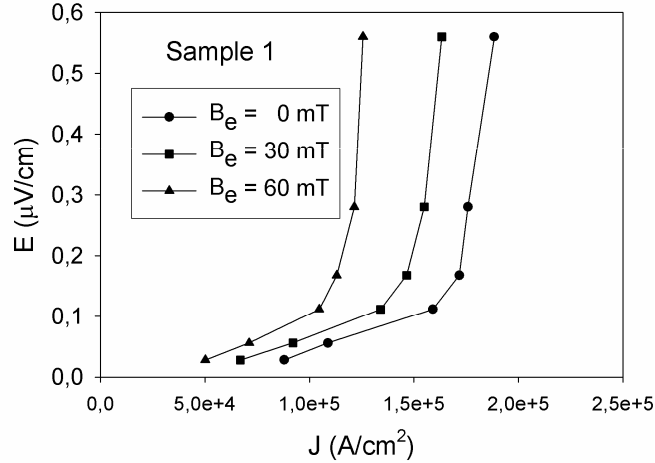
Fig. 35 *J-E* characteristics of the sample 1 determined from the measured hysteresis loops for magnetic fields 0, 30 and 60 mT at 77 K.
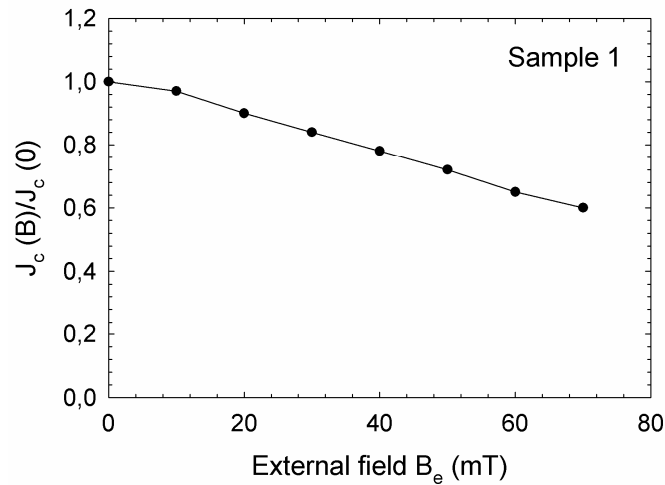
Fig. 36 Normalised $J_C(B)$ characteristics for magnetic fields from 0 to 70 mT for the sample 1, the value of $J_C(0) = 2.1 \times 10^5$ A/cm^2, J_C criterion 1 μV/cm.

In summary

Using the Hall probe method in the static regime (persistent magnetization currents) we determined the critical current density in the self field $J_C = 2.1 \times 10^5$ Acm^{-2} and $J_C = 6.75 \times 10^4$ Acm^{-2} for the samples 1 and 2, respectively. The sample 3 exhibited only intragranular currents. This method confirmed a better homogeneity of the samples prepared by the non-contact mercuration. By the measurement in the dynamic regime we determined *J-E* curves of the sample 1 at various magnetic fields with an electric field sensitivity of the

order of 10 nV/cm. Large resistive sections on *J-E* curves of the sample 1 were observed. This behaviour indicates either the presence of defects or the dependence of intergranular contact resistances on the electric field. From the shape of hysteresis loops and *J-E* curves we can conclude that the conductivity of the grains in the superconducting layer depends on the electric field in the sample. The uniformity of the film can be determined from the shape of the measured magnetic field profiles and their amplitudes. The described non-destructive method does not require any electrical contacts on the sample surface and it overcomes the problems with contacting of thin films.

These results were published in the *Physica C* **435** (2006) 41-46.

3. Influence of the partial pressure of mercury on the film synthesis using non-contact mercuration

Syntheses of the Hg-based superconductors are usually performed in the one-zone configuration where the starting materials (HgO and Ba-Ca-Cu-O precursor) are kept at the same temperature. Two-zone technique with independent control of the precursor and HgO source temperatures was used for the preparation of the Hg-1201 phase only [13]. In this case Hg source and the precursor material were placed in the zones with different annealing temperatures and the superconducting phase was formed by vapour-solid reaction. Some groups reported the use of the two pellets (Hg-free (Re)-Ba-Ca-Cu-O and unreacted Hg,Re-Ba-Ca-Cu-O) for the mercuration to obtain a stable mercury vapour flow [87, 93, 94]. To the best of our knowledge, no publication reports on the preparation of the higher superconducting phases (Hg-1212, Hg-1223) by vapor-solid reaction using the mercuration with no contact between the precursor film and the source of mercury as it was used in our experiments. In this chapter we report the influence of the partial pressure of mercury on the preparation and properties of the Hg(Re)-based films prepared using no contact method.

The mercuration was performed using non-contact mercuration (see chapter 2.1). We studied the influence of the partial mercury pressure pHg on the properties of the final films. We tried to keep the partial pressure of oxygen constant by using the same amount of the HgO in the pellet source in every experiment so the partial mercury pressure was changed by the different amount of the liquid mercury in the sealed quartz tube. The synthesis temperature and annealing time were in the range 800 – 830 °C and 2 - 24 h, respectively.

First, the experiments with a low amount of Hg about 0.001 mol/cm^3 (low partial pressure of mercury) were performed. The synthesis temperature was 800, 820, 830 °C and time 2, 4 and 6 h.

At 800 °C, we obtained c-axis oriented Hg-1212 phase. The increase of the annealing time lead to the better c-axis orientation of this phase (Fig. 37). From the positions of the Bragg (00l) peaks we calculated c-parameter of the Hg-1212. The value of this parameter increased with rising time of the mercuration (c = 1.2508 nm for 2 h, c = 1.2553 nm for 6 h). In the XRD patterns we observed also diffractions of some parasitic phase. We suppose that these peaks belong to the rhenium containing phase $Re_{2-x}Ba_4Ca_{1+y}O_{12}$ with monoclinic structure (a = 5.771 nm, c = 28.0 nm) (Fig. 38) [92]. The details of the structure are in the Annexe. Only (00l) diffractions are visible in the XRD pattern so this phase is also textured

and its amount decreases with increasing time of the mercuration. The *c*-parameter increased with the annealing time which could be caused by the better development and crystallization of the film after longer synthesis time so the films are more relaxed and their parameters are closer to those of the bulk samples. However, *c*-parameter is smaller than in the case of unsubstituted Hg-1212 phase which is caused by incorporation of more rhenium to the superconducting phase with increasing time of the mercuration and thus insertion of additional oxygen in the structure. Chmaissem *et al.* [16] reported that the Re substitution brings four additional oxygen atoms into the structure. The linear decrease of *c*/*a* is consistent with the increase in the amount of the smaller Re atoms at the Hg sites.

We did not detect any other impurities in the prepared samples which suggest that they are textured and their peaks could have the same positions as the peaks of the superconducting phase or peaks of the substrate and buffer layer so they are difficult to detect by XRD analysis in *θ-2θ* configuration.

Fig. 37 XRD patterns of the films prepared at 800 °C with the amount of mercury about 0.001 mol/cm^3. Hg-1212 phase (**o**), Re-phase (⊗), sapphire (S), CeO$_2$ buffer layer (C).

Fig. 38 Basic cell of the $Re_{2-x}Ba_4Ca_{1+y}O_{12}$ compound.

Measurements of the *R(T)* dependences of the prepared films confirmed the presence of the superconducting phase. However, critical temperatures of the films annealed during 2 and 4 h are reduced probably due to the insufficient crystallization of the Hg-1212 and non-superconducting Re-phase (Fig. 39). The increase of the transition temperature is evident with the increase of annealing time due to the increased oxygen content in the superconducting phase [67].
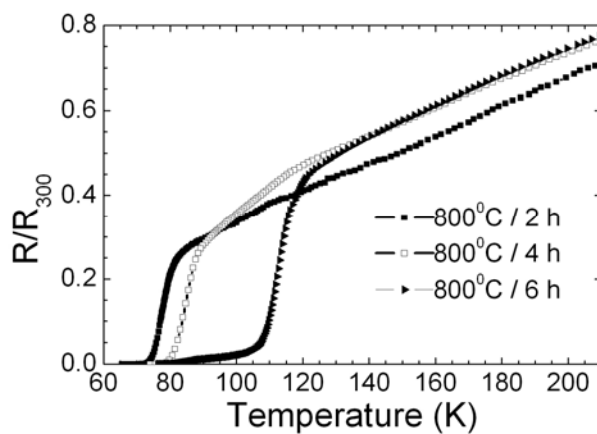
Fig. 39 *R*(*T*) dependences of the films prepared at 800 °C with the amount of mercury about 0.001 mol/cm^3.

Using mercuration at 820 °C with a small amount of the mercury (0.001 mol/cm^3) in the reaction system we obtained similar results as at 800 °C. Applying longer annealing time Hg-1212 phase was better crystallized and the amount of Re-phase decreased. After 6 hours of the mercuration this phase completely disappeared.

The values of the critical temperature were higher as in the case of the mercuration at 800 °C (T_{ON} up to 126 K, T_{C0} up to 107 K). This confirmed the growth of the films with better intragranular and intergranular properties (Fig. 40).
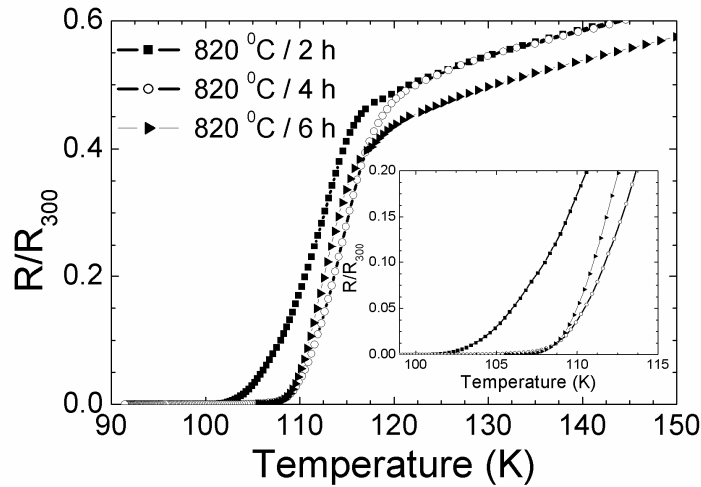
Fig. 40 *R(T)* dependences of the films prepared at 820 °C with the amount of mercury about 0.001 mol/cm^3.

For the mercuration at 830 °C we used only annealing time 2 and 4 hours because at this temperature the risk of the explosion is higher than at lower temperatures. At this temperature we risk also the reaction of the CeO_2 buffer layer with the precursor film and formation of the $BaCeO_3$ or another non-superconducting phase. Already after 2 hours of annealing we obtained pure *c*-axis oriented Hg-1212 superconducting phase (Fig. 41). This suggests that at a low content of the mercury in the reaction system (0.001 mol/cm^3) the formation of the parasitic phase containing rhenium can be avoided by using the higher annealing temperature. After 4 hours of the mercuration, the prepared films contained *c*-axis oriented Hg-1212 phase of good crystallinity with relatively high values of the critical temperatures (T_{ON} up to 131 K, T_{C0} up to 105 K) (Fig. 42).
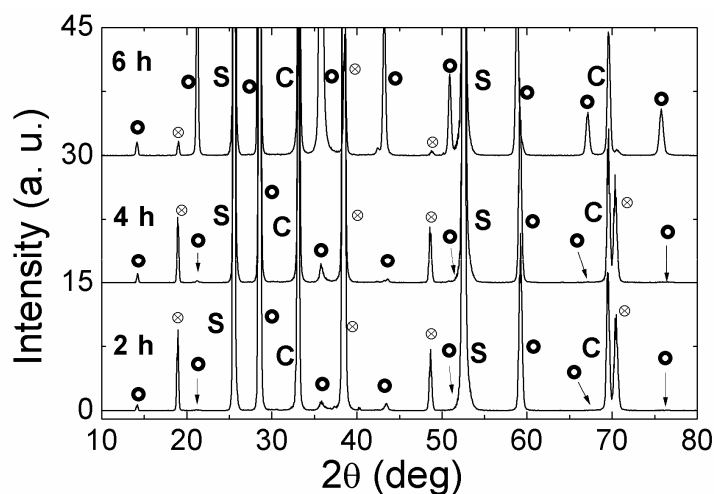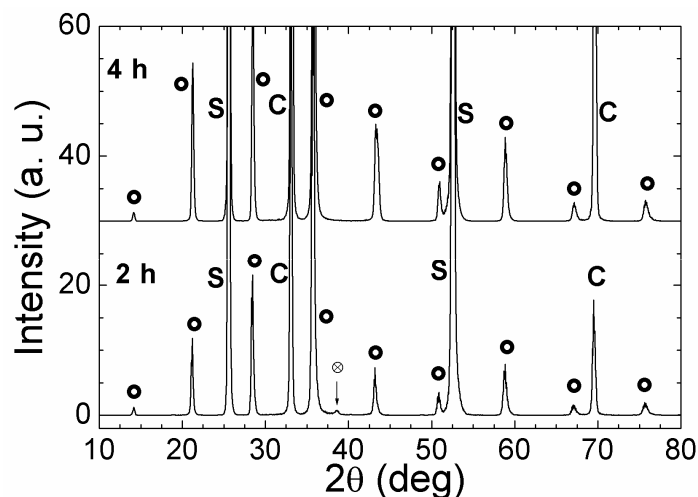
Fig. 41 XRD patterns of the films prepared at 830 °C with the amount of mercury about 0.001 mol/cm^3. Hg-1212 phase (o), Re-phase ($\otimes$), sapphire (S), CeO$_2$ buffer layer (C).
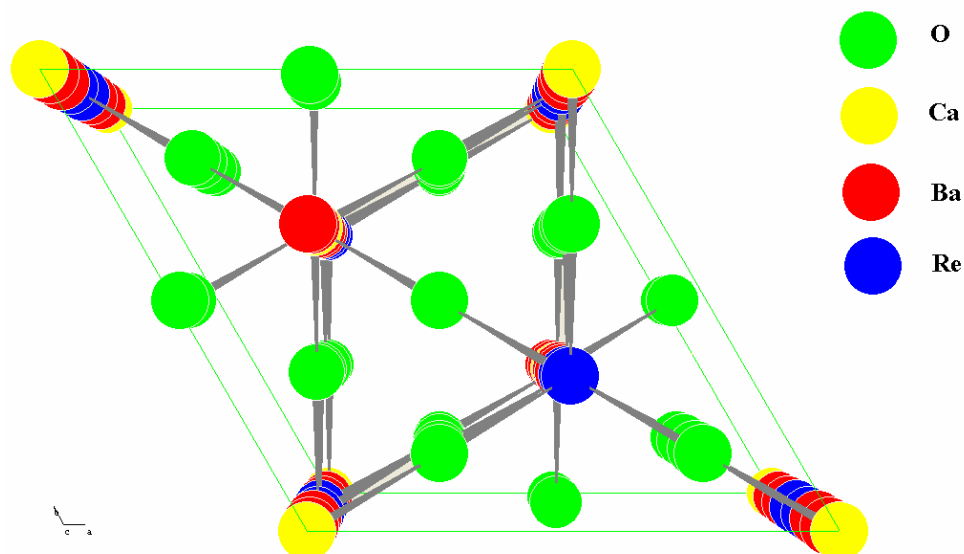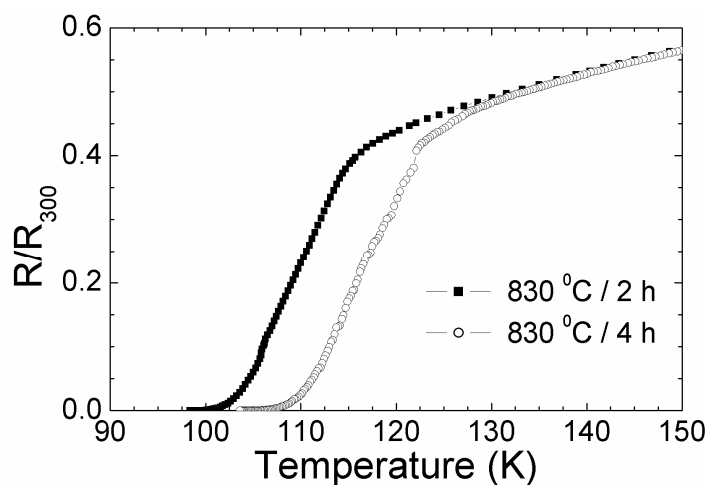

Fig. 42 $R(T)$ dependences of the films prepared at 830 °C with the amount of mercury about 0.001 mol/cm^3.

Then we started experiments with a higher content of the mercury in the reaction system so we increased the mercury pressure in the sealed quartz tube. We performed mainly experiments at 800 °C to prevent the explosion of the quartz tube. In the Fig. 43 we can see XRD patterns of the samples prepared at 800 °C / 5 h with different amounts of mercury in the quartz tube ($1.04 \times 10^{-3} - 1.77 \times 10^{-3}$ mol/cm^3).
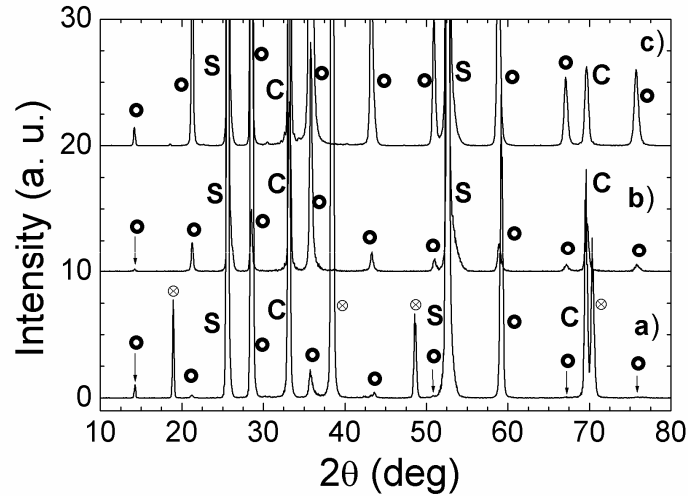
Fig. 43 XRD patterns of the films prepared at 800 °C / 5 h with different amounts of mercury: 1.04×10^{-3} mol/cm^3 (a), 1.26×10^{-3} mol/cm^3 (b) and 1.77×10^{-3} mol/cm^3 (c). Hg-1212 phase (o), Re-phase (⊗), sapphire (S), CeO$_2$ buffer layer (C).

At the low amount of the mercury 1.04×10^{-3} mol/cm^3 c-axis oriented Hg-1212 and Re-containing phase is formed. Addition of the further mercury inhibited the creation of the parasitic Re-based phase and supported the growth of the superconducting phase. This suggests that the increase of the mercury content in the reaction system improves the kinetics of the Hg-1212 formation and consequently its combination with Re-based phase $Re_{2-x}Ba_4Ca_{1+y}O_{12}$. In all cases Hg-1212 phase was also bi-axially aligned (see ϕ-scans in the Fig. 44) with $\Delta\phi < 1°$. Also the values of the critical temperatures T_{C0} increased up to 115 K (Fig. 45).
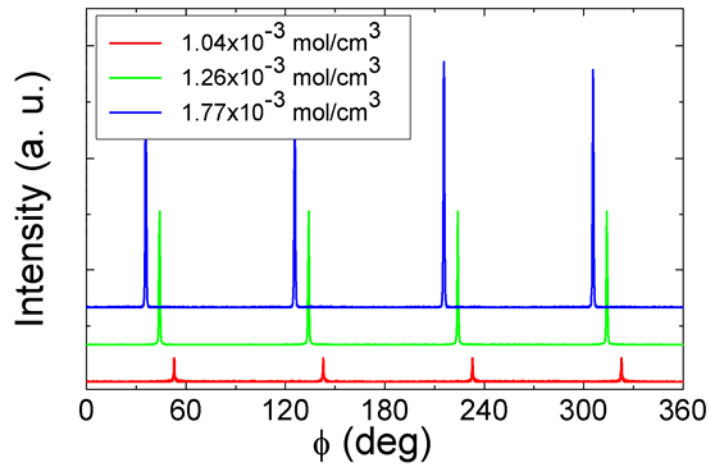
Fig. 44 ϕ-scans of the films prepared at 800 °C / 5 h with different amounts of mercury.
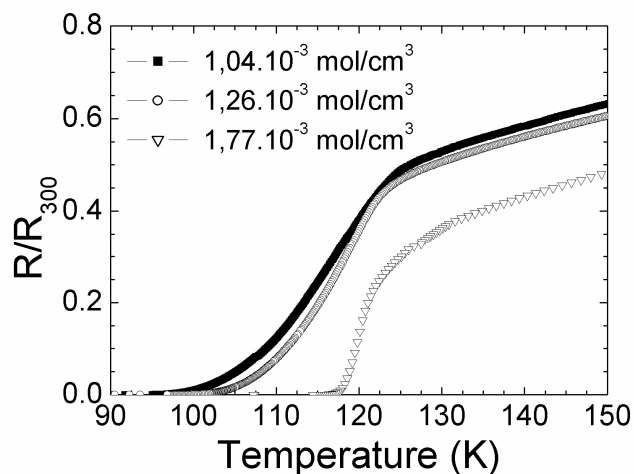
Fig. 45 *R*(*T*) dependences of the films prepared at 800 °C / 5 h with different amounts of mercury.

Increasing of the amount of the mercury in the reaction system leads to the formation of the Hg-1212 pure phase without parasitic Re-containing phase so it had the same effect as elevated temperature during the mercuration without the risk of the reaction between the CeO_2 buffer layer and the precursor film.

Then we studied the influence of the length of the mercuration with a higher amount of the mercury on the properties of the final films. The precursor films were mercurated 12 and 24 h at 800 °C. We observed that the prolongation of the annealing time caused the degradation of the superconducting Hg-1212 phase (Fig. 46) ((00*l*) Bragg peaks of the Hg-1212 phase were not so pronounced, probably due to the formation of the $BaCeO_3$ or another phase), however, the critical temperature values were similar to those prepared after 5 h annealing (Fig. 47). From this we can conclude that with a higher amount of the mercury 5 hours of the mercuration annealing are sufficient for the formation of the good quality Hg-1212 films on the CeO_2 buffered R-plane sapphire.
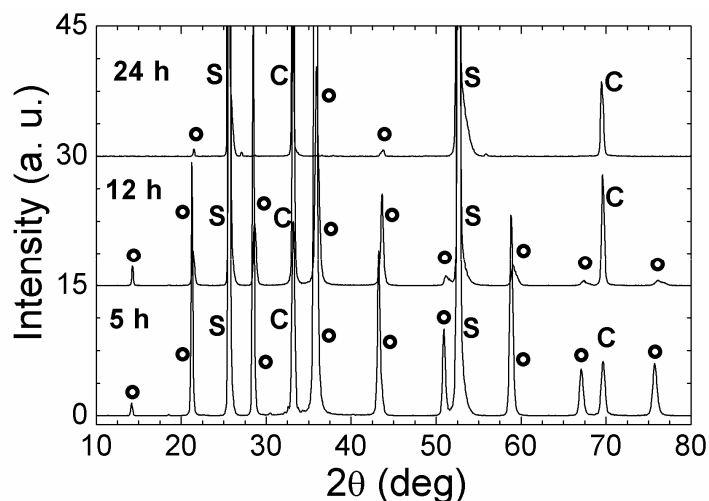
Fig. 46 XRD patterns of the films prepared at 800 °C during 5, 12 and 24 h with a higher amount of mercury ($\sim 1.9 \times 10^{-3}$ mol/cm^3). Hg-1212 phase (o), sapphire (S), CeO$_2$ buffer layer (C).
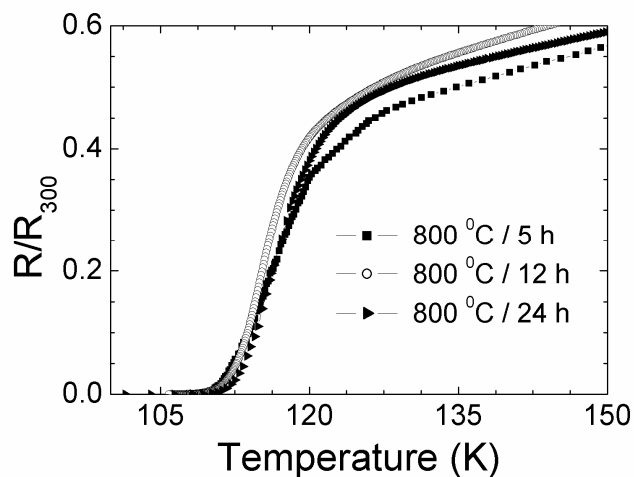
Fig. 47 $R(T)$ dependences of films prepared at 800 °C with a higher amount of mercury ($\sim 1.9 \cdot 10^{-3}$ mol/cm^3).

From the SEM analysis we can compare the microstructure of the films prepared at the same conditions (800 °C / 5 h) with a different amount of the mercury in the reaction system (Fig. 48). The films prepared with the higher mercury content are smoother than those prepared with the smaller amount of the mercury in the reaction system and contain less impurities.
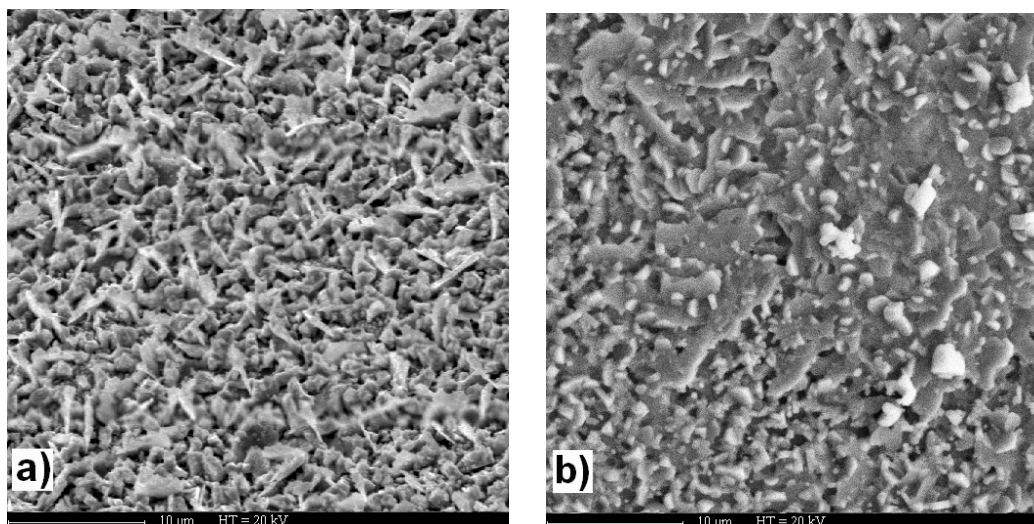
Fig. 48 SEM images of the superconducting film prepared with different amounts of the mercury in the reaction system: a) 1.0×10^{-3} mol/cm^3, b) 1.8×10^{-3} mol/cm^3.

In summary

Thin superconducting Hg-based films were prepared on the R-plane sapphire with the CeO$_2$ buffer layer by a two step process which involves RF magnetron sputtering of the amorphous precursor and ex-situ mercuration in sealed quartz tube. The films were prepared by the mercuration without contact between the source of the mercury and the precursor film so the superconducting phase is formed thanks to the mercury vapour. We studied the influence of the amount of the mercury in the reaction system on the structural and electrical properties of the final films. At 800 ºC using low amount of the mercury the textured parasitic phase Re$_{2-x}$Ba$_4$Ca$_{1+y}$O$_{12}$ is formed. The amount of this phase decreased with longer time of the mercuration and higher annealing temperature. The use of the higher amount of the mercury inhibited the creation of this phase and also advanced the formation of the superconducting phase and improved the critical temperatures in the prepared films; however, higher amount of the mercury (higher pHg) did not provide the formation of the Hg-1223 phase on the CeO$_2$ buffered R-plane sapphire in our experimental conditions.

These results were published in the *Central European Journal of Physics* **5** (2007) 446-456.

4. Influence of the CeO₂ buffer layer on the properties of the thin superconducting films based on mercury

The substrate and the buffer layer plays important role in the formation of the thin films. One of the most important factors is the lattice mismatch ε between the film and the substrate (buffer layer). If the lattice mismatch is too high ($\varepsilon > 15$ %), often no texturation is obtained in the film. The *c*-axis oriented or epitaxial (oriented also in the *a-b* plane) films could be obtained when the lattice mismatch is smaller than 15 %. De Barros et *al*. [93] studied the influence of the substrate on the growth of the HgBCCO films. They used LAO (010) and MgO (001) substrates with the lattice mismatch with the Hg-1212 phase are 1.4 % and -8.7 %, respectively. They found out, that on the LAO, the Hg-1212 was formed while on the MgO, the main phase was the Hg-1223 obtained. This suggests that the substrate plays very important role in the phase formation of the Hg-based superconducting phases.

In our experiments we used CeO₂ buffered R-plane sapphire substrate. The lattice mismatch between the Hg-phase and the CeO₂ is only 0.3 %. Although we used a Ba:Ca:Cu = 2:2:3 precursor, only Hg-1212 phase was present in our films. This is in agreement with the work of De Barros et *al*. [93]. When the lattice parameters of the film and the substrate (buffer layer) are very close, 2D growth is favourable and epitaxial Hg-1212 phase is formed. As the used buffer layer is epitaxial having no disorder in the structure the material needed for the following formation of the Hg-1223 phase (Ca, Cu, O) is excluded on the top of the film and higher superconducting phase could not be created. We suppose that the quality of the buffer layer can strongly influence the properties of the final films. To the best of our knowledge, there is no publication studying this issue.

In this section we report the study of the influence of the thickness of the buffer layer on the structural and electrical properties of the Hg-based superconducting films.

First, the CeO₂ buffer layers with different thickness (10, 70 and 120 nm) were prepared using RF magnetron sputtering as described previously (see chapter 1.3 in this section). In the Figs. 49-51 we can see the results from the XRD analyses. In the θ-2θ scan (Fig. 49) we observed only (00*l*) diffractions of the CeO₂ in all cases which suggests 2D (layer by layer) growth of the buffer layer. The intensity of the peaks increased with the film thickness. Bragg peaks of the very thin buffer layer (10 nm) are shifted and enlarged due to the large mismatch between the substrate and the buffer layer and the films are constrained.

The strain in the film decreases with the increasing thickness and the lattice parameter decreases, too. The formation of the domains is possible in the case of the thicker films.
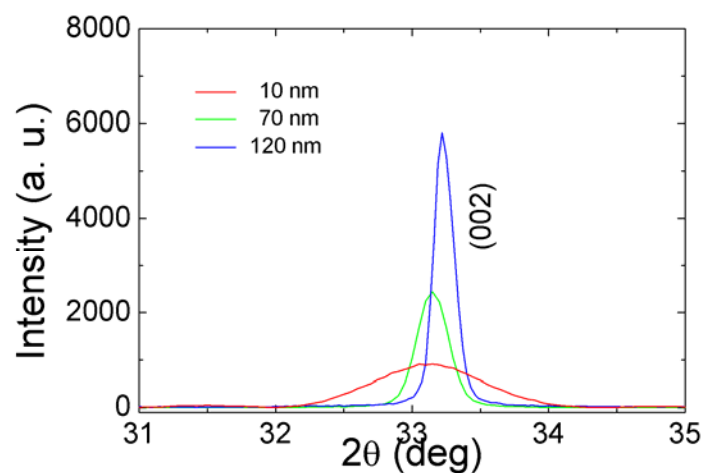
Fig. 49 (002) reflection of the CeO_2 films with the different thickness.

The ω-scans confirmed c-axis orientation of the CeO_2 films. The FWHM depends on the film thickness and increases with the increased thickness. The ω-scan (Fig. 50) is sensitive to the out-of-plane mosaicity and to the width of the domains [122]. From the Fig. 49 we can see that we have two populations of the grains in the thicker films. This suggests that in the very thin film the mosaicity is very small and it increases with the film thickness so the domains are formed. The ϕ-scans (Fig. 51) suggest also the texturation in *a-b* plane with (FWHM) $\Delta\phi = 0.2 - 1°$.
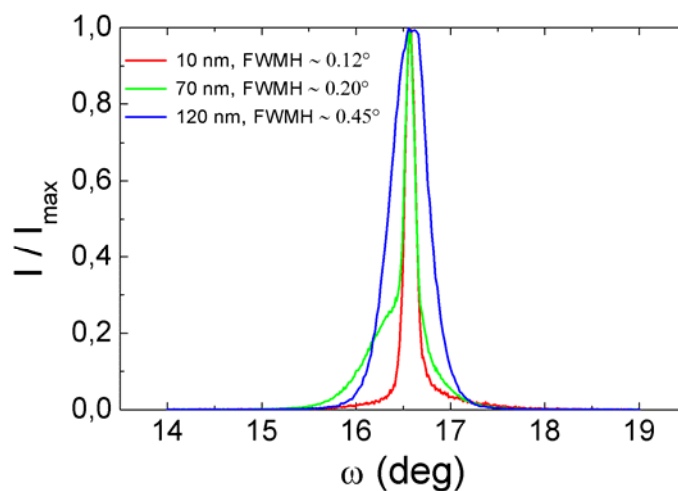
Fig. 50 ω-scans of the CeO_2 films with the different thickness.
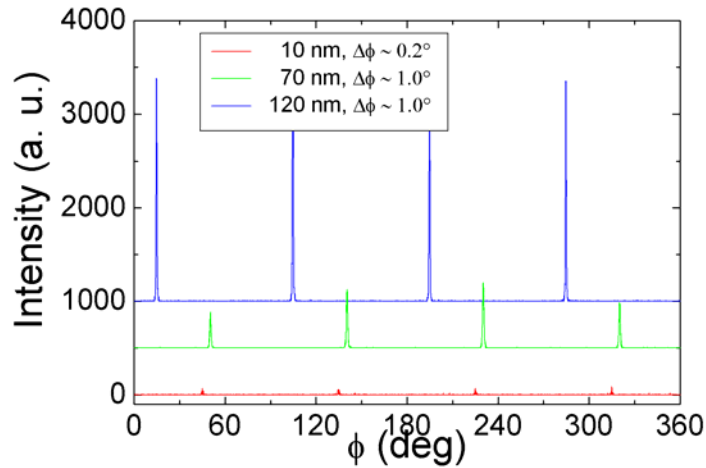
Fig. 51 ϕ-scans of the CeO$_2$ films with the different thickness.

The precursor films (300 nm thick) with the nominal composition of Re$_{0.15}$Ba$_2$Ca$_2$Cu$_2$O$_x$ were deposited by RF magnetron sputtering on the R-plane sapphire substrates with the different thicknesses of the CeO$_2$ buffer layer. Precursor films were then mercurated using non-contact mercuration (described in the Chapter 2.1) with the total amount of mercury about 1.7×10^{-3} mol/cm^3. The synthesis temperature and time were 800 ºC and 3-5 h, respectively.

First, the precursor films deposited on the sapphire with the CeO$_2$ buffer layer of different thickness were mercurated at 800 ºC / 3 h. We obtained the mixture of the *c*-axis oriented Hg-1223, Hg-1212 and intergrowth phase with the majority of the Hg-1223 (Fig. 52) in all cases, however, the ratio between the phases was different. Using the precursor film on the thinnest CeO$_2$, Hg-1223 phase was in majority. The amount of the Hg-1223 phase decreased with the increasing thickness of the buffer layer.

The results of XRD analyses suggest that very thin buffer layer is suitable for the formation of the Hg-1223 phase. When the CeO$_2$ is very thin ($\sim$ 10 nm), it is constrained (not relaxed) and thus enables the formation of the Hg-1223 due to the diffusion (intercalation) of the Ca-Cu-O dislocations into the grains of the Hg-1212 and consequent transformation to the Hg-1223 [28]. In the case of the thicker CeO$_2$ (70, 120 nm), the buffer layer is relaxed and the Ca-Cu-O material is excluded on the top of the film during the formation of the Hg-1212 phase and does not have access to the Hg-1212 grains to form Hg-1223 phase.
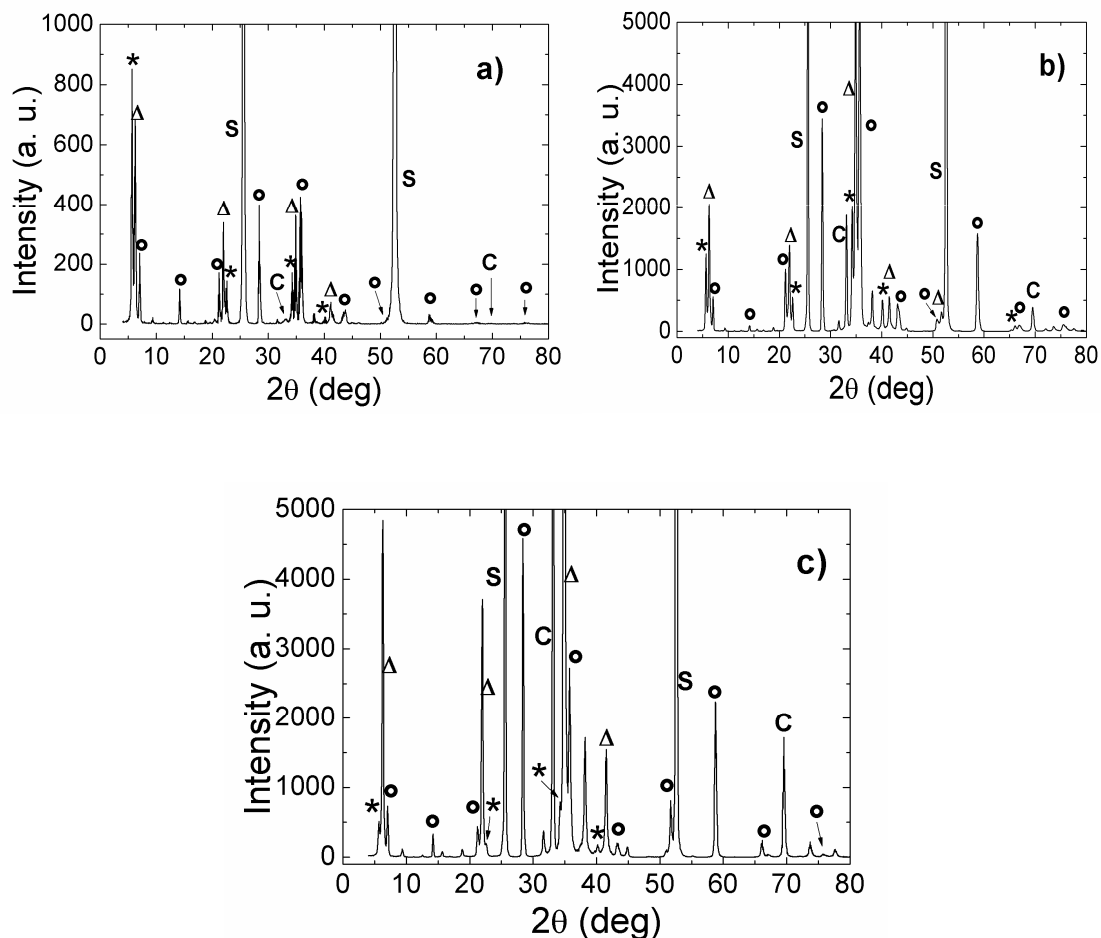
Fig. 52 XRD patterns of the films mercurated 800 ºC / 3 h with the 10 nm (a), 70 nm (b) and 120 nm (c) thick CeO_2 buffer layer. oHg-1212 phase, ★ Hg-1223 phase, Δ intergrowth phase, S-substrate, C-CeO_2.
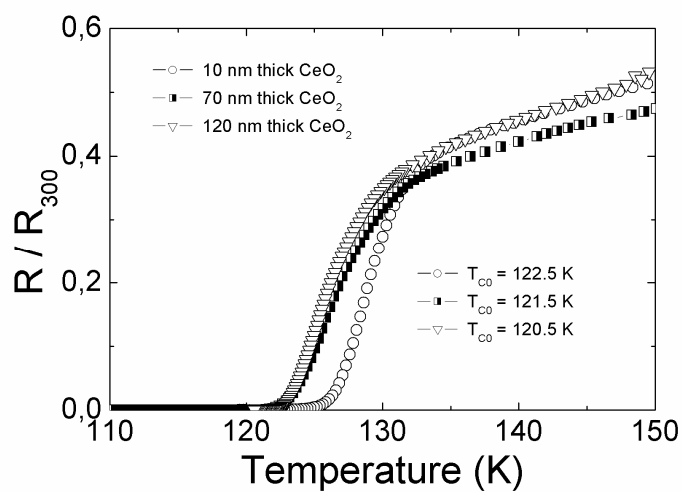
Fig. 53 $R(T)$ dependence of the film mercurated 3 h with the 10, 70 and 120 nm thick CeO_2 buffer layer.

The critical temperatures of the films prepared after 3 h mercuration were very close (Fig. 53), however, the highest T_{C0} had sample containing the majority of Hg-1223 phase prepared on the thinnest CeO_2 (T_{C0} = 122.5 K) which is in agreement with XRD analyses.

The prepared films were studied also by SEM. The images of the samples prepared by 3 h mercuration on the substrate with the different thicknesses of the CeO_2 are in the Fig. 54. The film prepared on the thinnest buffer layer contains fewer impurities comparing to the films prepared on the thicker buffer layer. If we suppose that the precursor film had the composition Ba:Ca:Cu = 2:2:3, we suggest that this could be due to the higher content of the Hg-1223 phase in the sample.
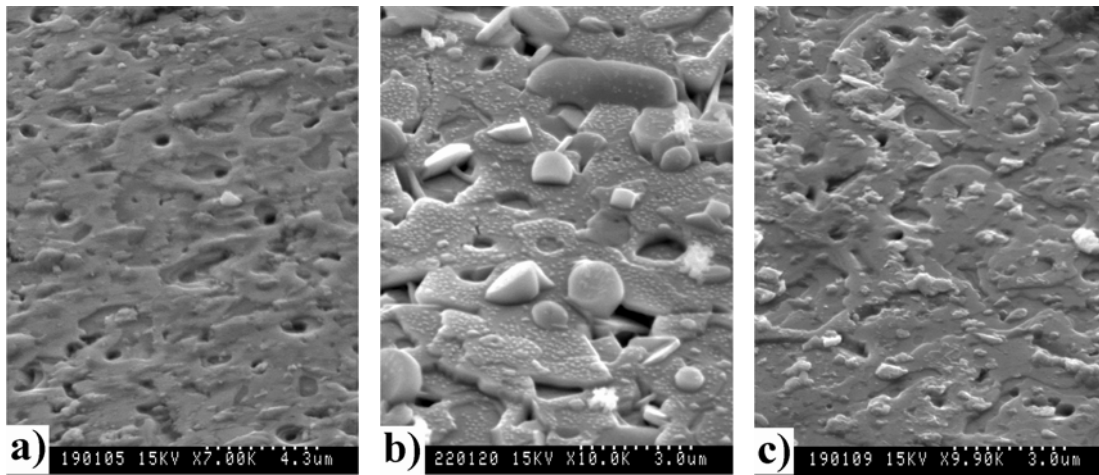
Fig. 54 SEM images of the Hg-based superconducting films with the 10 nm (a), 70 nm (b) and 120 nm (c) thick CeO_2 buffer layer mercurated 3 h.

The current density of the prepared films was estimated from the magnetic measurements using the Hall probe method. In the Fig. 55 we can see the dependence of the critical current density determined from the magnetic measurement on the external magnetic field at 77 K for the films prepared by the 3 h mercuration on the buffer layers with different thickness. The values of the critical current density are comparable for all samples. The highest value has the film prepared on the thickest CeO_2 suggesting that this film was the most compact and homogenous and the impurities on the top of this film did not influence the superconducting properties of the final films.
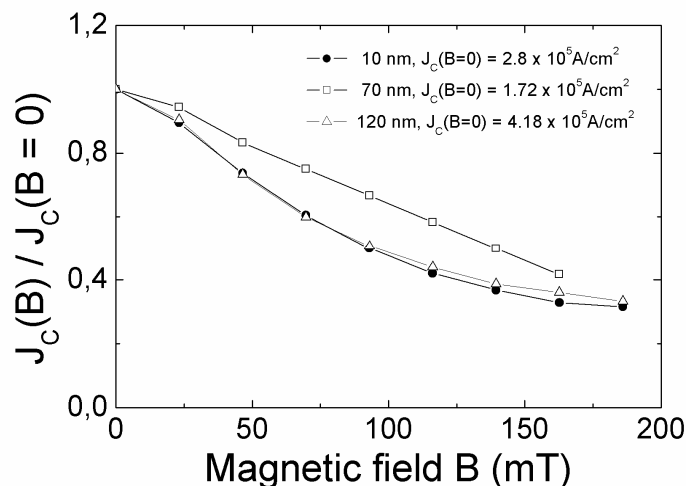
Fig. 55 Dependence of the critical current density determined from the magnetic measurement on the external magnetic field at 77 K for the films prepared by the 3 h mercuration on the buffer layers with different thickness.

Then we performed the same experiments with prolonged annealing time (5 h).
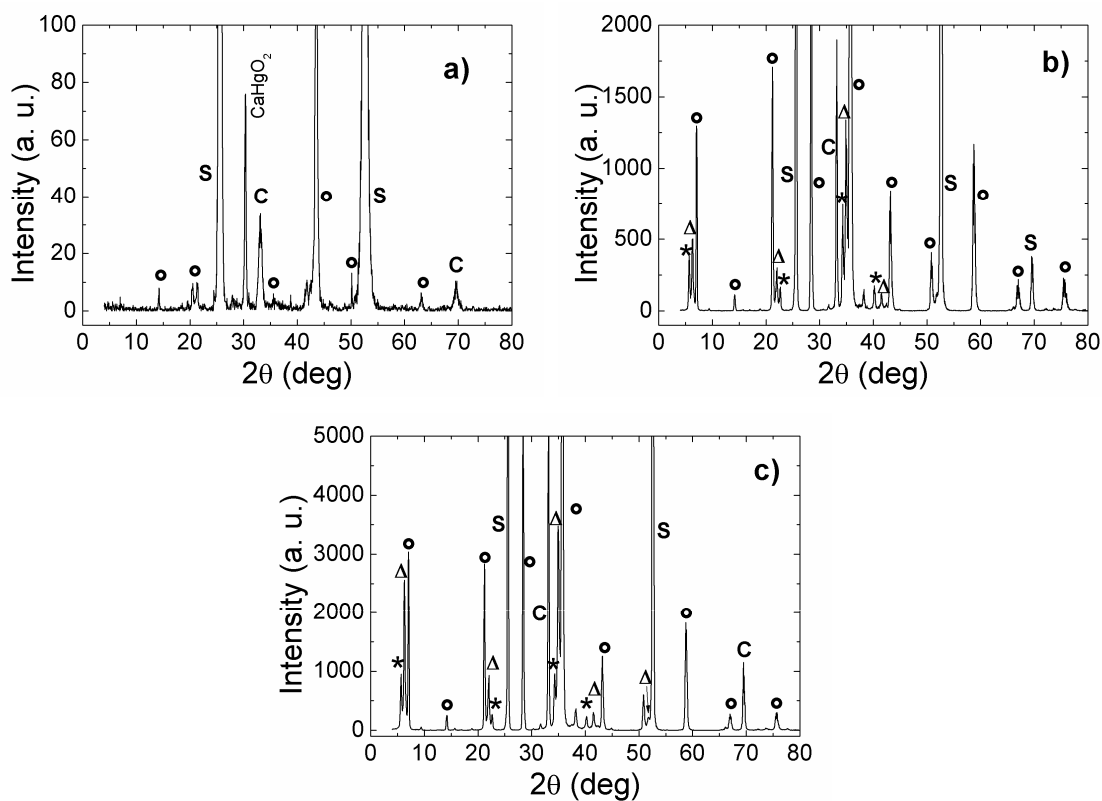
Fig. 56 XRD patterns of the films mercurated 5 h with the 10 nm (a), 70 nm (b) and 120 nm (c) thick CeO$_2$ buffer layer. ○Hg-1212 phase, ★ Hg-1223 phase, Δ intergrowth phase, S-substrate, C-CeO$_2$.

From the XRD patterns (Fig. 56) we can see that also the annealing time of the mercuration had an influence on the phase composition of the prepared Hg-based films. In the case of the films prepared on very thin buffer layer after 5 h mercuration the films contained only Hg-1212 phase with the low intensity probably due to the degradation of the buffer layer caused by the longer annealing time. Using thicker CeO_2 the amount of the Hg-1212 phase increased after 5 h mercuration. Longer annealing time decreased the amount of the Hg-1223 superconducting phase.

In the Fig. 57 we can see the $R(T)$ dependences of the Hg-based films after 5 h mercuration. Critical temperature T_{C0} decreased with the annealing time. This could be caused by the lower amount of the Hg-1223 phase in the final film. The film prepared on the sapphire with the 10 nm thick CeO_2 was not superconducting.
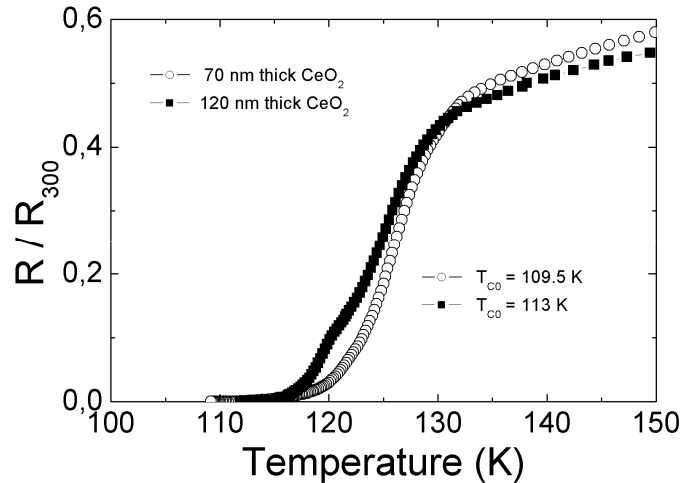
Fig. 57 $R(T)$ dependences of the film mercurated 5 h with the 10, 70 and 120 nm thick CeO_2 buffer layer.

Longer time of the mercuration had changed also the morphology of the final films. From the SEM micrographs (Fig. 58) we can see that we obtained films containing larger grains especially in the case of the film on the thickest buffer layer. However, on the top of the films we observed more impurities due to the lower content of the Hg-1223 phase.
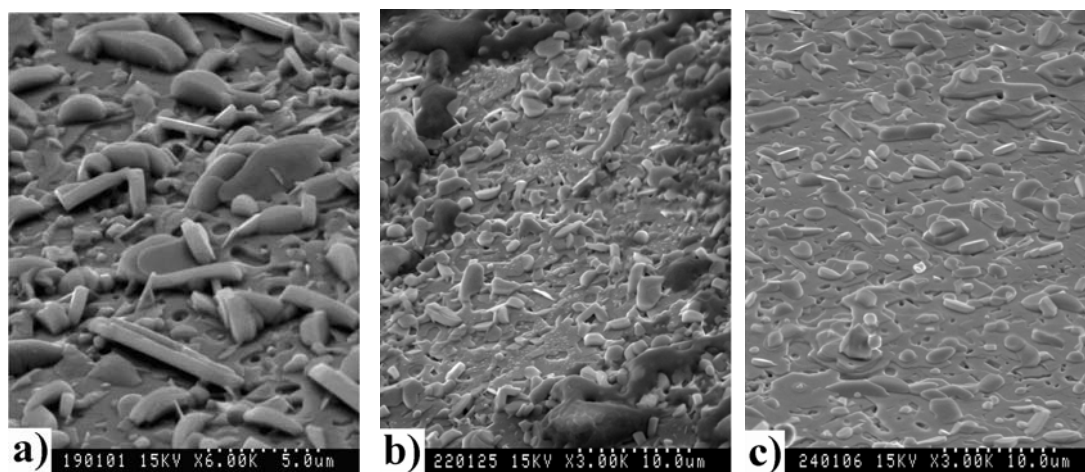
Fig. 58 SEM images of the Hg-based superconducting films with the 10 nm (a), 70 nm (b) and 120 nm (c) thick CeO$_2$ buffer layer mercurated 5 h.

In summary

Thin mercury based superconducting films were prepared by a two step process involving RF magnetron sputtering and non-contact mercuration. We found out that we can change the phase composition of the final films varying the thickness of the CeO$_2$ buffer layer. Using very thin CeO$_2$ film (~ 10 nm) we can prepare Hg-1223 phase on the R-plane sapphire due to the diffusion (intercalation) of the Ca-Cu-O dislocations into the grains of the Hg-1212 and consequent transformation to the Hg-1223.

These results were published in the *Superconductor Science and Technology* **20** (2007) 900-903.

5. Superconducting structures

To receive more complex information about the properties of the films suitable as cryoelectronic devices a method of temperature dependence of microwave losses MMMA was applied (Fig. 59) [123]. Using this method we can determine the Josephson loses which can influence the behaviour of the superconducting structures due to the increase of noise. The superconducting films were placed in the cavity resonator filled with the sapphire rod. Microwave losses caused by the presence of weak links and dynamic vortices were analysed using magnetic modulation microwave absorption.
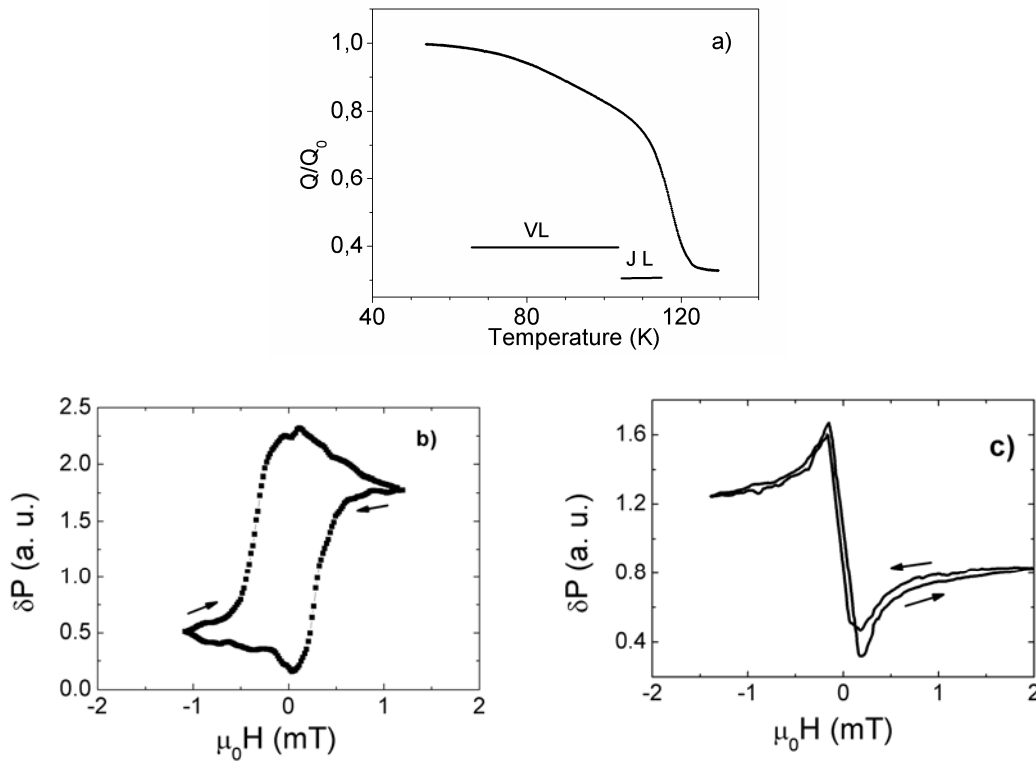
Fig. 59 Temperature dependence of the microwave quality of the superconducting film (a). In the picture the temperature regions of vortex (VL) and Josephson losses (JL) detected by MMMA method (figures b and c, respectively) are denoted.

The gradual increase of the resonator quality with the decreasing temperature in the upper part of the curve (80 – 110 K) [112] confirms some dissipation in coupling strength between the grains probably due to the existence of a nonstoichiometric material as a consequence of not optimal 223 precursor for the Hg-1212 phase. MMMA study exhibits the

existence of Josephson losses (JL) in the intergranular weak link medium just below the transition to the superconducting state while the viscous vortex motion (VL) is marked below 105 K. This fact enables to use our Hg-based films at working temperatures 77K without a noise effect due to the existence of intergranular weak links.

The fabrication of the Hg-based superconducting structures is a very complicated process. There are several difficulties which have to be solved to obtain functional structures. The first one is the sensitivity of the Hg-based compounds to water as we already mentioned (see chapter II., part 3.4). Despite this, we tried to pattern the deposited Re-Ba-Ca-Cu-O amorphous precursor as well as the mercurated films (Hg-1212) using photolithography and ion milling. These experiments were not successful because we did not succeed to remove the entire precursor (Hg-1212 film) from the substrate (Fig. 60). The structures prepared this way were not suitable for the applications so we were forced to use another method for fabrication of the Hg-based superconducting structures.
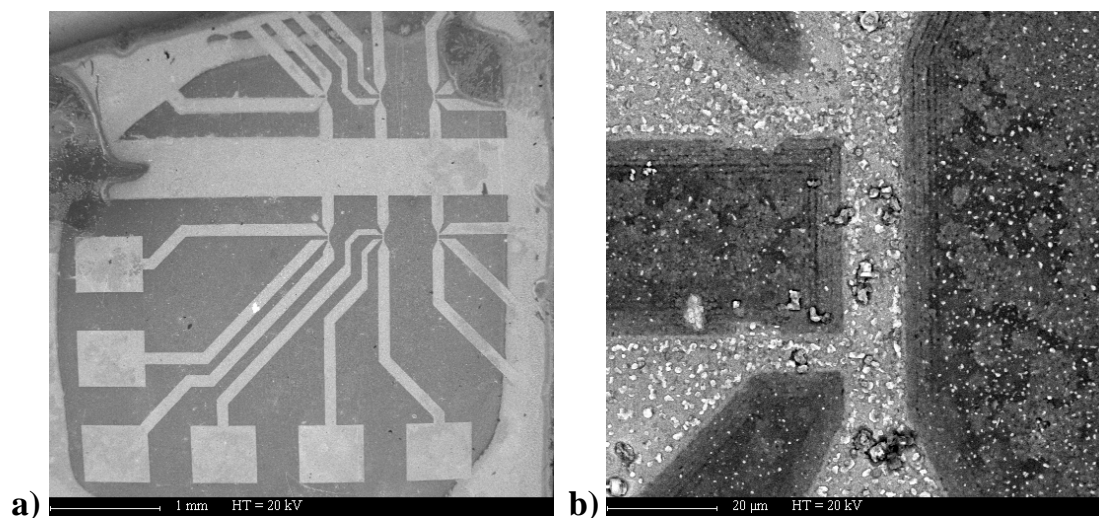
Fig. 60 SEM images of the Hg-1212 film on the CeO_2 buffered R-plane sapphire patterned by photolithography and ion milling. a) general overview, b) detail of the edged structure.

We decided to use lift-off patterning process. This process is based on the patterning of the resist and subsequent deposition of the precursor film.

In the lift-off method, first, the positive resist (150 μm or more) is spinned on top of the substrate and then annealed at 80 ºC during 10 minutes. Then the sample is dipped into the chlorobenzene for a few minutes to form a modified film with the top of the film having a

smaller developing rate. The next step of the process is its exposition. After dipping the exposed film to the developer, the developing rate of the resist is lower in the beginning, however, after the development of the modified surface layer the developing rate of the resist increases significantly. This creates undercuts of the edges of the patterned resist which allow the separation of the deposited film on the top of the patterned photoresist mask from the desired patterned structures on the substrate after the application of the acetone (see Fig. 14).

Re-Ba-Ca-Cu-O thin films have been prepared mostly on the CeO_2 buffered R-plane sapphire and $LaAlO_3$ substrates in a two step process. First, the substrate was covered with the patterned resist for the application of the lift-off process. Then, 200-600 nm thick precursor films with a nominal composition of $Re_{0.25}Ba_2Ca_2Cu_3O_x$ were deposited by RF magnetron sputtering from a single target of the same stoichiometry as described previously. Subsequently, the sample is dipped into the acetone to form a final structure.

We prepared several types of structures: coplanar structures, limiters and microbridges (Fig. 61) suitable for different types of applications. Then the Re-Ba-Ca-Cu-O precursor films were mercurated in a closed quartz tube as described previously. The precursor film was placed face to face with contact or without contact with the unreacted pellet. The synthesis temperatures and times were varied between 700-850 °C and 1-5 h.
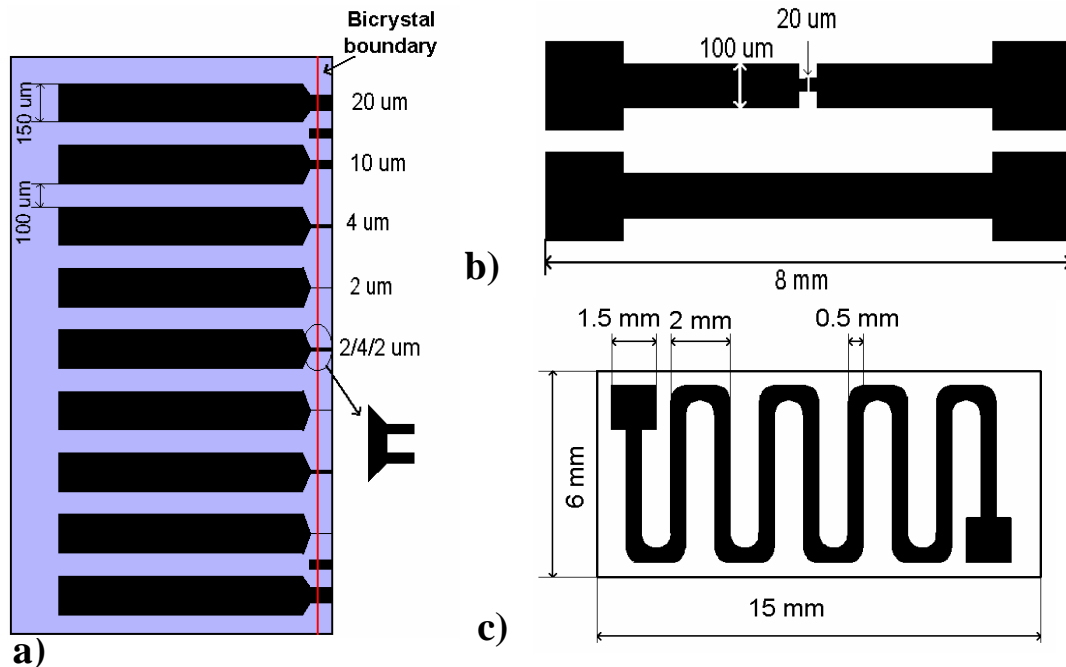
Fig. 61 Design of the microstrips on the bicrystal boundary (a), coplanar (b) and limiter (c) structures.

In first experiments, we used the mercuration with the contact between the precursor film and the source of the mercury. As we have already mentioned, this type of the mercuration is the source of several problems such as: high irreproducibility of the experiments, sticking of the films on the source pellet, ejection of some particles from the mercury source pellet to the surface of the film and subsequent short-circuiting between the strips of the superconducting structures. All these problems had a considerable influence on the fabrication of the superconducting structures.

These problems were solved by the use of the non-contact mercuration (see section 2.1 in this chapter). This method decreases considerably the amount of the particles originated from the source pellet and avoids sticked residua and thus the risk of short-circuits between the different parts of the superconducting structure.

Using XRD analyses we identified Hg-1212 phase in the prepared patterned structures. The *c*-axis crystallographic parameters reach 1.250-1.255 nm which is in a good agreement with the reported data [124]. In some cases few peaks belonging to the Hg-1223 phase were also observed in the XRD patterns. ϕ-scan of Hg-1212 films confirmed that these films were textured in the *a-b* plane, too. This suggests that the lift-off process used for the patterning of the precursor films did not influence the composition of the precursor and thus is suitable for the fabrication of the Hg-based superconducting structures.

The SEM investigations of the surface morphology of the Hg,Re-Ba-Ca-Cu-O structures prepared from the Re-doped precursors indicate a uniform character of the film surface over the substrate (Fig. 62). The detail of the surface reveals the existence of the typical plate-like crystal growth of the film and some precipitates on the surface. We suppose that these precipitates are a consequence of the fact that the composition of the (Ba-Ca-Cu-O) precursor was (223), while the final films had Hg-1212 phase. However, experiments with a precursor having a composition (212) offered worse superconducting properties. Some of the precipitates have an origin in the mercuration pellet (when we used contact mercuration). The presence of the particles on the surface of our Hg-1212 films indicates that these films are not suitable for the preparation of sandwich planar Josephson junctions. However, plate like grains with diameters few µm (Fig. 62) offer a possibility of the preparation of the intrinsic Josephson junction using FIB technique [125].
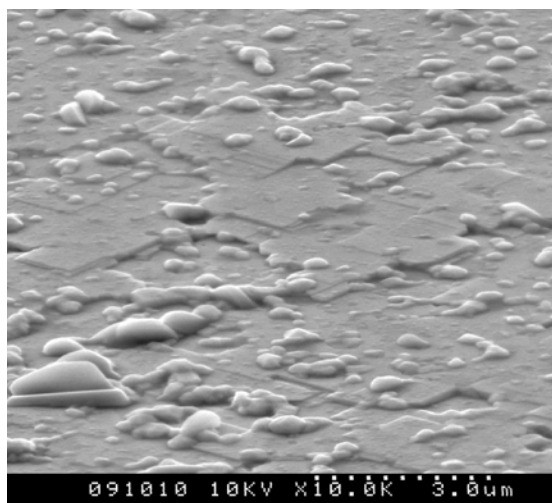
Fig. 62 The SEM investigations of the surface morphology of the Hg-Ba-Ca-Cu-O films prepared from the Re-doped precursors indicate a uniform character of the film surface over the substrate.

The use of the non-contact mercuration was very useful mainly for the preparation of the coplanar structures potential for the photodetector (Fig. 63) where we have a gap between two coplanar strips 10 or 20 μm on the length ~ 8 mm. The non-contact method of the mercuration process decreases considerably the amount of particles originated from the source pellet and avoid sticked residua and avoids the formation of short circuits between the strip lines.
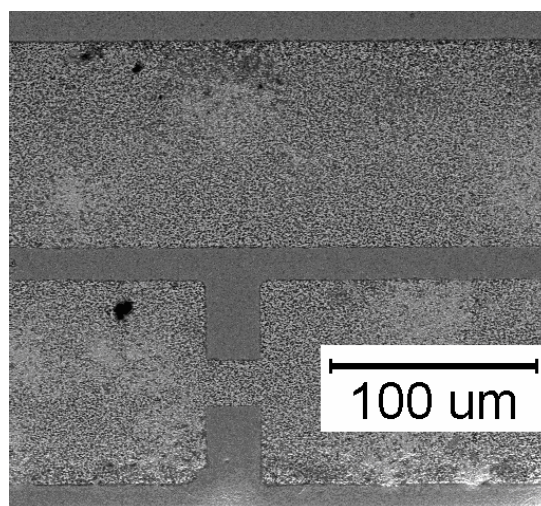
Fig. 63 SEM image of the coplanar strips of the superconducting structure fabricated using non-contact mercuration.

Using the mercuration with the contact between the precursor film and the source of the mercury allows to prepare superconducting single where the critical temperatures reaches 118 K, however, they were often not usable for applications due to the short-circuits between the strips. After applying the non-contact mercuration, the experiments were much more successful. As prepared Hg-1212 films showed the maximum T_{C0} values of the final films ~ 122 K at the film thickness of 350 nm and 4 - 20 μm wide strips had maximum T_{C0} ~ 110 K (Fig. 64).
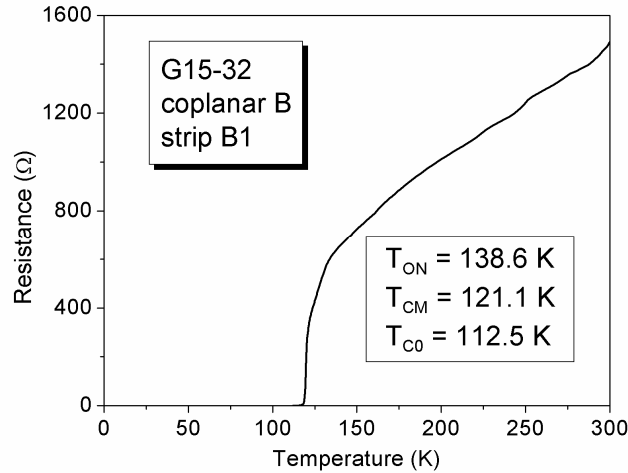
Fig. 64 $R(T)$ dependence of a 20 μm wide strip which is a part of the coplanar structure on the LaAlO$_3$ substrate for ultrafast photodetectors.

The most important request on precursor film is air stable properties after applied lift-off technique. We have found that precursor (Ba-Ca-Cu-O) films doped with rhenium (Re-Ba-Ca-Cu-O) are stable in air and suitable for the preparation of Hg-based films [126]. We found out that the patterned precursor films can be mercurated even after a few weeks to produce acceptable ($T_{C0} > 100K$) superconducting structures.

Recently we have shown that in the case of Hg-based films the Cooper-pair dynamics is not limited by the phonon bottleneck, which makes this HTS compound a material-of-choice for ultrafast optoelectronics applications [127]. An important step for the optoelectronic application is the creation of Hg,Re-Ba-Ca-Cu-O microbridges embedded into a coplanar strip to observe transient voltage signals generated in a current biased microbridge expose to a femtosecond–in–duration laser excitation. We were successful at the preparation of such structures on the top of the LaAlO$_3$ substrate by the above presented technology. Fig. 65 shows photoresponse signal (μV) versus time of such a structure where the dependence can be tuned by the biased current for a given temperature and for the parameters

of the incident laser pulse. A detailed study of the photoresponse dynamic was presented elsewhere [128] and is submitted for a publication.
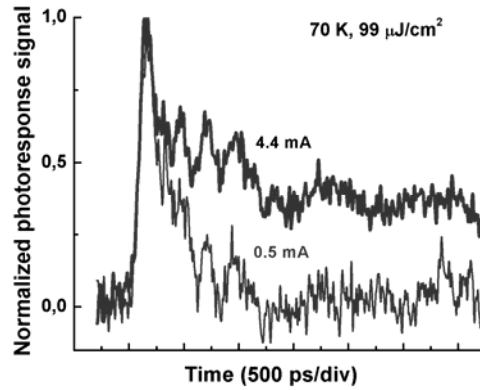
Fig. 65 Photoresponse versus time for the bias current 4.4 mA and 0.5 mA at a temperature of 70K and a laser beam energy of $99 \mu J/cm^2$. The fast first signal is related to the kinetic inductive response, while the nanosecond signal shoulder is due to the resistive response.

At low temperatures, and under low bias and low excitation conditions, was observed the fast, ~90-ps (system-limited), kinetic-inductive response, associated with the Cooper-pair breaking and quasiparticle recombination processes. At high temperatures, close to T_C, the photoresponse was a superposition of the fast kinetic-inductive and slower resistive signals, with the fast part essentially the same as the one observed at low temperatures and under low bias. The bolometric (resistive) component corresponded to the heat transfer from the film to the substrate. The observed fast kinetic-inductive relaxation dynamics in our Hg-Ba-Ca-Cu-O devices make this material very promising for ultrafast photodetector applications.

Another activity consisted to attempt the preparation of microstrips through a 24° tilted bicrystal boundary on the CeO_2 buffered R-plane bicrystal sapphire substrate. Fig. 66a presents $R(T)$ dependences of such strips. 4 μm wide strips have still $T_{C0} \sim 110K$. However, I-V characteristics (Fig. 66b) do not follow RSJ (resistively shunted junction) model [129]. We observed a rounding of the dependence near the critical current (probably a consequence of a noise). We know that the CeO_2 buffer layer itself consists of almost parallel epitaxial blocks misoriented few tenths of a degree in the a-b plane. In the case of d-wave superconductors, the maximum Josephson current I_C of the weak link depends, besides of the extrinsic wave function (φ) but also on the intrinsic angles (α, β) of the superconducting wave function [130]. As it has recently been shown by theoretical analyses [131, 132], a monotonic

temperature dependence of the Josephson current $I_C(T)$ exists when $\alpha = \beta$, it become convex for $\alpha = 0$ or concave for $\alpha = \pi / 4$ but frequently also linear at $\alpha \approx \pi / 8$ (as we show in Fig. 67), the angle close to the angle of our bicrystal substrate.
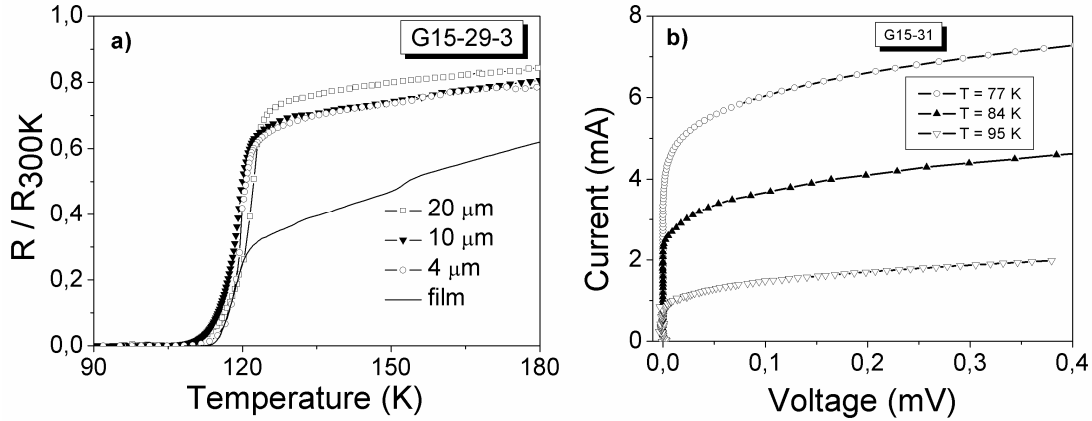
Fig. 66 R-T dependence of the microstrips over the bicrystal boundary for different wide of the strips and the film made in the same mercuration process (a). I-V characteristics of the 4 μm wide strip at different temperatures (b).
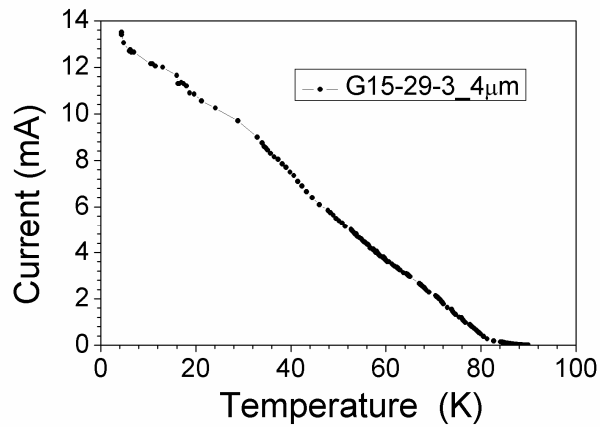
Fig. 67 $I_C (T)$ dependence of the 4 μm wide strip over the bicrystal boundary.

The next activity was the preparation of a model structure for the Hg-based superconducting fault current limiter. The limiters (~ 40 mm longs) were prepared on the LAO and CeO_2 buffered R-plane sapphire substrates using non-contact mercuration technique. Lift-off process was used for the patterning of the precursor films. Using XRD analyses c-axis oriented Hg-1212 phase was identified in the both cases (Fig. 68).
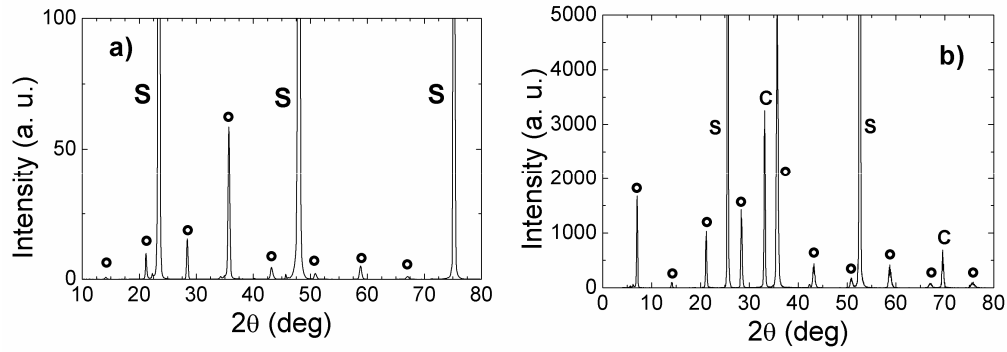
Fig. 68 XRD pattern of the limiter prepared on the LAO (a) and CeO$_2$ buffered R-plane sapphire (b) substrate. ○Hg-1212 phase, S-substrate, C-CeO$_2$.

The critical temperatures were measured in small sections of the limiter to compare the superconducting properties on its different parts (Fig. 69). From these dependences we can see that the limiter prepared on the sapphire substrate has higher critical temperature than the one prepared on the LAO. The structures were homogenous having very close critical temperatures T_{C0} in the different parts of the structure.
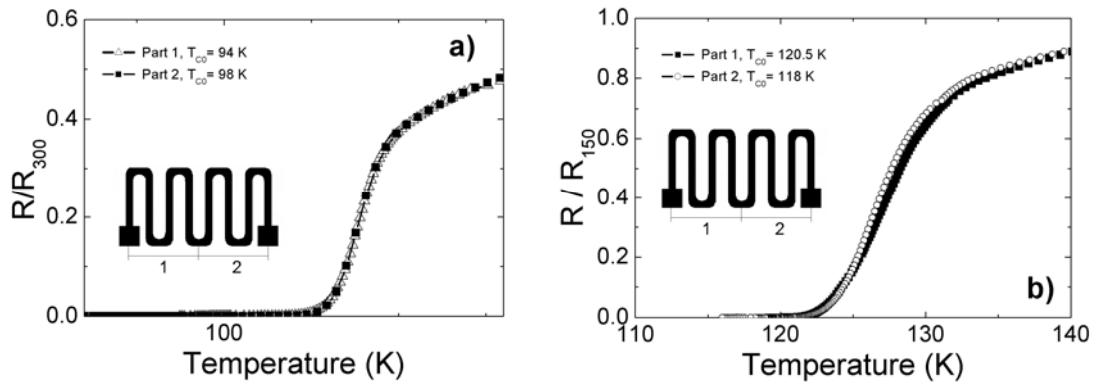
Fig. 69 $R(T)$ dependences of the limiter prepared on the LAO (a) and CeO$_2$ buffered R-plane sapphire (b) substrate.

The critical current density was measured on the limiter structure prepared on the R-plane sapphire with the CeO$_2$ buffer layer using transport measurements. The J_C values were estimated at 100 K ($\sim$ 1×10^4 Acm^{-2}) and at 77 K ($\sim$ 1×10^5 Acm^{-2}). These results are comparable to those obtained for the films using magnetic measurements suggesting that the patterning of the precursor film did not influence the superconducting properties of the structures.

In summary

In this part we describe a fabrication method of the Hg-based superconducting patterned structures. We present the preparation and patterning of Hg,Re-Ba-Ca-Cu-O superconducting films suitable for coplanar structures usable as possible photodetectors and for microbridges. We found out that we cannot use the direct patterning method of our Hg-based films via ion milling because using this method we are not able to remove the film up to the substrate and thus as prepared structures are not suitable for the applications. Therefore we used a lift-off patterning process based on the patterning of the (Re-Ba-Ca-Cu-O) precursor for the preparation of the superconducting structures. We studied different types of the mercuration processes and their impact on the superconducting properties of the structures.

Using non-contact mercuration enabled the fabrication of high quality Hg-based superconducting structures (coplanars, microbridges, limiters) convenient for cryoelectronic applications. High values of the critical temperatures (up to 110 K for the coplanar strips and microbridges, up to 120 K for limiter model structures) provide the stability of the superconducting properties (coherent length, energy gap, etc.) at the working temperature of the superconductor (77 K). We fabricated model structures of fault current limiters (~ 40 mm longs) without any defects as well as coplanar structures where a fast, ~90-ps (system-limited), kinetic-inductive response, associated with the Cooper-pair breaking and quasiparticle recombination processes was observed. These results strongly suggest that thin Hg-based superconducting films could find interesting applications in the field of cryoelectronics.

VII. Conclusion

In the frame of my dissertation thesis we studied the conditions of the mercuration process with the aim of the improvement of the structural and the superconducting properties of the final films and the synthesis of the Hg-1223 phase possessing the highest critical temperature T_{C0} from all known superconducting materials.

For the fabrication of our thin films of the Hg-based superconductors we used a two step process including an RF magnetron sputtering of the amorphous precursor (Re-Ba-Ca-Cu-O) and an *ex situ* mercuration in the sealed quartz tube. R-plane sapphire with the CeO_2 buffer layer was used as a substrate in the majority of experiments.

The experiments were focused on the solution of these main difficulties:

- The increase of the reproducibility of the mercuration process studying the influence of the configuration of the mercuration on the structural and electrical properties of the prepared films. Optimization of the mercuration process.

- Study of the influence of the substrate and the buffer layer on the phase composition of the final films. Optimization of the phase composition of the films to obtain Hg-1223 phase with the best electrical properties.

- Patterning of the precursor films using lift-off process and the consequent mercuration of the patterned structure, the study of the prepared structures to find some practical applications.

New knowledge obtained during my work on the dissertation thesis:

1. Non-contact mercuration

The main difficulty in the fabrication of the thin Hg-based superconducting films is that in some cases, parts of the films were translucent indicating very small thickness. We suppose that this was caused by sticking of the films to the surface of the mercury source during the mercuration process and the contact between the precursor film and the source of the mercury makes the mercuration very unreproducible with a small recovery.

We developed a *new method for the mercuration* of the precursor films. We used a sample holder with the special shape made of porous alumina which provided no contact between the precursor film and the Hg source.

We studied the influence of the mercuration process on the structural and electrical properties of the films. The films prepared without contact between the precursor film and the

source of the mercury were bi-axially textured Hg-1212 phase which is the evidence that the mercury is incorporated in the precursor film through the mercury vapour. When the films were prepared with a contact between the precursor films and the source of mercury, a dominating bi-axially Hg-1212 phase is also formed but another populations of grains is detected, suggesting that the contact caused the secondary nucleation centres. The critical temperatures in both methods were comparable in the range of 100-115 K. However, the non-contact mercuration is more reproducible thus more suitable for the preparation of thin superconducting films based on mercury for cryoelectronic applications.

We studied magnetic properties of the samples prepared by contact and non-contact mercuration. Using the Hall probe method in the static regime (persistent magnetization currents) we determined the critical current density in the self field $J_C = 2.1 \times 10^5$ A cm^{-2} and $J_C = 6.75 \times 10^4$ A cm^{-2} for the samples 1 (contact mercuration) and 2 (non- contact mercuration), respectively. The J_C value was higher in the case of the film prepared by the contact mercuration (sample 1); however the film prepared by non-contact mercuration (sample 2) was more homogenous than those prepared with the contact.

There is no report in the literature about the critical current densities of the Hg-based thin films prepared on the CeO_2 buffered R-plane sapphire. Only Stelzner and Schneidewind [108, 109] published the fabrication of the Hg-1212 phase on the R-plane sapphire with the CeO_2 using Tl-Hg cation exchange process. They used Tl-2212 films as the precursor films and the final films showed the critical current densities up to 6 MAcm^2 at 77 K in the self field. Our results are slightly lower but comparable to those obtained using Tl-Hg cation exchange process.

2. Influence of the partial pressure of mercury on the film synthesis using non-contact mercuration

The partial pressure of the mercury is very important parameter influencing the synthesis of the Hg-based compounds. It depends on the total amount of the mercury in the reaction system and on the synthesis temperature. We tried to keep the partial pressure of oxygen constant by using the same amount of the HgO in the pellet source in every experiment so the partial mercury pressure was changed by the different amount of the liquid mercury in the sealed quartz tube. We studied the influence of the amount of the mercury in the reaction system on properties of the final films to find out the best conditions for the non-contact mercuration of our films. At 800 °C using low amount of the mercury (lower pHg) the textured parasitic phase $Re_{2-x}Ba_4Ca_{1+y}O_{12}$ is formed. The amount of this phase decreased with

longer time of the mercuration and higher annealing temperature. The use of the higher amount of the mercury inhibited the creation of this phase even at lower synthesis temperature (800 °C) and also advanced the formation of the superconducting phase and improved the critical temperatures in the prepared films; however, higher amount of the mercury (higher pHg) did not provide the formation of the Hg-1223 phase on the CeO_2 buffered R-plane sapphire in our experimental conditions.

3. Influence of the CeO_2 buffer layer on the properties of the thin superconducting films based on mercury

The lattice mismatch ε between the film and the substrate (buffer layer) is one of the most important factors influencing the growth of the epitaxial films. The CeO_2 buffered R-plane sapphire substrate was used in our experiments. The lattice mismatch between the Hg-phase and CeO_2 is only 0.3 %. We found out that using high quality epitaxial buffer layer (60 nm thick) we can obtain only c-axis oriented Hg-1212 phase. We wanted to find out the influence of the thickness of the CeO_2 buffer layer on the structural and electrical properties of the Hg-based superconducting films.

After the experiments with the CeO_2 films on the sapphire of different thickness (10, 70 and 120 nm) we found out that we can change the phase composition of the final Hg-based films varying the thickness of the CeO_2 buffer layer. Using very thin CeO_2 film (~ 10 nm) we can prepare Hg-1223 phase on the R-plane sapphire due to the diffusion (intercalation) of the Ca-Cu-O dislocations into the grains of the Hg-1212 and consequent transformation to the Hg-1223. In the case of the thicker buffer layers the amount of the Hg-1223 decrease because the buffer layers are relaxed thus the Ca-Cu-O material is excluded on the top of the film during the formation of the Hg-1212 phase and does not have access to the Hg-1212 grains to form Hg-1223 phase.

4. Superconducting structures

The combination of the Hg-based superconducting film with the sapphire substrate is highly desirable for cryoelectronic microwave applications. An important step at the fabrication of cryoelectronic structures on the mercury cuprates is the patterning technique. Hg-1212 films are susceptible to water or water-based chemicals used in the standard photolithography process making fabrication of Hg-1212 devices difficult.

To overcome these difficulties a lift off process based on the patterning of the (Re-Ba-Ca-Cu-O) precursor films was used. Other difficulties in the fabrication of the superconducting structures were high irreproducibility of the experiments, sticking of the films on the source pellet, ejection of some particles from the mercury source pellet to the surface of mercurated precursor structure and subsequent short-circuiting between the strips of the superconducting structures.

These problems were solved by the use of the non-contact mercuration. This method decreases considerably the amount of the particles originated from the source pellet and avoids sticked residua. Using this method we prepared HgBCCO superconducting structures suitable for coplanar structures usable as possible photodetectors and for microbridges where the direct patterning on Hg-1212 was avoided by patterning of the (Re-Ba-Ca-Cu-O) precursor film using a lift off technique.

High values of the critical temperatures (up to 110 K for the coplanar strips and microbridges, up to 120 K for limiter model structures) provide the stability of the superconducting properties and parameters (coherent length, energy gap, etc.) at the working temperature of the superconductor (77 K). We fabricated the coplanar structures where the the fast, ~90-ps (system-limited), kinetic-inductive response, associated with the Cooper-pair breaking and quasiparticle recombination processes was observed as well as the model structures of the fault current limiters (~ 40 mm longs) without defects. The observed fast kinetic-inductive relaxation dynamics in our Hg-Ba-Ca-Cu-O devices make this material very promising for ultrafast photodetector applications.

Obtained results suggest that the thin Hg-based superconducting films can find applications in the field of cryoelectronics.

Conclusion

Dans le cadre de ma thèse, j'ai étudié les conditions d'élaboration de couches minces à base de cuprates de mercure en vue d'obtenir la phase Hg-1223 qui possède la température critiques la plus grande de tous les composés connus. J'ai cherché notamment à améliorer les propriétés structurales et supraconductrices de ces couches.

La fabrication de couches minces à base de cuprate de mercure utilise un procédé en deux étapes: dépôt d'une couche précurseur amorphe (Re-Ba-Ca-Cu-O) par pulvérisation magnétron suivi de sa mercuration *ex situ* en ampoule de quartz scellée. On a utilisé dans la plus part des cas un substrat de saphir coupé selon le « plan –R » puis recouvert d'une couche tampon de CeO_2.

Les expériences ont été focalisées sur la résolution des difficultés suivantes:

- augmenter la reproductibilité du procédé de mercuration. Pour ce faire on a étudié l'influence de la configuration de l'étape de mercuration sur les propriétés structurales et électrique des couches minces. Ceci a permis d'améliorer le procédé de mercuration.
- Comprendre l'influence du substrat et de la couche tampon sur la composition des films obtenu après mercuration, en vue de s'approcher de la phase Hg-1223 avec les meilleures propriétés électriques possibles.
- Développer une méthodologie simple pour structurer les films et identifier des applications possibles.

Les connaissances nouvelles obtenues pendant mon travail de thèse concernent ces quatre thématiques :

1. La mercuration sans contact

Un exemple de difficulté rencontrée dans la fabrication des couches minces à base de mercure est que dans certains cas des parties du film sont translucides indiquant une épaisseur très faible. On suppose que ça pu être causé par l'arrachement du film collé à la source de mercure, ce qui rend la méthode très non - reproductible et de faible rendement.

On a donc développé une nouvelle méthode de mercuration en utilisant un porte échantillon de forme spéciale, fabriqué en alumine poreuse qui a permit la mercuration sans contact de la couche précurseur avec la source de mercure.

On a étudié l'influence du procédé de mercuration sur les propriétés structurales et électriques des couches. Les couches préparées « sans contact » sont composées de la phase Hg-1212 ; c'est une preuve que le mercure est incorporé dans la couche précurseur par une réaction avec la vapeur de mercure. Ces couches sont texturées bi-axialement grâce à une croissance quasi-épitaxiale sur le substrat monocristallin avec la couche tampon épitaxiale. Les couches préparées par mercuration « avec contact » sont aussi texturées bi-axialement mais d'autres orientations ont été détectées dans ce cas. Ainsi le contact physique est la cause de centres de nucléations secondaires. Cette géométrie n'a pas d'incidence sur la température critique des échantillons qui se situaient dans le domaine 100-115 K que ce soit « avec contact » ou « sans contact ». La mercuration sans contact est plus reproductible donc convient mieux à la préparation des couches minces à la base de mercure pour les applications cryoeléctroniques.

On a étudié les propriétés magnétiques des couches minces préparées par mercuration « avec et sans contact ». En utilisant une sonde de Hall en régime statique, on a déterminé la densité de courent critique J_C en champ propre. Dans un échantillon préparé par « avec contact » le J_C était 6.75×10^4 A cm^{-2} et valait $J_C = 2.1 \times 10^5$ A cm^{-2} pour un échantillon préparé « sans contact ». Bien que valeur de J_C soit plus grande pour la mercuration « avec contact », les couches préparées sans contact étaient plus homogènes.

Dans la littérature, très peu de publications rapportent des données de densités de courant critiques de couches de cuprates de mercure préparées sur CeO$_2$/saphir. On trouve seulement Stelzner et Schneidewind [108, 109] pour avoir publié l'obtention de la phase Hg-1212 sur CeO$_2$/saphir par échange cationique Tl-Hg en partant de couches Tl-2212 comme couches précurseur. Les couches finales ont montrés des J_C atteignant 6 MAcm^{-2} à 77 K en champ propre montrant une marge d'amélioration possible de la voie que nous utilisions.

2. Influence de la pression partielle de mercure sur la synthèse des couches en conditions « sans contact »

La pression partielle de mercure est un paramètre influant de la synthèse des supraconducteurs à la base de mercure. Elle est fonction du volume total de mercure dans l'ampoule de synthèse et de la température. Pendant les expériences, on a essayé d'avoir une pression partielle d'oxygène constante en utilisant toujours la même quantité d'HgO, source d'Hg et O$_2$ dans l'ampoule. La pression partielle de mercure est ajustée par addition de différents volumes de mercure liquide. On a étudié l'influence du volume de mercure ajouté sur les propriétés des couches préparées pour identifier les meilleures conditions pour la

mercuration de nos couches « sans contact ». A 800 ºC et pour les plus faibles taux de mercure (faible pression de mercure), la phase parasite texturée $Re_{2-x}Ba_4Ca_{1+y}O_{12}$ est formée. La quantité de cette phase baisse avec une augmentation de la durée de synthèse et de la température de synthèse. L'utilisation de volumes de mercure plus élevés inhibe l'apparition de la phase parasite même dans le bas du domaine de température (800 ºC) et a permis de renforcer la formation de la phase supraconductrice et d'améliorer les températures critiques des couches préparées. Malheureusement, même les taux du mercure les plus élevés n'ont pas permis la formation de la phase Hg-1223 sur saphir muni d'une couche tampon de CeO_2.

3. Influence d'une couche tampon en CeO_2 sur les propriétés des couches minces de cuprate de mercure

Un désaccord dans les paramètres de maille ε entre la couche et le substrat (ou la couche tampon) est un des facteurs les plus importants influençant la croissance épitaxiale. Dans nos expériences, nous avons utilisé une coupe selon le plan R du saphir sur lequel a été déposée la couche tampon en CeO_2. Le désaccord de maille entra les phases de cuprate supraconducteur et CeO_2 est seulement de 0.3 % mais entre CeO_2 et le saphir c'est presque 20 %. On a trouvé que l'épaisseur des couches de CeO_2 avait une influence sur la composition des couches supraconductrices formées. Ainsi une couche très fine (~ 10 nm) permet la préparation de la phase Hg-1223 sur saphir (mais toutefois pas totalement pure), mais le taux de Hg-1223 diminue quand on augmente l'épaisseur des couches de CeO2 dont les contraintes sont alors relaxées. Il semble donc que la matière nécessaire à la formation d'Hg-1223 à partir d'Hg-1212 (Ca-Cu-O) puisse diffuser plus aisément quand la couche sous-jacente est contrainte et induise, de ce fait, un ensemble de dislocations favorable à la diffusion dans la couche supraconductrice

4. Des films supraconducteurs structurés

L'utilisation de substrats en saphir est très intéressante pour les applications en cryoeléctroniques micro-ondes. Cependant un pas très important à franchir pour aller dans cette direction est celui de la fabrication de structures par les techniques de gravure. Les couches d'Hg-1212 comme celles d'YBCO sont très sensibles à l'eau et aux produits chimiques utilisés dans la photolithogravure qui sont en général aqueux. C'est la principale difficulté dans la structuration de ces matériaux.

Pour prévenir ces difficultés on a utilisé un procédé de gravure par lift-off des couches précurseur (Re-Ba-Ca-Cu-O). Une autre source de difficultés résidait dans la non reproductibilité des expériences liées à un collage des couches minces sur la source de mercure ainsi qu'à des dépôts de particules provenant de cette source. Ces particules venaient se mettre sur la surface de la structure créant des courts-circuits entre les lignes des structures supraconductrices gravées.

La méthode de mercuration « sans contact » a permis de résoudre ces problèmes pour préparer des structures supraconductrices de HgBCCO coplanaires avec microponts utilisables comme photodétecteurs et des méandres de longueur totale 40 mm destinés a l'étude de la limitation du courant.

La haute valeur de la température critique observée dans ces structures (jusqu'au 110 K pour les lignes coplanaires et les microponts et jusqu'au 120 K pour les méandres pour limiteur de courant) assurent la stabilité des propriétés supraconductrices à la température de l'azote liquide (77 K) à laquelle sont testés ces dispositifs. Plusieurs structures co-planaires ont été fabriquées et testées avec succès sous impulsions lumineuses. Leur réponse ultra rapide (~90-ps, à 77 K) est associée avec la brisure des paires de Cooper et la recombinaison des quasiparticles résultantes. L'observation de telle dynamique de relaxation est très prometteuse pour des applications de photodétection ultra rapides à base de Hg-Ba-Ca-Cu-O fonctionnant peut-être à des températures supérieures à celle des autres matériaux. L'étude des méandres pour la limitation est en cours.

Les résultats obtenus suggèrent que les couches minces à la base de cuprates de mercure puissent être utilisées en cryoélectronique.

VIII. Summary and future development of research

The Hg-based superconductors are materials with the highest critical temperatures from all known superconductors. Their application as the devices for the everyday use is, however, limited due to the difficulties in their fabrication. The optimization of the preparation methods will open large possibilities for the cryoelectronic applications.

Within the frame of my dissertation thesis we tried to optimize the parameters of the synthesis of the thin Hg-based films. The development of the non-contact method for the mercuration of the thin films confirmed the film formation via Hg vapour phase which will enable the development of the devices for the mercuration of the larger samples (few cm). The lift-off method used for the patterning of the precursor films prevents the water contamination of the films and thus their degradation. The non-contact mercuration also enabled the fabrication of the Hg-based superconducting structures with the minimal risk of the short-circuits between the single parts of the structure. The formation of the Hg-1223 decreased the amount of the impurities on the top of the films which will enable the fabrication of the sandwich planar Josephson junctions, too.

The prepared coplanar structures are suitable for the use in the ultra-fast detectors. The structures containing microbridges can serve for the study of the superconductivity in the micro- and submicro- scale and for the fabrication of the Josephson junctions of such dimensions. The model structure of the superconducting fault-current limiter was the first step for the fabrication of the real limiter structure and will be used for the study of the superconducting properties on this type of the structure. The use of the sapphire substrate allows the application of the Hg-based superconducting structures also for the microwave devices.

All the structures had high values of the critical temperatures (up to 110 K for the coplanar strips and microbridges, up to 120 K for the limiter model structures) which provide the stability of the superconducting properties and parameters (coherent length, energy gap, etc.) at the working temperature of the superconductor (77 K).

In the future we want to continue with the optimization of the mercuration process with a view to improve the surface quality of the films and thus the fabrication of the different types of the structures, especially the sandwich planar Josephson junctions. Decreasing the film thickness we will be able to prepare the structures suitable for the different types of devices such as bolometers.

IX. References

[1]   Handbook of Superconducting Materials, edited by D. A. Cardwell and D. S. Ginley, IOP publishing, Bristol 2003.

[2]   J. G. Bednorz, K. A. Müller, *Z. Physik B* **64** (1986) 189.

[3]   M. K. Wu, J. R. Ashburn, C. J. Torng, P. H. Hor, R. L. Meng, L. Gao, Z. J. Huang, Y. Q. Wang, C. W. Chu, *Phys. Rev. Lett.* **58** (1987) 908.

[4]   S. N. Putilin, E. V. Antipov, O. Chmaissem, M. Marezio, *Nature* **362** (1993) 226.

[5]   A. Schilling, M. Cantoni, J. D. Guo, H. R. Ott, *Nature* **363** (1993) 56.

[6]   C. W. Chu, L. Gao, F. Chen, Z. J. Huang, R. L. Meng, Y. Y. Xue, *Nature* **365** (1993) 323.

[7]   E. V. Antipov, S. M. Loureiro, C. Chaillout, J. J. Caponi, P. Bordet, J. L. Tholence, S. N. Putilin, M. Marezio, *Physica C* **215** (1993) 1.

[8]   R. L. Meng, L. Beauvais, X. J. Zhang, Y. Y. Sun, Y. Y. Xue, C. W. Chu, *Physica C* **216** (1993) 21.

[9]   B. A. Scott, E. Y. Suard, C. C. Tsuei, D. B. Mitzi, T. R. McGuire, B. H. Chen, D. Walker, *Physica C* **230** (1994) 239.

[10]   M. Marezio, E. V. Antipov, J. J. Capponi, C. Chaillout, S. Loureiro, S. N. Putilin, A. Santoro, J. L. Tholence, *Physica B* **197** (1994) 570.

[11]   E. V. Antipov, A. M. Abakumov, S. N. Putilin, *Supercond. Sci. Technol.* **15** (2002) R31.

[12]   M. A. C. Aranda, *Adv. Mater.* **6** (1994) 905.

[13]   S. S. P. Parkin, V. Y. Lee, A. I. Nazzal, R. Savoy, R. Bayers, S. J. La Placa, *Phys. Rev. Lett.* **61** (1998) 750.

[14]   R. Sugise, M. Hirabayashi, N. Terada, M. Jo, T. Shimonura, H. Ihara, *Japan. J. Appl. Phys.* **27** (1988) L1709.

[15]   A. Morosin, R. J. Baughman, D. S. Ginley, J. E. Schriber, E. L. Venturini, *Physica C* **161** (1990) 115.

[16]   O. Chmaissem, P. Guptasarma, U. Welp, D. G. Hinks, J. D. Jorgensen, *Physica C* **292** (1997) 305.

[17]   O. Chmaissem, J. D. Jorgensen, D. G. Hinks, B. G. Storey, B. Dabrowski, H. Zhang, L. D. Marks, *Physica C* **279** (1997) 1.

[18]   G. Villard, D. Pelloquin, A. Maignan, *Physica C* **307** (1998) 128.

[19]   H. Schwer, E. Kopnin, R. Molinski, J. Jun, G. I. Meijer, K. Conder, C. Rossel, J. Karpinski, *Physica C* **276** (1997) 281.

[20]   D. Pelloquin, H. Hardy, A. Maignan, B. Raveau, *Physica C* **273** (1997) 205.

[21]   X. Chen, Z. Xu, J. Wang, Z. Jiao, Q. Zhang, *Chemical Physics Letters* **258** (1996) 1.

[22]   Y. S. Sung, X. F. Zhang, D. J. Miller, *Appl. Phys. Lett.* **69** (1996) 3420.

[23]   K. H. Sandhage, P. K. Gallagher, in: A. M. Hermann, J. V. Yakhmi (Eds.), Thallium-Based High-Temperature Superconductors Chap. 19, Marcel Dekker, New York, 1994.

[24]   X. F. Zhang, Y. S. Sung, D. J. Miller, *Physica C* **301** (1998) 221.

[25]   Th. Hopfinger, O. O. Shcherban, Ph. Galez, R. E. Gladyshevkii, M. Lomello-Tafin, J. L. Jorda, M. Couach, *J. Alloys and Compounds* **333** (2002) 237.

[26]   E. V. Antipov, J. J. Capponi, C. Chaillout, O. Chmaissem, S. M. Loureiro, M. Marezio, S. N. Putilin, A. Santoro, J. L. Tholence, *Physica C* **218** (1993) 348.

[27]   S. Adachi, A. Tokiwa-Yamamoto, A. Fukuoka, R. Usami, T. Tatsuki, Y. Moriwaki, K. Tanabe, in: A. V. Narlikar (Ed.), Studies of High Temperature Superconductors, vol 23, Nova Science, New York, 1997, p. 163.

[28]   M. Reder, L. Schmidt, J. Wiesmann, H. C. Freyhardt, *Physica C* **339** (2000) 53.

[29]   L.-W. Wu, Y.-L. Wang, W. Bian, Y. Zhu, T. R. Thurston, R. L. Sabatini, P. Haldar, M. Suenaga, *J. Mater. Res.* **12** (1997) 305.

[30]   Y. R. Sun, J. R. Thompson, J, Schwartz, D. K. Christen, Y. C. Kim, M. Paranthaman, *Phys. Rew. B* **51** (1995) 581.

[31]   Y. R. Sun, K. M. Amm, J. Schwartz, *IEEE Trans. Appl. Supercond.* **5** (1995) 1870.

[32]   J. Krelaus, M. Reder, J. Hoffmann, H. C. Freyhardt, *Physica C* **314** (1999) 81.

[33]   U. Welp, U. W. Crabtree, J. L. Wagner, D. G. Hinks, *Physica C* **218** (1993) 373.

[34]   Z. J. Huang, Y. Y. Xue, R. L. Meng, C. W. Chu, *Phys. Rew. B* **49** (1994) 4218.

[35]   A. Schilling, O. Jeaundupeux, J. D. Guo, H. R. Ott, *Physica C* **216** (1993) 6.

[36]   K. Isawa, T. Higuchi, T. Machi, A. Tokiwa-Yamamoto, S. Adachi, M. Murakami, M. Yamauchi, *Appl. Phys. Lett.* **64** (1994) 1301.

[37]   J. Shimoyama, K. Kishio, S. Hahakura, K. Kitazawa, K. Yamaura, Z. Hiroi, M. Takano, *Advances in Superconductivity* **7** (1995) 287.

[38]   Y. Moriwaki, T. Sugano, S. Adachi, K. Tanabe, *IEEE Trans. Appl. Supercond.* **9** (1998) 2390.

[39]   A. Salem, G. Jakob, H. Adrian, *Physica C* **388-389** (2003) 747.

[40]   B. A. Hunter, J. D. Jorgensen, J. L. Wagner, P. G. Radaelli, P. G. Hinks, H. Shaked, R. L. Hitterman, R. B. Von Dreele, *Physica C* **221** (1994) 1.

[41]   M. Nuñez-Regueiro, J. L. Tholence, E. V. Antipov, J. J. Caponi, M. Marezio, *Science* **262** (1993) 97.

[42]   H. Takahashi, A. Tokiwa-Yamamoto, N. Môri, S. Adachi, H. Yamauchi, S. Tanaka, *Physica C* **218** (1993) 1.

[43]   L. Gao, F. Chen, R. L. Meng, Y. Y. Xue, C. W. Chu, *Phil. Mag. Lett.* **68** (1993) 345.

[44]   L. Gao, Y. Y. Xue, F. Chen, Q. Xiong, R. L. Meng, D. Ramirez, C. W. Chu, J. H. Eggert, H. K. Mao, *Phys. Rew. B Rapid Commun.* **50** (1994) 4260.

[45]   B. Gromoll, G. Ries, W. Schmidt, H.-P. Kraemer, B. Seebacher, B. Utz, R. Nies, H.-W. Neumueller, E. Baltzer, S. Fischer, B. Heismann, *IEEE Trans. Appl. Supercond.* **9** (1999) 656.

[46]   L. R. Gilbert, R. Messier, S. V. Krishnaswamy, *J. Vac. Sci. Technol.* **17** (1980) 389.

[47]   S. M. Rossnagel, J. J. Cuomo, *Conf. Proc.* **165** (1988) 106.

[48]   X. X. Xi, G. Linker, O. Meyer, E. Nold, B. Obst, F. Ratzel, R. Smithley, B. Strehlau, F. Weschenfelder, J. Geerk, *Z. Phys. B* **74** (1989) 13.

[49]   N. Newman, B. F. Cole, S. M. Garrison, K. Char, R. Taber, *IEEE Trans. Magn.* **27** (1991) 1276.

[50]   C. B. Eom, J. Z. Sun, K. Yamamoto, A. F. Marshall, K. E. Luther, T. H. Geballe, S. S. Laderman, *Appl. Phys. Lett.* **55** (1989) 595.

[51]   U. Poppe, J. Schubert, R. R. Arons, W. Evers, C. R. Freiburg, W. Reichert, K. Schmidt, W. Sybertz, K. Urban, *Solid State Commun.* **66** (1988) 661.

[52]   J. Schneider, J. Einfeld, P. Lahl, T. Königs, R. Kutzner, R. Wördenweber, *Applied superconductivity* (ed H. Rogalla, D. Blank Inst. Phys. Conf. Ser. **158** 1997) 221.

[53]   G. Ockenfuss, R. Wördenweber, T. A. Scherer, R. Unger, W. Jutzi, *Physica C* **243** (1995) 24.

[54]   R. Wördenweber *et al* unpublished.

[55]   Y. Suzuki, J. M. Triscone, C. B. Eom, M. R. Beasley, T. H. Geballe, *Phys. Rew. Lett.* **73** (1994) 328.

[56]   O. Fischer, J. M. Triscone, P. Fivat, M. Anderson, M. Decroux, *Proc. SPIE* **2157** (1994) 134.

[57]   P. Wagner, U. Frey, F. Hillmer, A. Hadish, G. Jakob, H. Adrian, T. Steinborn, L. Ranno, A. Elschner, I. Heyvaert, Y. Bruynseraede, *J. Supercond.* **7** (1994) 217.

[58]   T. Satoh, H. Adachi, Y. Ichikawa, K. Setsune, K. Wasa, *J. Mater. Res.* **9** (1994) 1961.

[59]   G. Jakob, V. V. Moshchalkov, Y. Bruynserade, *Appl. Phys. Lett.* **66** (1995) 2564.

[60]   T. Aytug, Y. Yu, S. L. Yan, Y. Y. Xie, J. Z. Wu, *Physica C* **325** (1999) 56.

[61]   A. Tsukamoto, K. Takagi, Y. Moriwaki, T. Sugano, S. Adachi, K. Tanabe, *Applied Physics Letters* **73** (1998) 990.

[62]   A. Tsukamoto, N. Inoue, T. Sugano, S. Adachi, K. Tanabe, K. Takagi, *Physica C* **357-360** (2001) 1459.

[63]   N. Inoue, T. Sugano, T. Utagawa, Y. Wu, S. Adachi, K. Tanabe, *Physica C* **357-360** (2001) 1444.

[64]   R. S. Aga Jr., Y. Y. Xie, S. L. Yan, J. Z. Wu, S. S. Han, *Applied Physics Letters* **79** (2001) 2417.

[65]   L. Krusin-Elbaum, C. C. Tsuei, A. Gupta, *Nature* **373** (1995) 679.

[66]   L. Krusin-Elbaum, G. Blatter, J. R. Thompson, D. K. Petrov, R. Wheeler, J. Ullmann, C. W. Chu, *Phys. Rew. Lett.* **81** (1998) 3948.

[67]   A. Fukuoka, A. Tokiwa-Yamamoto, M. Itoh, R. Usami, S. Adachi, K. Tanabe, *Phys. Rew. B* **55** (1997) 6612.

[68]   S. M. Loureiro, C. Stott, L. Philip, F. M. Gorius, M. Perroux, S. Le Floch, J. J. Capponi, D. Xenikos, P. Toulemonde, J. L. Tholence, *Physica C* **272** (1996) 94.

[69]   A. Sin, A. G. Cunha, A. Calleja, M. T. D. Orlando, F. G. Emmerch, E. Baggio Saitovich, M. Segarra, S. Piñol, X. Obrados, *Supercond. Sci. Technol.* **12** (1999) 120.

[70]   S. N. Putilin, E. V. Antipov, M. Marezio, *Physica C* **212** (1993) 266.

[71]   P. Odier, A. Sin, P. Toulemonde, A. Bailly, S. Le Floch, *Supercond. Sci. Technol.* **13** (2000) 1120.

[72]   W. Lechter, L. Toth, M. Osofsky, M. Skelton, R. J. Soulen Jr., S. Quadri, J. Schwartz, J. Kessler, C. Wolters, *Physica C* **249** (1995) 213.

[73]   A. Tampieri, G. Celestani, G. Celotti, C. Micheletti, D. Rinaldi, *Physica C* **298** (1998) 10.

[74]   V. A. Alyoshin, D. A. Mikhailova, E. V. Antipov, *Physica C* **255** (1995) 173.

[75]   A. Sin, A. G. Cunha, A. Calleja, M. T. D. Orlando, F. G. Emmerich, E. Baggio-Saitovich, S. Piñol, J. M. Chimenos, X. Obrados, *Adv. Mater.* **10** (1998) 1126.

[76]   A. Sin, A. G. Cunha, A. Calleja, M. T. D. Orlando, F. G. Emmerich, E. Baggio-Saitovich, S. Piñol, J. M. Chimenos, X. Obrados, *Physica C* **306** (1998) 34.

[77]   K. M. Amm, Ch. Wolters, D. C. Knoll, S. C. Peterson, J. Schwartz, *IEEE Trans. Appl. Supercond.* **7** (1997) 1973.

[78]   R. L. Meng, B. Hickey, Y. Q. Wang, Y. Y. Sun, L. Gao, Y. Y. Xue, C. W. Chu, *Appl. Phys. Lett.* **68** (1996) 3177.

[79]   J. Schwartz, K. M. Amm, Y. R. Sun, Ch. Wolters, *Physica B* **216** (1996) 261.

[80]   J. Su, P. V. P. S. S. Sastry, J. Schwartz, *IEEE Trans. Appl. Supercond.* **11** (2001) 3118.

[81]   G. B. Peacock, I. Gameson, P. P. Edwards, M. Khaliq, G. Yang, T. C. Shields, J. S. Abell, *Physica C* **273** (1997) 193.

[82]   Y. Tsabba, S. Reich, *Physica C* **269** (1996) 1.

[83]   S. Reich, Y. Tsabba, *Adv Mater.* **9** (1997) 329.

[84]   S. H. Yoo, K. W. Wong, Y. Xin, *Physica C* **273** (1997) 189.

[85]   H. K. Singh, A. K. Saxena, O. N. Srivastava, *Physica C* **273** (1997) 181.

[86]   S. H. Yun, J. Z. Wu, B. W. Kang, A. N. Ray, A. Gadup, Y. Yang, R. Farr, G. F. Sun, S. H. Yoo, Y. Xin, W. S. He, *Appl. Phys. Lett.* **67** (1995) 2866.

[87]   S. H. Yun, J. Z. Wu, S. C. Tidrow, D. W. Eckart, *Appl. Phys. Lett.* **68** (1996) 2565.

[88]   S. H. Yun, J. Z. Wu, *Appl. Phys. Lett.* **68** (1996) 862.

[89]   S. H. Yun, J. D. Pedargin, R. Rössel, D. Bäuerle, X. Obrados, *Appl. Phys. Lett.* **77** (2000) 1369.

[90]   Y. Moriwaki, T. Sugano, C. Gasser, A. Fukuoka, K. Nakanishi, S. Adachi, K. Tanabe, *Appl. Phys. Lett.* **69** (1996) 3423.

[91]   A. Sin, Z. Supardi, A. Sulpice, P. Odier, F. Weiss, L. Ortega, M. Núñez-Regueiro, *IEEE Trans. Appl. Supercond.* **11** (2001) 2877.

[92]   D. De Barros, *DSc. Thesis*, INPG, Grenoble France, April 2004.

[93]   D. De Barros, L. Ortega, Ch. Peroz, F. Weiss, P. Odier, *Physica C* **440** (2006) 45.

[94]   Y. Moriwaki, T. Sugano, A. Tsukamoto, C. Gasser, K. Nakanishi, S. Adachi, K. Tanabe, *Physica C* **303** (1998) 65.

[95]   V. A. Alyoshin, D. A. Mikhailova, E. V. Antipov, *Physica C* **271** (1996) 197.

[96]   K. Knížek, E. Pollert, D. Sedmidubský, I. Bryntse, *Physica C* **371** (2002) 111.

[97]   K. Knížek, M. Veverka, E. Hadová, J. Hejtmánek, D. Sedmidubský, E. Pollert, *Physica C* **302** (1998) 290.

[98]   D. Sedmidubský, J. Leitner, K. Knížek, A. Štrejc, M. Veverka, *Physica C* **329** (2000) 191.

[99]   Y. Y. Xue, R. L. Meng, Q. M. Lin, B. Hickley, Y. Y. Sun, C. W. Chu, *Physica C* **281** (1997) 11.

[100] T. Tsuchiya, K. Fueki, *Physica C* **288** (1997) 47.

[101] T. Tsuchiya, K. Fueki, T. Koyama, *Physica C* **298** (1998) 49.

[102] V. A. Alyoshin, D. A. Mikhailova, E. B. Rudnyi, E. V. Antipov, *Physica C* **383** (2002) 59.

[103] K. A. Lokshin, D. A. Pavlov, M. L. Kovba, S. N. Putilin, E. V. Antipov, I. Bryntse, *Physica C* **366** (2002) 263.

[104] A. A. Gapud, T. Aytug, S. H. Yoo, Y. Y. Xie, B. W. Kang, S. D. Gapud, J. Z. Wu, S. W. Wu, W. Y. Liang, X. T. Cui, J. R. Liu, W. K. Chu, *Physica C* **308** (1998) 264.

[105] W. N. Kang, R. L. Meng, C. W. Chu, *Appl. Phys. Lett.* **73** (1998) 381.

[106] W. N. Kang, S. Lee, C. W. Chu, *Physica C* **315** (1999) 223.

[107] J. Z. Wu, S. L. Yan, Y. Y. Xie, *Appl. Phys. Lett.* **74** (1999) 1469.

[108] Th. Stelzner, H. Schneidewind, *Physica C* **398** (2003) 37.

[109] H. Schneidewind, Th. Stelzner, E. Gaganidze, J. Halbritter, *Physica C* **411** (2004) 152.

[110] Y. Y. Xie, J. Z. Wu, A. A. Gapud, Y. Yu, Y. Xin, *Physica C* **322** (1999) 19.

[111] M. Bindi, F. Fuso, E. Arimondo, A. Tampieri, G. Celotti, D. Rinaldi, *Physica C* **377** (2002) 319.

[112] Š. Chromik, V. Štrbík, M. Polák, Š. Gaži, D. De Barros, P. Odier, F. Hanic, Applied superconductivity 2003, in: A. Andreone et al., *Proc. of the 6th EUCAS*, Sorrento 2003. IoP Conf. Ser. No **181**, Bristol: IoP 2004, p. 1507.

[113] M. Polák, V. Windte, W. Schauer, J. Reiner, A. Gurevich, H. Wuhl, *Physica C* **174** (1991) 14.

[114] A. Sin, P. Odier, *Advanced Materials* **10** (1998) 1126.

[115] A. Sin, P. Odier, M. Núñez-Regueiro, *Physica C* **330** (2000) 9.

[116] A. Sin, P. Odier, F. Weiss, M. Núñez-Regueiro, *Physica C* **341-348** (2000) 2459.

[117] A. Sin, F. Alsina, N. Mestres, A. Sulpice, P. Odier, M. Núñez-Regueiro, *J. Solid State Chem.* **161** (2001) 355.

[118] Š. Chromik, M. Španková, I. Vávra, Š. Gaži, M. Cannaerts, L. Hellemans, D. Machajdík, Š. Beňačka, *Acta Physica Slovaca* **50** (2000) 403.

[119] M. Španková, I. Vávra, Š. Gaži, D. Machajdík, Š. Chromik, K. Fröhlich, L. Hellemans, Š. Beňačka, *J. of Crystal Growth* **218** (2000) 287.

[120] Š. Chromik, M. Cannaerts, Š. Gaži, C. Van Haesendonc, M. Španková, P. Kúš, Š. Beňačka, *Physica C* **371** (2002) 301.

[121] Y. C. Kim, J. R. Thompson, D. K. Christens, Y. R. Sun, M. Paranthaman, E. D. Specht, *Phys. Rew. B* **52** (1995) 4438.

[122] N. Inoue, T. Sugano, A. Tsukamoto, T. Utagawa, S. Adachi, K. Tanabe: *Physica C* **330** (2000) 94.

[123] Š. Chromik, M. Jergel, Š. Gaži, V. Štrbík, F. Hanic, C. Falcony, M. Vaško, Š. Beňačka: *Physica C* **354** (2001) 429.

[124] Y. Q. Wang, R. L. Meng, Y. Y. Sun, K. Ross, Z. J. Huang, C. V. Chu: *Appl Phys. Lett.* **63** (1993) 3084.

[125] P. A. Warburton, A. R. Kuzhakhmetov, C. Bell, G. Burnell, M. G. Blamire, H. Wu, C. R. M. Grovenor, H. Schneidewind, *IEEE Transactions Appl. Supercond.* **1**3 (2003) 821.

[126] Š. Chromik, D. De Barros, V. Štrbík, P. Odier, A. Sin, F. Hanic, I. Kostič: *J.Phys. IV France* **11** (2001) Pr11.

[127] X. Li, Y. Xu, Š. Chromik, V. Štrbík, P. Odier, .D. De Barros, R. Sobolewski: *IEEE Trans. Applied Supercond.* **15** (2005) 622-625.

[128] X. Li, M. Khafizov, R. Sobolewski, Š. Chromik, M. Valeriánová, V. Štrbík, P. Odier: *Proc. of the ASC 2006*, Seattle 2006, will be published.

[129] M. Tinkham, Introduction to Superconductivity, 2nd edition, McGraw-Hill, Inc., New York 1996, 202.

[130] M. Sigrist, T. M. Rice: *Rev. Mod. Phys.* **67** (1995) 503.

[131] Y. Tanaka, S. Kashiwaya, Y. Asano, T. Yokoyama: *Physica C* **435** (2006) 1.

[132] S. Kashiwaya, Y. Tanaka: *Rep. Progr. Phys.* **63** (2000) 1641.

PHYSICAL PROPERTIES	
Chemical formula	Al_2O_3
Crystal structure	Hexagonal system (rhombohedral)
Unit cell dimension	a = 4.758 Å , c = 12.991 Å
Density	3.98 g cm^{-3}
Hardness	9 mohs, 1525-2000 Knoop
Melting point	2040 °C
Boiling point	2980 °C
THERMAL PROPERTIES	
Thermal conductivity (60° to c-axis) at 25 °C	0.065 cal cm^{-1} s^{-1} °C^{-1}
Thermal expansion coefficient (60° to c-axis) 25 - 800 °C	8.40 x 10^{-6} °C^{-1}
Specific heat at 25 °C	0.10 cal g^{-1}
Heat capacity at 25 °C	18.6 cal °C^{-1} mol^{-1}
MECHANICAL PROPERTIES*	
Tensile strength	40,000-60,000 psi (design criterion)
Flexural strength	70,000-130,000 psi (design criterion)
Young's modulus	345 GPa
Compressive modulus	379.5 GPa
Flexural modulus	359 GPa
Rigidity modulus	148 GPa
Volumetric modulus of elasticity (bulk modulus)	241.5 GPa
Poisson's ratio	0.29
ELECTRICAL PROPERTIES	
Volume resistivity	10^{14} Ohm-cm
Dielectric strength	480,000 V cm^{-1}
Dielectric constant:	
E perpendicular to c-axis	9.4
E parallel to c-axis	11.5
Dissipation factor, *tan delta*	10^{-4}

A1. Main characteristics of the sapphire.

Material	Structure	Tm [°C]	a_0 (300 K) [nm]	L_m	Misfit R-plane sapphire [%]	Misfit Hg-1212 [%]
YSZ	cubic/fluorite	2680	5.13	3.63	-23.7	5.8
$Gd_2Zr_2O_7$	cubic/pyrochlore		10.52	3.72	-21.8	3.3
Y_2O_3	cubic/Mn_2O_3	>2400	10.6	3.75	-21.2	2.5
$LaAlO_3$	rhomboedral/perovskite	2100	5.36	3.79	-20.3	1.4
$La_2Zr_2O_7$	cubic/pyrochlore	2300	10.8	3.82	-19.7	0.6
Gd_2O_3	cubic/Mn_2O_3	>2400	10.81	3.82	-19.7	0.6
$CaTiO_3$	orthorhombic/perovskite		5.38×5.44	3.83	-19.5	0.3
CeO_2	cubic/fluorite	2600	5.41	3.83	-19.5	0.3
Eu_2O_3	cubic/Mn_2O_3	>2300	10.87	3.84	-19.3	0.01
$LaNiO_3$	rhomboedral/perovskite		5.45	3.85	-19.1	-0.2
$NdGaO_3$	orthorhombic/perovskite	1670	5.43×5.5	3.86	-18.9	-0.5
Sm_2O_3	cubic/Mn_2O_3	>2300	10.93	3.86	-18.9	-0.5
La_2NiO_4	tetragonal		3.86	3.86	-18.9	-0.5
Sr_2RuO_4	tetragonal		3.87	3.87	-18.7	-0.7
LSMO	rhomboedral/perovskite		5.49	3.88	-18.5	-1.0
NdBCO	orthorhombic		3.87×3.92	3.89	-18.2	-1.2
Gd_2CuO_4	tetragonal		3.89	3.89	-18.2	-1.2
$SrTiO_3$	cubic/perovskite	2080	3.91	3.91	-17.8	-1.7
Nd_2O_3	cubic/Mn_2O_3	>2300	11.08	3.92	-17.6	-2.0
$SrRuO_3$	orthorhombic/perovskite		5.57×5.54	3.93	-17.4	-2.2
Nd_2CuO_4	tetragonal		3.94	3.94	-17.2	-2.5
$BaTiO_3$	tetragonal/perovskite		3.99	3.99	-16.1	-3.7
$LaMnO_3$	orthorhombic/perovskite		5.54×5.74	3.99	-16.1	-3.7
$SrZrO_3$	orthorhombic/perovskite	2800	5.79×5.82	4.1	-13.8	-6.3
$BaSnO_3$	cubic/perovskite		4.12	4.12	-13.4	-6.7
NiO	cubic/rocksalt	1984	4.17	4.17	-12.4	-7.8
$BaZrO_3$	cubic/perovskite	2690	4.19	4.19	-11.9	-8.3
MgO	cubic/rocksalt	3100	4.21	4.21	-11.5	-8.7

a(sapphire) = 4.758 nm

a(Hg-1212) = 3.8425 nm

A2. Buffer layers suitable for the thin films of high temperature superconductors.
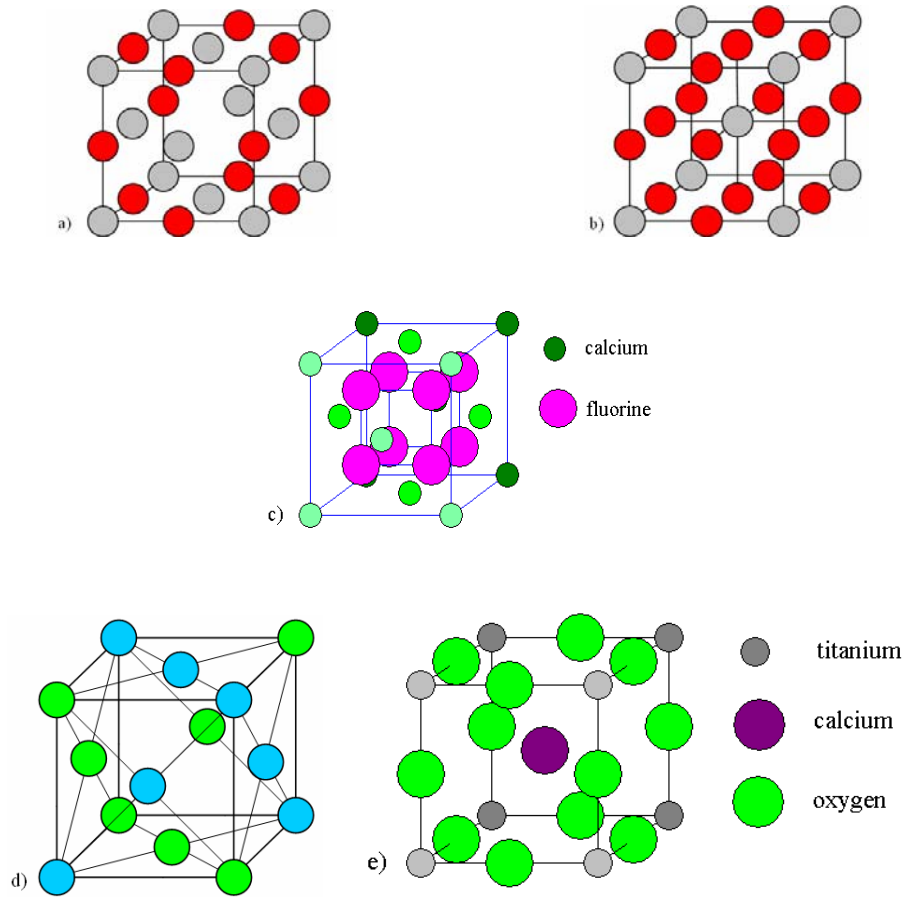
A3. Structural types: a) rocksalt NaCl, b) A_2O_3 (Mn_2O_3), c) fluorite $CaCl_2$, d) pyrochlore $A_2B_2O_7$, e) perovskite $CaTiO_3$.

Al2O3

Aluminum Oxide

Rad.: CuKa1λ: 1.54060 Filter: d-sp: Calculated

Cut off: 17.7 Int.: Calculated I/Icor.: 1.02
Ref: Calculated from ICSD using POWD-12++, (1997)
Ref: Sawada, H., Mater. Res. Bull., 29, 127 (1994)

Sys.: Rhombohedral S.G.: R$\bar{3}$c (167)

a: 4.7589(4) b: c: 12.9919(3) A: C: 2.7300

α: β: γ: Z: 6 mp:

Ref: Ibid.

Dx: 3.987 Dm: ICSD # : 075560

Peak height intensity. R-factor: 0.000. Al2 O3 type. PSC:
hR10. Mwt: 101.96. Volume[CD]: 254.81.

2θ	Int	h	k	l
25.597	683	0	1	2
35.180	999*	1	0	4
37.809	461	1	1	0
41.713	5	0	0	6
43.391	958	1	1	3
46.219	14	2	0	2
52.598	471	0	2	4
57.552	919	1	1	6
59.795	24	2	1	1
61.186	33	1	2	2
61.359	84	0	1	8
66.580	349	2	1	4
68.273	531	3	0	0
70.483	11	1	2	5
74.372	13	2	0	8
76.950	148	1	0	10
77.312	87	1	1	9
80.498	8	2	1	7
80.779	57	2	2	0
83.300	6	0	3	6
84.442	46	2	2	3
85.227	3	1	3	1
86.440	34	3	1	2

2θ	Int	h	k	l
86.592	27	1	2	8
89.091	63	0	2	10

A4. Diffraction data of the sapphire.

LaAlO3

Lanthanum Aluminum Oxide

Rad.: CuKa1λ: 1.54060 Filter: d-sp: Calculated

Cut off: 17.7 Int.: Calculated   I/Icor.: 4.71
Ref: Calculated from ICSD using POWD-12++, (1997)
Ref: Geller, S., Bala, V.B., Acta Crystallogr., 9, 1019 (1956)

Sys.: Rhombohedral   S.G.: R$\bar{3}$m (166)

a: 5.357   b: c: A: C: 1.0000

α: 60.100   β: γ: Z: 2   mp:

Ref: Ibid.

Dx: 6.520   Dm: ICSD # : 035551

Peak height intensity. R-factor: 0.136. C.D. Cell: a=5.365,
c=13.112, c/a=2.4439, S.G.=R-3m(166). PSC: hR10. Mwt:
213.89. Volume[CD]: 326.85.

2_θ	Int	h	k	l
20.260	1	0	1	0
20.260		1	1	1
23.448	642	1	1	0
33.374	999*	1	1	0
33.374	*	1	2	1
41.191	389	0	2	0
41.278	325	2	2	2
47.957	400	2	2	0
54.083	121	1	3	2
59.683	262	2	1	1
59.683		1	3	0
59.782	184	3	3	2
63.837	1	3	3	3
70.100	99	2	2	0
70.221	107	2	4	2
75.060	49	1	3	0
75.238	35	3	3	4
79.923	78	3	2	1
80.010	79	3	4	1
84.727	60	2	4	0
84.842	34	2	4	4
89.423	37	0	4	0
89.651	26	4	4	4

A5. Diffraction data of the LaAlO$_3$.

CeO2

Cerium Oxide

2θ	Int	h	k	l
28.541	999*	1	1	1
33.074	285	2	0	0
47.474	458	2	2	0
56.330	361	3	1	1
59.076	71	2	2	2
69.399	58	4	0	0
76.683	125	3	3	1
79.057	87	4	2	0
88.408	103	4	2	2

Rad.: CuKa1λ: 1.54060 Filter: d-sp: Calculated

Cut off: 17.7 Int.: Calculated   I/Icor.: 15.07
Ref: Calculated from ICSD using POWD-12++, (1997)
Ref: Wolcyrz, M., Kepinski, L., J. Solid State Chem., 99, 409
(1992)

Sys.: Cubic   S.G.: Fm3m (225)

a: 5.4124(1) b: c: A: C:

α: β: γ: Z: 4   mp:

Ref: Ibid.

Dx: 7.211   Dm: ICSD # : 072155

Peak height intensity. R-factor: 0.072. Ca F2 type. PSC:
cF12. Mwt: 172.12. Volume[CD]: 158.55.

A6. Diffraction data of the CeO$_2$.

HgBa2CaCu2O6

Mercury Barium Calcium Copper Oxide

Rad.: CuKa1λ: 1.54060 Filter: d-sp: Calculated

Cut off: 17.7 Int.: Calculated   I/Icor.: 6.48
Ref: Calculated from ICSD using POWD-12++, (1997)
Ref: Hunter, B.A et al., Physica C: Superconductivity, 221, 1
(1994)

Sys.: Tetragonal   S.G.: P4/mmm (123)

a: 3.8425(1) b: c: 12.6007(5) A: C: 3.2793

α: β: γ: Z: 1   mp:

Ref: Ibid.

Dx: 6.591   Dm: ICSD # : 075729

Peak height intensity. R-factor: 0.000. PSC: tP12. Mwt:
738.42. Volume[CD]: 186.05.

2θ	Int	h	k	l
7.00	170	0	0	1
14.045	8	0	0	2
21.135	41	0	0	3
23.128	17	1	0	0
24.195	122	1	0	1
27.160	999*	1	0	2
28.307	67	0	0	4
31.530	818	1	0	3
32.938	697	1	1	0
33.718	108	1	1	1
35.595	204	0	0	5
35.966	6	1	1	2
36.865	112	1	0	4
39.467	1	1	1	3
42.879	30	1	0	5
43.034	20	0	0	6
43.972	187	1	1	4
47.272	312	2	0	0
47.852	10	2	0	1
49.276	189	1	1	5
49.415	185	1	0	6
49.562	56	2	0	2
50.670	10	0	0	7

2θ	Int	h	k	l
52.320	10	2	0	3
53.263	3	2	1	0
53.795	20	2	1	1
55.372	217	2	1	2
56.018	40	2	0	4
56.398	123	1	0	7
57.935	216	2	1	3
58.555	28	0	0	8
60.549	125	2	0	5
61.408	32	2	1	4
61.768	8	1	1	7
63.812	24	1	0	8
65.713	12	2	1	5
65.829	8	2	0	6
66.757	6	0	0	9
68.842	34	1	1	8
69.082	81	2	2	0
69.540	4	2	2	1
70.786	46	2	1	6
71.684	6	1	0	9
71.802	10	2	0	7
73.156	3	2	2	3
73.939	1	3	0	0

2θ	Int	h	k	l
74.384	3	3	0	1
75.367	6	0	0	10
75.714	34	3	0	2
76.264	16	2	2	4
76.474	42	1	1	9
76.589	84	2	1	7
77.913	36	3	0	3
78.452	36	2	0	8
78.680	82	3	1	0
79.117	13	3	1	1
80.201	42	2	2	5
80.422	22	3	1	2
80.962	5	3	0	4
82.587	1	3	1	3
83.118	17	2	1	8
84.728	13	1	1	10
84.953	8	2	2	6
85.601	35	3	1	4
85.805	23	2	0	9
89.123	36	1	0	11
89.459	53	3	1	5

A7. Diffraction data of the Hg-1212 phase.

HgBa2Ca2Cu3O8.39

Mercury Barium Calcium Copper Oxide

Rad.: CuKa1λ: 1.54060 Filter: d-sp: Calculated

Cut off: 17.7 Int.: Calculated   I/Icor.: 4.31
Ref: Calculated from ICSD using POWD-12++, (1997)
Ref: Chmaissem, O et al., Physica C: Superconductivity, 217,
265 (1993)

Sys.: Tetragonal   S.G.: P4/mmm (123)

a: 3.8438(1) b: c: 15.7329(1) A: C: 4.0931

α: β: γ: Z: 1   mp:

Ref: Ibid.

Dx: 6.288   Dm: ICSD # : 080722

Peak height intensity. R-factor: 0.071. PSC: tP16.39. Mwt:
880.28. Volume[CD]: 232.45.

2θ	Int	h	k	l	2θ	Int	h	k	l
5.613	799	0	0	1	48.181	175	1	1	6
11.239	1	0	0	2	48.734	3	2	0	2
16.892	3	0	0	3	50.537	1	2	0	3
22.588	86	0	0	4	52.203	75	1	0	8
23.120	21	1	0	0	52.289	46	0	0	9
23.810	25	1	0	1	52.810	58	1	1	7
25.775	582	1	0	2	52.985	42	2	0	4
28.340	32	0	0	5	53.586	2	2	1	1
28.773	999*	1	0	3	54.603	96	2	1	2
32.544	705	1	0	4	56.022	20	2	0	5
32.927	925	1	1	0	56.271	228	2	1	3
33.429	185	1	1	1	57.903	68	1	0	9
34.166	226	0	0	6	58.553	190	2	1	4
34.896	4	1	1	2	59.593	122	2	0	6
36.886	290	1	0	5	61.408	107	2	1	5
37.229	12	1	1	3	63.189	11	1	1	9
40.085	54	0	0	7	63.652	36	2	0	7
41.661	18	1	0	6	63.879	34	1	0	10
43.986	174	1	1	5	64.797	4	2	1	6
46.118	1	0	0	8	65.171	2	0	0	11
46.782	52	1	0	7	68.167	1	2	0	8
47.255	469	2	0	0	68.684	21	2	1	7
47.628	22	2	0	1	68.902	53	1	1	10

2θ	Int	h	k	l
69.055	120	2	2	0
70.148	2	1	0	11
71.680	1	2	2	3
71.962	2	0	0	12
73.047	42	2	1	8
73.694	3	2	2	4
73.910	2	3	0	0
74.973	15	1	1	11
75.050	17	3	0	2
76.254	7	2	2	5
76.467	39	3	0	3
76.742	19	1	0	12
77.872	44	2	1	9
78.503	67	3	0	4
78.503		2	0	10
78.648	105	3	1	0
78.929	53	3	1	1
79.346	41	2	2	6
80.950	21	3	0	5
81.159	14	3	1	3
81.430	9	1	1	12
82.960	12	2	2	7
83.166	18	3	1	4
83.166		2	1	10
83.715	3	1	0	13
83.998	2	3	0	6
84.339	3	2	0	11
85.585	29	3	1	5
86.540	1	0	0	14
87.097	1	2	2	8
87.579	3	3	0	7
88.329	4	1	1	13
88.611	36	3	1	6
88.950	18	2	1	11

A8. Diffraction data of the Hg-1223 phase.

```
Re2-xBa4Ca1+yO12
source   : X-ray   Cu-Ka1   1,540598
2Theta   : 10,000  - 80,000
geometry : Bragg-Brentano, fixed slit, no anom. disp.


H   K   L   2Theta/deg   d/£     I/rel.   |F(hkl)|   Mu    FWHM
-----------------------------------------------------------------
1   0   1    18,015    4,92007   13,35    190,53     6    0,0707
0   1   2    18,838    4,70690    0,13     19,83     6    0,0707
0   0   6    19,002    4,66667   18,84    414,21     2    0,0707
1   0   4    21,833    4,06750   15,13    247,41     6    0,0707
0   1   5    23,844    3,72879    0,02     10,18     6    0,0707
1   0   7    28,560    3,12295   97,00    831,06     6    0,0707
0   0   9    28,671    3,11111    0,02     21,46     2    0,0707
1   1   0    30,966    2,88550  100,00    920,14     6    0,0707
0   1   8    31,172    2,86690    0,15     35,87     6    0,0707
1   1   3    32,451    2,75676    0,04     12,85    12    0,0707
0   2   1    36,056    2,48902    1,11    114,23     6    0,0707
2   0   2    36,495    2,46004    0,81     99,28     6    0,0707
1   1   6    36,585    2,45424   22,70    371,57    12    0,0707
1   0  10    36,763    2,44276    8,92    331,17     6    0,0707
0   2   4    38,211    2,35345    6,34    291,36     6    0,0707
0   0  12    38,553    2,33333    1,86    276,01     2    0,0707
2   0   5    39,456    2,28202    2,97    206,78     6    0,0707
0   1  11    39,706    2,26821    6,66    311,56     6    0,0707
0   2   7    42,626    2,11933   53,63    957,13     6    0,0707
1   1   9    42,704    2,11562    0,06     22,34    12    0,0707
2   0   8    44,514    2,03375    0,41     87,68     6    0,0707
1   0  13    45,839    1,97799   10,33    455,86     6    0,0707
2   1   1    48,247    1,88472    2,40    164,77    12    0,0707
1   2   2    48,595    1,87204    0,02     13,73    12    0,0707
0   0  15    48,744    1,86667    0,39    164,81     2    0,0707
0   2  10    48,807    1,86439    7,00    403,01     6    0,0707
0   1  14    49,019    1,85684    9,96    482,91     6    0,0707
2   1   4    49,968    1,82376    3,70    212,85    12    0,0707
1   1  12    50,245    1,81435    0,02     17,40    12    0,0707
1   2   5    50,980    1,78991    0,00      5,36    12    0,0707
2   0  11    51,185    1,78323    4,41    337,61     6    0,0707
2   1   7    53,611    1,70811   34,58    704,71    12    0,0707
3   0   0    55,082    1,66594   20,27    786,83     6    0,0707
1   2   8    55,211    1,66234    0,04     24,65    12    0,0707
1   0  16    55,598    1,65167    0,42    114,53     6    0,0707
0   3   3    56,028    1,64002    0,00      8,28     6    0,0707
3   0   3    56,028    1,64002    0,00      8,28     6    0,0707
0   2  13    56,348    1,63147    6,98    473,65     6    0,0707
3   0   6    58,807    1,56897    3,02    327,25     6    0,0707
0   3   6    58,807    1,56897    3,01    326,78     6    0,0707
1   1  15    58,876    1,56730    1,34    154,38    12    0,0707
2   1  10    58,932    1,56596    4,65    287,74    12    0,0707
0   1  17    59,000    1,56430    8,23    542,06     6    0,0707
2   0  14    59,117    1,56147    7,81    529,01     6    0,0707
0   0  18    59,365    1,55556    0,40    208,32     2    0,0707
1   2  11    61,035    1,51693    4,02    277,99    12    0,0707
0   3   9    63,269    1,46864    0,01     21,24     6    0,0707
3   0   9    63,269    1,46864    0,01     21,24     6    0,0707
2   2   0    64,540    1,44275   19,16    913,08     6    0,0707
0   2  16    65,010    1,43345    0,10     66,95     6    0,0707
2   2   3    65,402    1,42582    0,00      7,19    12    0,0707
2   1  13    65,693    1,42019    7,30    406,29    12    0,0707
1   0  19    66,043    1,41352    0,03     35,08     6    0,0707
1   3   1    67,613    1,38445    0,92    149,06    12    0,0707
3   1   2    67,894    1,37940    0,00      9,38    12    0,0707
2   2   6    67,952    1,37838    4,02    312,25    12    0,0707
2   0  17    68,130    1,37521    8,68    651,15     6    0,0707
1   2  14    68,238    1,37329    7,48    427,92    12    0,0707
1   1  18    68,467    1,36926    1,67    202,93    12    0,0707
1   3   4    69,013    1,35975    1,49    193,33    12    0,0707
3   0  12    69,241    1,35583    0,01     19,83     6    0,0707
0   3  12    69,241    1,35583    0,01     19,83     6    0,0707
0   1  20    69,695    1,34811    2,66    369,20     6    0,0707
3   1   5    69,847    1,34554    0,00      0,74    12    0,0707
0   0  21    70,581    1,33333    0,14    147,05     2    0,0707
1   3   7    72,049    1,30974   14,64    632,45    12    0,0707
2   2   9    72,105    1,30886    0,01     19,86    12    0,0707
3   1   8    73,412    1,28876    0,01     20,12    12    0,0707
2   1  16    73,744    1,28377    0,38    103,60    12    0,0707
0   2  19    74,721    1,26939    0,42    155,98     6    0,0707
4   0   1    76,212    1,24822    0,20    110,18     6    0,0707
0   4   2    76,480    1,24451    0,05     54,24     6    0,0707
3   0  15    76,595    1,24293    0,31    136,89     6    0,0707
0   3  15    76,595    1,24293    0,31    136,89     6    0,0707
1   3  10    76,644    1,24226    2,21    260,37    12    0,0707
1   2  17    76,704    1,24143    7,88    491,74    12    0,0707
1   0  22    77,299    1,23336    0,55    184,09     6    0,0707
4   0   4    77,548    1,23002    0,78    221,01     6    0,0707
2   2  12    77,766    1,22712    0,84    162,42    12    0,0707
2   0  20    78,200    1,22138    2,38    388,57     6    0,0707
0   4   5    78,346    1,21947    0,22    119,18     6    0,0707
3   1  11    78,509    1,21735    2,03    254,76    12    0,0707
1   1  21    79,051    1,21036    0,62    141,82    12    0,0707
```

A9. Diffraction data of the $Re_{2-x}Ba_4Ca_{1+y}O_{12}$ phase calculated using Powdercell program.

List of conference contributions

1. <u>M. Valeriánová</u>, Š. Chromik, V. Štrbík, G. Plesch: Thin film preparation of high-temperature superconductors based on thallium substituted by rhenium, 13th Conference of Slovak physicists, august 2003, Smolenice castle, Slovac republic.

2. D. De Barros, **<u>M. Valeriánová</u>**, P. Odier, L. Ortega, F. Weiss, Š. Chromik, V. Štrbík, J. C. Villegier: Properties of mercury cuprates films grown on CeO_2 buffered R-cut sapphire and $LaAlO_3$, Electroceramics IX, june 2004, Cherbourg, France.

3. <u>M. Valeriánová</u>, Š. Chromik, V. Štrbík, G. Plesch, Z. Matkovičová: Tl-based superconductors prepared on CeO_2 buffered sapphire, Solid State Chemistry, September 2004, Prage, Czech Republic.

4. <u>M. Valeriánová</u>, D. De-Barros, Š. Chromik, P. Odier, V. Štrbík, L. Ortega, G. Plesch: Mercuration and thallination for superconducting films without physical contact, Eco-Net meeting, November 2004, Bratislava, Slovak Republic (lecture).

5. <u>M. Valeriánová</u>, P. Odier, S. Pairis, V. Štrbík: Are mercury superconducting films grown by vapour phase or by bulk mass transfer?, Workshop on Weak Superconductivity 2005, Sept. 2005, Bratislava, Slovak Republic

6. <u>M. Valeriánová</u>, P. Odier, Š. Chromik, V. Štrbík: Role of the mercury pressure during reaction synthesis of $HgBa_2Ca_{n-1}Cu_nO_{2n+2+\delta}$ superconducting films: structural and electrical properties, Workshop on Weak Superconductivity 2005, Sept. 2005, Bratislava, Slovak Republic

7. M. Polák, **<u>M. Valeriánová</u>**, Š. Chromik, J. Kvitkovič, P. Mozola, P. Odier: Contactless testing of mercury based thin films, Workshop on Weak Superconductivity 2005, Sept. 2005, Bratislava, Slovak Republic

8. P. Odier, D. De Barros, **<u>M. Valeriánová</u>**, V. Štrbík, Š. Chromik: Growth of cuprate mercury based films, Workshop on Weak Superconductivity 2005, Sept. 2005, Bratislava, Slovak Republic

9. <u>M. Valeriánová</u>, P. Odier, Š. Chromik, V. Štrbík: Thin films of Hg-based superconductors, Eco-Net meeting, July 2006, Annecy, France (lecture)

10. <u>M. Valeriánová</u>, P. Odier, Š. Chromik, V. Štrbík: Role of the mercury pressure during reaction synthesis of Hg-based superconducting films using no contact mercuration, Cryoprague 2006, July 2006, Prague, Czech Republic

Published papers:

1. <u>Valeriánová</u>, <u>M.,</u> Chromik, Š., Štrbík, V., Plesch, G., Matkovičová, Z.: Rhenium doped Tl-based superconductors prepared on CeO_2 buffered sapphire, *Acta Physica Slovaca* **56** (2006) 35-39.

2. <u>Valeriánová</u>, <u>M.</u>, Odier, P., Pairis, S., and Štrbík, V.: Do mercury superconducting films grown by vapour phase or by bulk mass transfer?, *Physica C* **435** (2006) 31-36.

3. Polák, M., Kvitkovič, J., **<u>Valeriánová</u>, <u>M.</u>**, Chromik, Š., Mozola, P., Odier, P.: Contactless testing of mercury based thin films, *Physica C* **435** (2006) 41-45.

4. Li, X., Khafizov, M., Chromik, Š., **<u>Valeriánová, M.</u>**, Štrbík, V., Odier, P., Sobolewski, R.: Ultrafast photoresponse dynamics of current-biased Hg-Ba-Ca-Cu-O superconducting microbridges, *IEEE Transaction on Applied Superconductivity* **17** (2007) 3648-3651.

5. Dujavová, A., **<u>Valeriánová, M.</u>**, Štrbík, V., Matkovičová, Z., Plesch, G.: The influence of the reaction conditions on the formation of Tl(Re)-Ba-Ca-Cu-O superconductong thin films by thallination in open system, *Central European Journal of Physics* **5** (2007) 229-235.

6. Chromik, Š., **<u>Valeriánová</u>, <u>M.,</u>** Štrbík, V., Gaži, Š., Odier, P., Li, X., Xu, Y., Sobolewski, R., Hanic, F., Plesch, G., Beňačka, Š.: Hg-based cuprate superconducting films patterned into structures for ultrafast photodetectors, accepted to *Applied Surface Science*.

7. Matkovičová, Z., Štrbík, V., Plesch, G., **<u>Valeriánová</u>, <u>M.</u>**, and Dujavová, A.: Tl-based superconducting films prepared by aerosol spray deposition and thallinated in an open system, *Central European Journal of Physics* **5** (2007) 398-404.

8. <u>Valeriánová</u>, <u>M.</u>, Chromik, Š., Odier, P., and Štrbík, V.: Role of the mercury pressure during reaction synthesis of Hg(Re)-based superconducting films, *Central European Journal of Physics* **5** (2007) 446-456.

9. <u>Valeriánová, M.</u>, Odier, P., Chromik, Š., Štrbík, V., Polák, M., and Kostič, I.: Influence of the buffer layer on the growth of superconducting films based on mercury, *Superconductor Science and Technology* **20** (2007) 900-903.

Abstract

The Hg-based superconductors are materials with the highest critical temperatures from all known superconductors. Their application as the devices for the everyday use is, however, limited due to the difficulties in their fabrication. The optimization of the preparation methods will open large possibilities for the cryoelectronic applications.

Within the frame of my dissertation thesis we tried to optimize the parameters of the synthesis of the thin Hg-based films. The development of the non-contact method for the mercuration of the thin films confirmed the film formation via Hg vapour phase which will enable the development of the devices for the mercuration of the larger samples (few cm). The lift-off method used for the patterning of the precursor films prevents the water contamination of the films and thus their degradation. The non-contact mercuration also enabled the fabrication of the Hg-based superconducting structures with the minimal risk of the short-circuits between the single parts of the structure. The formation of the Hg-1223 decreased the amount of the impurities on the top of the films which will enable the fabrication of the sandwich planar Josephson junctions, too.

The prepared coplanar structures are suitable for the use in the ultra-fast detectors. The structures containing microbridges can serve for the study of the superconductivity in the micro- and submicro- scale and for the fabrication of the Josephson junctions of such dimensions. The model structure of the superconducting fault-current limiter was the first step for the fabrication of the real limiter structure and will be used for the study of the superconducting properties on this type of the structure. The use of the sapphire substrate allows the application of the Hg-based superconducting structures also for the microwave devices.

All the structures had high values of the critical temperatures (up to 110 K for the coplanar strips and microbridges, up to 120 K for the limiter model structures) which provide the stability of the superconducting properties and parameters (coherent length, energy gap, etc.) at the working temperature of the superconductor (77 K).

Résumé

Les supraconducteurs à base de mercure sont les matériaux ayant les températures critiques les plus élevées de tous les supraconducteurs connus. Mais leurs applications dans des dispositifs d'utilisation pratique est limitée en raison de leurs difficultés d'élaboration. L'optimisation des méthodes de préparation ouvrira d'importantes possibilités pour les applications cryoeléctroniques.

Dans le cadre de ma thèse j'ai essayé d'optimiser les paramètres de synthèse de couches minces à la base de cuprates de mercure (Hg-1212 ou Hg-1223). Le développement d'une méthode de mercuration sans contact a confirmé que la formation de couches se faisait par phase vapeur. Ceci permettra d'envisager une fabrication d'échantillons de plus grandes dimensions (quelque cm) que celle de ceux que nous fabriquons actuellement. L'utilisation du procédé lift-off de gravure des couches précurseur a permis d'éviter la contamination des couches de cuprates de mercure et donc la dégradation de leurs propriétés supraconductrices. On a ainsi pu réaliser des motifs supraconducteurs au micron intéressants. La mercuration sans contact a aussi permis une limitation de la pollution par les grains de la source de mercure. C'est une amélioration importante pour éviter la création de courts-circuits entre des lignes co-planaires utilisées pour tester la photo-réponse de ce type de supraconducteur. On a trouvé que l'épaisseur de la couche tampon avait une influence sur la formation de la phase supraconductrice. L'épaisseur de la couche de CeO_2 modifie les contraintes et l'arrangement des défauts dans cette couche, or ces défauts jouent un rôle critique dans la diffusion de Ca-Cu-O nécessaire à la formation de Hg-1223. L'amélioration de la formation de Hg-1223 diminue le volume des impuretés en surface ce qui permettra d'envisager la fabrication de structures planaires sandwich pour des jonctions de Josephson.

Les structures co-planaires de la phase Hg-1212, sont compatibles pour leur utilisation dans des détecteurs ultra rapides. Ces structures comportent des micro-ponts et peuvent servir pour les études de la supraconductivité à l'échelle micronique ainsi qu'à la fabrication de jonctions Josephson à cette échelle. Dans un autre domaine, on a pu réaliser une structure modèle destinée à l'étude de limiteurs de courants supraconducteurs utilisant ce matériau. L'utilisation de saphir comme substrat permettra d'accéder aux domaines micro-ondes.

Toutes ces structures étaient supraconductrices avec des températures critiques élevées (jusqu'au 110 K pour les lignes co-planaires et les microponts, et jusqu'au 120 K pour les structures modèles pour le limiteur de courant). Cette haute température critique assure la stabilité des propriétés supraconductrices à la température de l'azote liquide (77 K) à laquelle seront testés ces dispositifs.